Terms and Conditions of Use of Digitised Theses from Trinity College Library Dublin

Copyright statement

All material supplied by Trinity College Library is protected by copyright (under the Copyright and Related Rights Act, 2000 as amended) and other relevant Intellectual Property Rights. By accessing and using a Digitised Thesis from Trinity College Library you acknowledge that all Intellectual Property Rights in any Works supplied are the sole and exclusive property of the copyright and/or other IPR holder. Specific copyright holders may not be explicitly identified. Use of materials from other sources within a thesis should not be construed as a claim over them.

A non-exclusive, non-transferable licence is hereby granted to those using or reproducing, in whole or in part, the material for valid purposes, providing the copyright owners are acknowledged using the normal conventions. Where specific permission to use material is required, this is identified and such permission must be sought from the copyright holder or agency cited.

Liability statement

By using a Digitised Thesis, I accept that Trinity College Dublin bears no legal responsibility for the accuracy, legality or comprehensiveness of materials contained within the thesis, and that Trinity College Dublin accepts no liability for indirect, consequential, or incidental, damages or losses arising from use of the thesis for whatever reason. Information located in a thesis may be subject to specific use constraints, details of which may not be explicitly described. It is the responsibility of potential and actual users to be aware of such constraints and to abide by them. By making use of material from a digitised thesis, you accept these copyright and disclaimer provisions. Where it is brought to the attention of Trinity College Library that there may be a breach of copyright or other restraint, it is the policy to withdraw or take down access to a thesis while the issue is being resolved.

Access Agreement

By using a Digitised Thesis from Trinity College Library you are bound by the following Terms & Conditions. Please read them carefully.

I have read and I understand the following statement: All material supplied via a Digitised Thesis from Trinity College Library is protected by copyright and other intellectual property rights, and duplication or sale of all or part of any of a thesis is not permitted, except that material may be duplicated by you for your research use or for educational purposes in electronic or print form providing the copyright owners are acknowledged using the normal conventions. You must obtain permission for any other use. Electronic or print copies may not be offered, whether for sale or otherwise to anyone. This copy has been supplied on the understanding that it is copyright material and that no quotation from the thesis may be published without proper acknowledgement.

FUNCTIONAL EXPRESSION OF THE EPITHELIAL SODIUM CHANNEL δ-SUBUNIT IN HUMAN RESPIRATORY EPITHELIAL CELLS

by

Elena Schwagerus

(Staatsexamen Pharmazie, Jena, Germany)

A dissertation submitted for the degree of Doctor of Philosophy

at the

University of Dublin, Trinity College

This research was conducted at the School of Pharmacy and Pharmaceutical Sciences,

Trinity College, Dublin 2, Ireland

Under the direction and supervision of

Dr. rer. nat. Carsten Ehrhardt

2012

Declaration

This thesis has not been submitted as an exercise for a degree at this or any other University. Except where stated otherwise, the work described herein has been carried out by the author alone. This thesis may be borrowed or copied upon request with the permission of the Librarian, University of Dublin, Trinity College.

Signature of Author

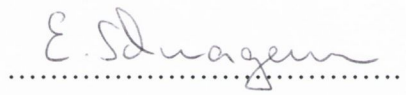

Elena Schwagerus

Summary

Mammalian amiloride-sensitive epithelial Na^+ channel (ENaC) can be composed by different combinations of four homologous subunits, α, β, γ and δ. The canonical αβγ-ENaC, abundantly expressed in Na^+ absorbing epithelia, is thoroughly investigated and well known for its crucial role in Na^+ homoeostasis. Via aldosterone-controlled Na^+ re-uptake in the kidney, ENaC regulates blood volume and pressure. In the lung, it facilitates the maintenance of alveolar lining fluid layer and efficient gas exchange. Delta-ENaC, mainly expressed in non-epithelial tissues, has recently been described in human airway epithelia. Its physiological role, however, remains largely hypothetical and is primarily based on the expression data as well as the biophysical characteristics of the heterologously expressed protein. This work sought to gain insight into the physiological role of δ-ENaC in human respiratory epithelium *in vitro*, in particular, to provide evidence for its contribution to the net transepithelial ion transport in the lung. To achieve this aim, continuous respiratory epithelial cell lines (alveolar A549, bronchiolar H441 as well as bronchial 16HBE14o- and Calu-3) and alveolar epithelial type I and type II cells in primary culture (ATI and ATII) were used. The first part of this work focused on expression and cellular localisation of δ-ENaC in the selected organotypic models. Messenger RNA transcripts encoding α-, β-, γ- and δ-subunits were detected in A549, 16HBE14o- and Calu-3 cell lines. At protein level, expression of δ-ENaC was demonstrated in H441 and Calu-3 as well as in ATI cells, using an anti-δ-ENaC antibody of confirmed specificity. Furthermore, cell surface biotinylation and immunofluorescence microscopy were carried out to study the subcellular localisation of the protein in the respective cells. In the second step, transepithelial measurements in modified Ussing chambers were performed to test the functionality of δ-ENaC protein. To this end, Evans blue, capsazepine and icilin, previously characterised as specific

modulators of δ-ENaC function in *Xenopus laevis* oocytes expression system, were used as pharmacological tools. The substances stimulated or inhibited short-circuit currents (I_{SC}) across monolayers of H441, Calu-3 and ATI-like cells. However, compound effects in our hands differed from previous observations in *X. laevis* oocytes. Moreover, analysis of Na^+ and Cl^- dependencies of the observed outcomes suggested that these were likely not to originate from exclusive modulation of δ-ENaC as target. Therefore, in the last part of this work, experiments aiming to up- and down-regulate δ-ENaC expression were performed to test whether any of the effects, induced by the alleged δ-ENaC modulators in human airway epithelial cells, were δ-ENaC-mediated. None of the utilised knock-down strategies (i.e. RNAi technique, dominant negative cDNA constructs) succeeded to down-regulate δ-ENaC expression and/or to significantly change the pharmacological responses to Evans blue, capsazepine or icilin in H441 and Calu-3 cells, respectively. When δ-ENaC was stably over-expressed in H441 cells, on the other hand, capsazepine and icilin increased I_{SC} levels, consistent with the prior characterisation of the compounds as δ-ENaC activators and opposed to the I_{SC} reduction observed with both substances in the wild-type H441 cells. Also, interdependencies of δ-ENaC activators with the channel inhibitors Evans blue and amiloride indicated interaction of all substances with the same target, i.e., δ-ENaC. Hence, elevating δ-ENaC expression levels in H441 cells, endogenously expressing the protein, revealed that the effects induced by δ-ENaC modulators in the wild-type H441 cells were not δ-ENaC-mediated. Consequently, since no δ-ENaC activity was detectable in human respiratory epithelial cells *in vitro,* δ-ENaC, expressed on both mRNA and protein levels in these cells, is likely non-functional and does not contribute to the net transepithelial ion transport, at least under basal conditions.

Table of contents

CHAPTER 1

Introduction

1.1 Epithelial ion transport in the respiratory system

According to the classic concept of human lung architecture, the human lung consists of 24 generations of branching airways, with each airway dividing into two smaller airway tubes. The generations 0-14, which include tracheal tube, bronchi, bronchioles and terminal bronchioles, are regarded as conducting airways. Their main function is to pre-warm, humidify and filter the inhaled air from particles and pathogens while routing it to the sites of the gas exchange. From generation 15-16 on (transitional-respiratory bronchioles), the gas exchange starts to take place, as alveoli begin to be incorporated into airway walls. The airways continue to divide to alveolar ducts, until, in the last generation, they end in alveolar sacs (Weibel, 1963).

The surface of the airways is lined with a continuous epithelial layer, the cellular composition of which constantly changes as the airways are branching further, adjusting to the function of the respective segment (**Figure 1**). The bronchial epithelium is of pseudo-stratified nature and columnar morphology. It consists of a number of different cell types, but mainly ciliated cells, mucus-secreting goblet cells and small basal cells, the progenitor cells of the airway epithelium. The proportions in which these cells are found change, and the height of the epithelial layer decreases progressively towards the periphery, until the columnar epithelium (~50 μm in height) is replaced by the cuboidal epithelium (~10 μm) in the bronchioles and, finally, by the squamous epithelium in the alveoli. The latter is composed of only two distinct epithelial cell types, alveolar type I and type II cells (ATI and ATII), which are accompanied by alveolar macrophages, interstitial fibroblasts and endothelial cells of the microvasculature. The human alveolar barrier is extremely thin (~0.2 μm), therefore, providing just a minimal diffusion barrier for the gas exchange (Stone *et al.* 1992).

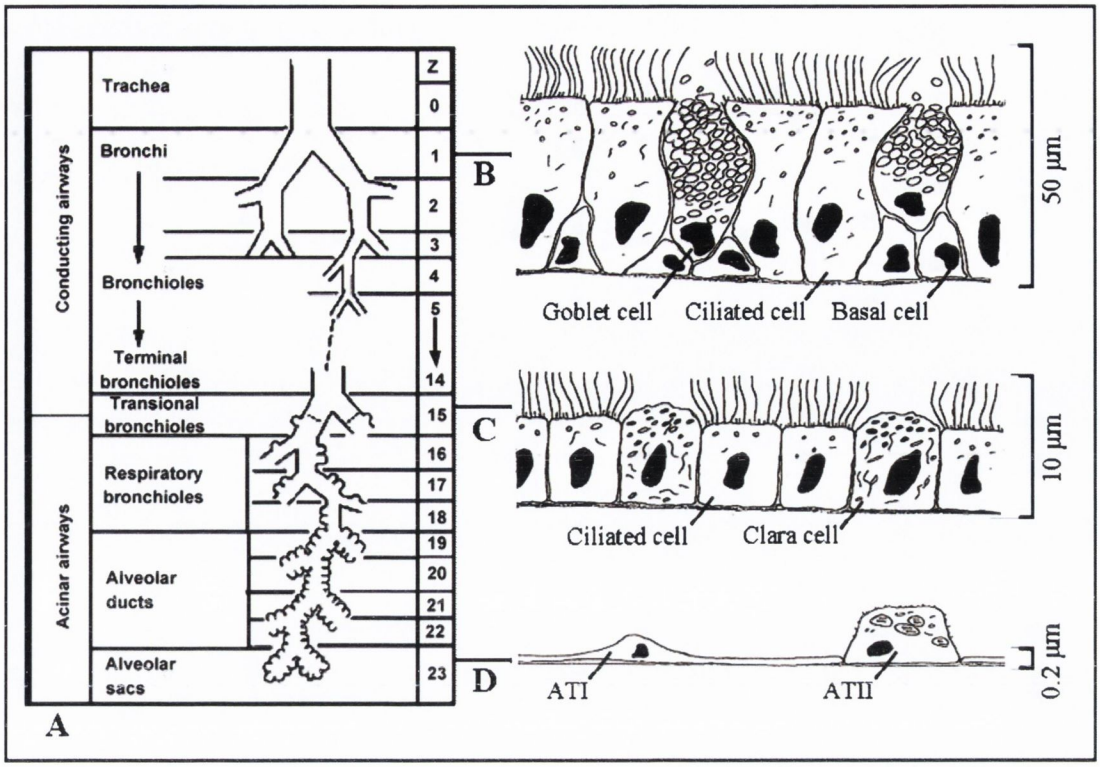

Figure 1. (A) The classic model of human lung architecture. *Adapted from Weibel, 1963.* Major cell types in different segments of human respiratory system. The pseudo-stratified epithelium of bronchi **(B)** is composed of ciliated, goblet and basal cells. In the bronchioles **(C)**, the epithelium mainly comprises ciliated cells with interspersed Clara cells. The alveolar epithelium **(D)** is composed of extremely thin, squamous alveolar epithelial type I (ATI) and cuboidal type II cells (ATII). The average height of the respective epithelium is indicated. *Modified from Forbes, 2000.*

1.1.1 Epithelial lining of the upper airways: cellular and molecular components involved in the regulation of the mucociliary clearance

The major function of the pseudo-stratified epithelium of the upper airways is the mucociliary clearance. The epithelial surface is covered with a thin biphasic liquid layer, formed by the periciliary liquid layer (PCL) that surrounds the cilia of the ciliated cells, and the overlying mucus, secreted by goblet cells and seromucous glands. The mucus blanket is constantly moved upwards by the ciliary beat, so that inhaled particles and pathogens trapped in the sticky mucus can be efficiently removed from the airways

(Braiman, Priel, 2008). Furthermore, various immunoreactive proteins are present in the airway surface liquid, i.e., Clara cell secretory protein or the surfactant proteins A and D (SP-A and SP-D) (Coppens *et al.* 2007; Kim *et al.* 2007). Thus, the bronchial epithelium represents an important part of the innate immune defence.

The height and composition of the PCL determines optimal mucociliary clearance. These parameters are primarily regulated by complementary Na^+ absorption and Cl^- secretion and the subsequent passive transepithelial water flow across the epithelial barrier (**Figure 2**). The **Na^+-K^+-ATPase**, located at the basolateral membranes of the airway epithelial cells, provides the driving force for the apical Na^+ uptake via **epithelial sodium channels (ENaC)**. Alpha-, β- and γ-ENaC subunits are present in human airway and nasal epithelium (Burch *et al.* 1995; Bangel *et al.* 2008). A fourth homologous subunit δ has been recently detected in human nasal epithelium as well as in human bronchial and bronchiolar cell lines (16HBE14o- and H441, respectively) (Zhao *et al.* 2012; Ji *et al.* 2006; Bangel-Ruland *et al.* 2009). Moreover, expression of **cyclic nucleotide-gated channels (CNG)** in rat tracheal, bronchial and bronchiolar epithelium has been reported (Schwiebert *et al.* 1997). Further details on Na^+ transporting proteins are provided in section 1.1.2.2 of this chapter.

Bronchial chloride secretion is mediated via Cl^- channels, with **cystic fibrosis transmembrane conductance regulator (CFTR)**, a cAMP activated apical Cl^- channel, being the most prominent contributor (Rich *et al.* 1990). Additionally, **Ca^{2+}-activated Cl^- channels (CaCC)** are also present at the apical surface of the airway epithelial cells. However, their molecular identity has not yet been identified (Rock *et al.* 2009). To enable apical Cl^- secretion, basolateral Cl^- supply is required. In airway epithelium, this is provided by **Na^+-K^+-2Cl^- cotransporters (NKCC)** as well as **HCO_3^-**

/Cl^- exchangers (Tessier *et al.* 1990; Al-Bazzaz *et al.* 2001). Furthermore, apically and basolaterally localised **K^+ channels** contribute to regulation of the membrane potential and maintenance of electrochemical gradient for the apical Cl^- secretion (Bardou *et al.* 2009).

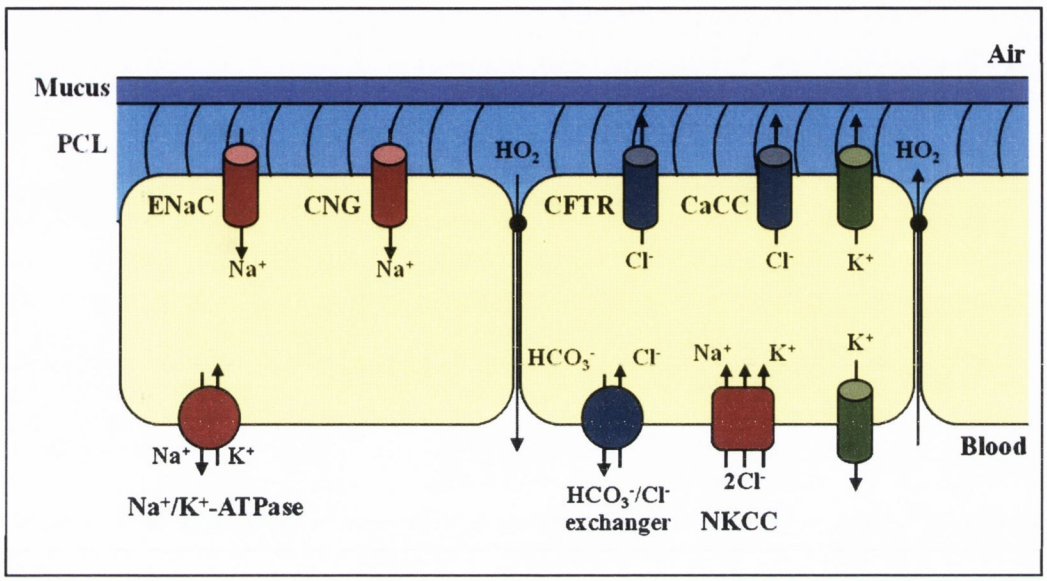

Figure 2. Schematic diagram of the airway epithelial layer composed of ciliated cells. Airway surface liquid layer, covering the epithelial surface, consists of the periciliary layer (PCL) including cilia and the overlying mucus blanket. The composition of the PCL is regulated by concerted apical Cl^--secretion and Na^+-absorption. The driving force for Na^+ uptake is provided by the basolateral Na^+-K^+-ATPase. On the apical side, epithelial sodium channels (ENaC) and, to a smaller extent, cyclic nucleotide-gated channels (CNG) mediate Na^+-absorption. The cystic fibrosis transmembrane conductance regulator (CFTR) is mainly responsible for the apical Cl^--secretion, in addition to Ca^{2+}-activated Cl^- channels (CaCC). The basolateral supply of Cl^- ions occurs via Na^+-K^+-2Cl^- cotransporters (NKCC) as well as HCO_3^- /Cl^- exchangers. Water molecules follow passively along the created osmotic gradient via the paracellular route.

1.1.2 Alveolar epithelium

1.1.2.1 Alveolar epithelial cell types involved in the alveolar fluid clearance

The alveolar epithelium consists of two major cell types: ATI and ATII cells. The smaller (~10 μm in diameter), cuboidal ATII cells are the better investigated pneumocytes, because their isolation and culture is less challenging. Among the known functions of ATII cells are the modulation of immune responses in the lung, repair of injured alveolar epithelium and the synthesis, secretion and re-uptake of pulmonary surfactant. Surfactant reduces the surface tension at the air-liquid interface and thus prevents alveoli from collapsing. Lamellar bodies, the intracellular storage organelles of surfactant components, belong to the distinctive morphological features of ATII cells (reviewed by Fehrenbach 2001). The large (~50-100 μm in diameter), squamous and extremely thin (0.05-0.2 μm) ATI cells line approximately 95% of the internal surface of the lung. ATI cell-specific functions, other than playing a role in gas exchange, were merely hypothetical for a long time. Recent data, however, suggest other important functions including alveolar fluid homoeostasis, protection from lung injury, host defence etc. (Qiao *et al.* 2003; Dahlin *et al.* 2004).

The alveolar surface is covered with an extremely thin fluid film, the so-called alveolar lining fluid (ALF) (Bastacky *et al.* 1995) composed of surfactant phospholipids and an aqueous subphase. The alveolar fluid originates mostly from the passive movement of capillary fluid across the alveolar epithelium due to the pressure gradient between the blood capillaries and the alveolar space. Increased ALF height (only 0.1-0.2 μm under normal physiologic conditions) represents a larger diffusion barrier and, thus, impairs gas exchange. Hence, a major role of alveolar epithelial cells is to regulate the alveolar fluid volume and, by this means, keep the lung sufficiently dry. This process, also called

alveolar fluid clearance (AFC), is pivotal for effective delivery of oxygen in the adult lung. In addition, it plays a key role at birth, when the mode of oxygen delivery changes from the placental to the atmospheric route and the lung switches from alveolar Cl^- and fluid secretion to net Na^+ and fluid absorption (Olver and Strang, 1974).

Although a lot still remains unknown and controversial, our knowledge about the exact molecular identity and spatial localisation of key mediators of AFC is getting more and more comprehensive, with more advanced cell isolation, culture techniques and model systems continuing to evolve. According to an early concept of AFC under physiologic conditions, Na^+ is absorbed in an amiloride-sensitive manner on the apical side of ATII cells and pumped actively from their basolateral surface into the lung interstitium by the Na^+-K^+-ATPase. Consequently, an osmotic gradient is generated with Cl^- following to preserve electroneutrality and water moving across both ATI and ATII cells via aquaporins (reviewed by Dobbs and Johnson 2007). While the general idea of AFC is still the same, evidence has emerged that Na^+ uptake is mediated by a wider range of ion channels than initially believed. It is also noted that both alveolar cell types are involved in the process, as ATI cells have also been shown to express the relevant Na^+ transport proteins. In addition, depending on the species and the stage of lung development, 20-70% of basal lung liquid absorption cannot be inhibited by amiloride (reviewed by Matthay *et al.* 2002), with the amiloride-insensitive component increasing with lung maturation. For example, amiloride can abolish the AFC completely in neonatal sheep, while by 6 months of age, only around 70% are inhibitable (Ramsden *et al.* 1992; Junor *et al.* 1999). These observations put the importance of amiloride-sensitive fluid absorption in adult lung under normal physiological conditions in question and highlight the relevance of the amiloride-insensitive component.

1.1.2.2 Molecular components of the alveolar fluid clearance

To generate an osmotic driving force across the epithelium, the presence of **Na^+-K^+-ATPase** on the basolateral side of the cells is crucial. Both rat ATI and ATII cells have been shown to express Na^+-K^+-ATPase subunits at mRNA and protein levels (Nici *et al.* 1991; Borok *et al.* 2002; Johnson *et al.* 2002). Immunohistochemistry confirmed the basolateral localisation of sodium pump *in situ* (Nici *et al.* 1991; Borok *et al.* 2002). Moreover, an inhibitor of Na^+-K^+-ATPase reduced AFC in isolated human lungs by approximately 45% (Sakuma *et al.*1994).

Aquaporins are transmembrane channels that enable water to follow the osmotic gradient created by Na^+ channels and the Na^+-K^+-ATPase. Four aquaporins have been identified in the lung so far (AQP1, AQP3, AQP4 and AQP5), one of them (AQP5) in the alveolar epithelium - more precisely in ATI cells (Nielsen *et al.* 1997). However, AQP5 knockout mice had reduced osmotic water permeability, but were able to clear alveolar fluid (Ma *et al.* 2000).

For a long time, the presence of **epithelial sodium channels (ENaC)** in alveoli has been the only explanation for the observed Na^+ uptake. Expression sites, biophysical characteristics and cellular regulation of this member of the epithelial sodium channel/degenerin family of non-voltage gated ion channels is discussed in detail in section 1.2 of this chapter. Briefly, the "classic" ENaC assembly, formed by homologous subunits α, β, and γ, is regarded to be the amiloride-sensitive component of Na^+ currents in epithelial cells. Knockout mice with inactivated β- or γ-subunit died from abnormal renal electrolyte re-absorption (Barker *et al.* 1998; McDonald *et al.* 1999). These data provided strong evidence that the functional expression of αβγ-ENaC in the distal nephron plays a crucially important role for the regulation of Na^+ balance

and, thus, also blood volume and pressure. In the lung, these three ENaC subunits have been detected at mRNA (Talbot *et al.* 1999) as well as at protein levels, most recently in both freshly isolated rat ATI and ATII cells by means of immunohistochemistry and Western blotting (Johnson *et al.* 2002). A crucial role of α-ENaC for the clearance of lung liquid at birth was demonstrated by Hummler *et al.* (1996), as mice lacking α-subunit died shortly after birth from inability to clear their lungs of fluid. The importance of α-ENaC for AFC in the adult lung, however, remains unclear. In recent studies by Li and Folkesson (2006), small interfering RNA (siRNA) against α-subunit, administrated intratracheally, failed to inhibit the basal AFC in adult rat by more than 30%.

The fourth homologous ENaC subunit δ, is able to generate amiloride-sensitive Na^+ currents on its own or in combination with other ENaC subunits (Waldmann *et al.* 1995; Ji *et al.* 2006). Delta-ENaC was found to be expressed in alveolar epithelium at mRNA level, in particular, in the alveolar epithelial A549 cell line, in ATII cells in primary culture as well in human lung tissue (Ji *et al.* 2006; Nie *et al.* 2009b; Zhao *et al.* 2012). However, its function in this tissue remains controversial. Delta-ENaC containing channels differ from α-containing channels in their biophysical and pharmacological properties, in particular showing around 30-fold lower affinity to amiloride ($K_{0.5\ (amiloride)}$ = 2.6 μM and 0.08 μM for δ- and α-ENaC, respectively; Waldmann *et al.* 1995) and distinct Na^+ conductances. Delta-ENaC has therefore been suggested to contribute, at least in part, to the less amiloride-sensitive component of AFC and to the variety of Na^+ conductances detected in alveolar epithelial cells, the presence of which cannot be explained by the expression of classic ENaC subunits alone (Ji *et al.* 2006).

Another possible pathway for amiloride-insensitive Na^+ transport in the lung is via

cyclic nucleotide-gated channels (CNG). These members of the superfamily of voltage-gated channels are permeable to mono- and divalent cations and are sensitive to, e.g., pimozide and dichlorobenzamil. They are expressed in different tissues such as retinal rods, testis, heart, and have also been detected in cultured ATII cells (Kemp *et al.* 2001) and freshly isolated ATI cells using patch-clamp technique (Johnson *et al.* 2006).

Moreover, various **K^+ channels** have been shown to be expressed in the alveolar epithelium. In addition to "n"-type, "l"-type (DeCoursey *et al.* 1988) and Ba^{2+}-sensitive K^+ channels (Johnson *et al.* 2006) as well as ATP-sensitive K^+ channels (K_{ATP}) are present. The main role of K^+ channels in epithelial tissues is usually the maintenance of the electrochemical gradient, which is required for ion and fluid transport. However, since K_{ATP} channel inhibitors have been shown to reduce both amiloride-sensitive Na^+ as well as forskolin-stimulated Cl^- currents in alveolar epithelial cells, K_{ATP} channels appear to have a more specific role and interact with both ENaC and **CFTR** (Leroy *et al.* 2004, 2006).

As a consequence of net Na^+ absorption taking place, either transcellular or paracellular anion transport is necessary in order to maintain electroneutrality. Recent studies have shown that CFTR is present in ATI and ATII cells (Brochiero *et al.* 2004; Johnson *et al.* 2006) and, thus, offers a transcellular pathway for Cl^- influx. Since CFTR inhibition does not affect basal fluid clearance in mice, but blocks cAMP-stimulated increase in fluid absorption instead, it has been suggested that CFTR channels are important for cAMP-activated AFC (Fang *et al.* 2006). Moreover, evidence for the presence of the **voltage-gated Cl^- channels, CLC-5 and CLC-2** in alveolar epithelial cells exists, as well as for **HCO_3^-/Cl^- exchangers** and **K^+-Cl^- cotransporters**, all important components of transepithelial chloride transport (Johnson *et al.* 2009; Lee *et al.* 2003).

1.1.2.3 Current concept of the alveolar epithelial ion transport

Considering that the molecular components involved in ion transport across the alveolar epithelium have been localised in both ATI and ATII cells, and taking into account the surface ratio of ATI:ATII cells, which is around 43:1, it has become increasingly clear that ATI cells play an important part in AFC and ion transport is involving the entire epithelium (i.e., ATI and ATII cells). **Figure 3** shows the revised concept of AFC as we understand it to date.

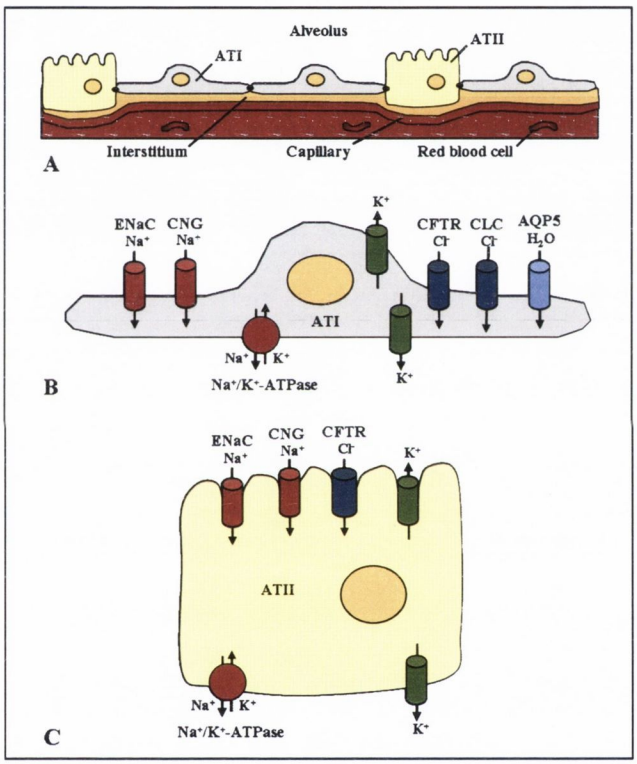

Figure 3. Schematic diagram of the alveolar epithelial layer, consisting of two distinct cell types **(A)**, as well as of the transport processes underlying the alveolar fluid clearance under physiologic conditions **(B, C)**. Na^+-K^+-ATPase, localised at the basolateral membrane of both ATI and ATII cells, pumps Na^+ actively into the interstitium of the lung. By this means, the electrochemical driving force for the Na^+ uptake is provided. This occurs at the apical surface of both cell types in amiloride-sensitive and amiloride-insensitive manner (via ENaC and CNG channels). Chloride follows via CFTR in both cell types and CLC channels in ATI cells to maintain electoneutrality. Due to the created osmotic gradient, water is transported from apical to basolateral side through aquaporins in ATI cells (AQP5) or by diffusion.

1.1.3 Clinical relevance of the functional ion transport in the airways: altered epithelial ion transport in cystic fibrosis

In cystic fibrosis (CF), a defect of the CFTR gene (most frequently caused by the ΔF508 mutation) leads to an impairment or loss of CFTR function and, thus, insufficient Cl^- secretion across epithelia. Whilst numerous tissues are affected by this autosomal recessive disease, the most severe effects are those in the respiratory system. Impaired Cl^- transport across airway epithelial barriers results in thickened mucus, which is too viscous to be efficiently cleared by the mucociliary escalator. Together with trapped bacteria, it accumulates in the airways, increasing the frequency and severity of pulmonary infections. These are especially dangerous in case of colonisation with *Pseudomonas aeruginosa*, since there is a high risk of chronic manifestation which is associated with increased mortality and morbidity in CF patients (O'Sullivan, Freedman, 2009).

Interestingly, impaired Cl^- secretion in CF is often accompanied by Na^+ hyperabsorption. Therefore, it has been proposed that CFTR is able to down-regulate ENaC activity (Kunzelmann *et al.* 1995; Mall *et al.* 1998). However, this hypothesis needs further confirmation, as according to some recent reports, Na^+ conductances are not elevated in CF epithelia (Chen *et al.* 2010; Itani *et al.* 2011).

1.1.4 Clinical relevance of the alveolar fluid balance: formation of pulmonary oedema

As mentioned above, alveolar fluid clearance is the prerequisite for efficient gas exchange and thus, indispensable for life. Impaired alveolar clearance leads to imbalance between fluid infiltration in the alveoli and fluid re-absorption, which is often associated with the formation of pulmonary oedema and may be caused by a number of conditions. Firstly, abnormally elevated pulmonary blood pressure may increase the fluid flux from the pulmonary capillaries into the alveolar airspace, aggravating gas exchange. The resulting local hypoxia down-regulates expression of ENaC and Na^+-K^+-ATPase (Clerici, Matthay, 2000), which, in turn, decreases AFC and promotes pulmonary oedema. Secondly, bacterial sepsis, acid aspiration, smoke inhalation, and reperfusion injury after lung transplantation may damage alveolar-capillary barrier causing the condition referred to as acute lung injury (ALI) or its more severe manifestation, the acute respiratory distress syndrome (ARDS). Both conditions are associated with increased epithelial permeability and oedema fuid infiltration into the lung (Mutlu, Sznajder, 2005). Furthermore, ventilator-induced lung injury (VILI), which is due to over-distention of the alveoli by artificial ventilation, is associated with formation of pulmonary oedema (Ricard *et al.* 2003). In patients with ALI or ARDS, impaired alveolar fluid clearance leads to significantly higher mortality from pulmonary oedema (Ware, Matthay, 2001). This observation taken together with the outcome of the knock-out studies in mice, in which mice lacking α-ENaC die at birth from inability to clear their lungs from fluid (Hummler *et al.* 1996), emphasises the importance of functional ion transport, in particular that of sodium, in the alveolar epithelium.

1.2 Epithelial sodium channel delta subunit (δ-ENaC)

Five homologous subunits of the epithelial sodium channel (ENaC) have been described so far: α-, β-, γ-, δ-, and ϵ-ENaC, most recently identified in *Xenopus laevis* (Babini *et al.* 2003). Functionally, so-called conducting or pore-forming subunits (i.e., α, δ, ϵ) that are able to form functional homomeric channels on their own, can be distinguished from accessory subunits (i.e., β, γ), which modify channel activity of the heteromeric ENaC. The "classic" α-, β-, γ-ENaC subunits, originally cloned from rat colon, are abundantly expressed in Na^+-absorbing epithelia of kidney, colon and lung (Canessa *et al.* 1993, 1994), but are also found in sweat and salivary ducts, keratinocytes as well as in a number of other predominantly epithelial expression sites (Duc *et al.* 1994; Brouard *et al.* 1999). Their crucial role in regulation of Na^+ homoeostasis and, thus, in regulation of blood volume and pressure via controlled, aldosterone-sensitive Na^+ re-absorption in the distal nephron as well as in maintenance of alveolar fluid layer in the lung has been imposingly demonstrated by *in vivo* studies in transgenic animals. Alpha-ENaC is essential for the clearance of lung liquid at birth, as knockout mice with inactivated α-subunit die shortly after birth from inability to clear their lungs of fluid (Hummler *et al.* 1996). Mice lacking β- or γ-subunit are able to clear their lung, but die from abnormal renal electrolyte re-absorption instead (Barker *et al.* 1998; McDonald *et al.* 1999). Due to the critical importance of αβγ-ENaC, the canonical subunits have been extensively investigated in relation to their biophysical and pharmacological properties, regulation and (patho)physiology. In contrast, the interest in the fourth homologous subunit, δ, which differs from α-ENaC in its tissue distribution, channel properties and, therefore, most likely in channel regulation and physiological role, has just recently emerged. In the following, an overview of the current knowledge about δ-ENaC is given.

1.2.1 ENaC/DEG superfamily

The homologous ENaC subunits belong to the epithelial sodium channel/degenerin (ENaC/DEG) family of amiloride-sensitive, non-voltage gated ion channels (**Figure 4**; Kellenberger, Schild, 2002). The degenerins in the neuronal cells of the nematode *Caenorhabditis elegans* were the first identified members of this family (Driscoll, Chalfie, 1991). Further members in invertebrates are FLR-1 in *C. elegans* (Take-Uchi *et al.* 1998), Phe-Met-Arg-Phe-NH_2-gated channel (FaNaC) in *Helix aspera* (Lingueglia *et al.* 1995) as well as Pickpocket (PPK/dmdNaC1) and Ripped Pocket (RPK/dGNaC1) in *Drosophila melanogaster* (Adams *et al.* 1998). In mammals, acid-sensing ion channels (ASIC) are expressed *inter alia* in neurons of both the central and peripheral nervous systems (Waldmann *et al.* 1997; Chen *et al.* 1998). Despite their functional heterogeneity and wide tissue distribution across Na^+ absorbing epithelia and neuronal excitable tissues, the ENaC/DEG family members share a common transmembrane topology as well as ~15-20% sequence homology, including some highly conserved domains (Kellenberger, Schild, 2002).

1.2.2 Delta-ENaC isoforms

The first δ-ENaC clone (δ_1-isoform) was isolated from a human kidney cDNA library by Waldmann *et al.* (1995). The 638 amino acid comprising protein shows 37, 27 and 29% amino acid sequence homology to α-, β- and γ-ENaC proteins, respectively, placing δ-ENaC phylogenetically closest to α-subunit. The predicted transmembrane topology with short cytoplasmic amino and carboxy termini, two hydrophobic membrane spanning domains and a large extracellular loop, resembles that of other ENaC subunits and ENaC/DEG family members. The second δ-ENaC isoform (δ_2) was

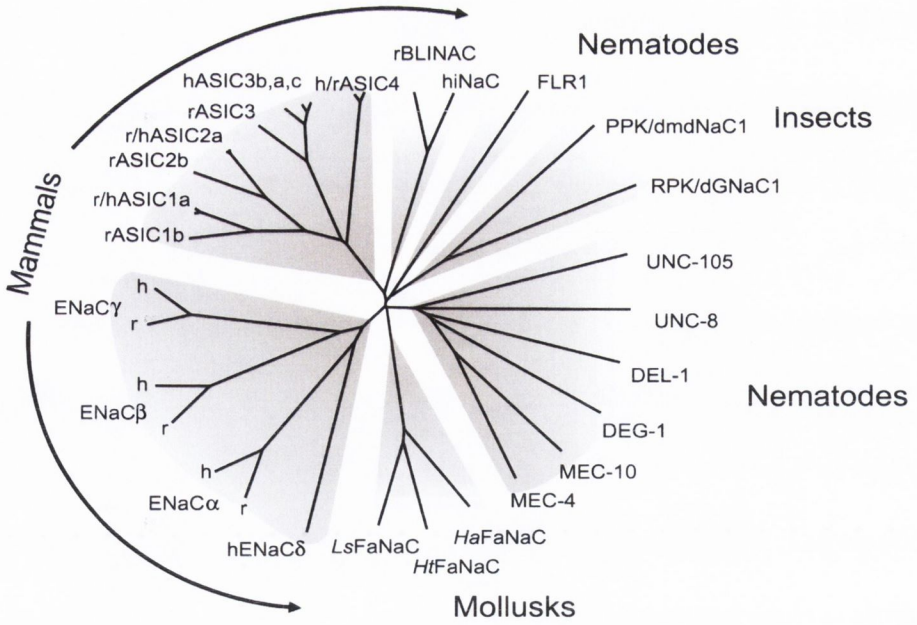

Figure 4. Phylogenetic tree of the ENaC/DEG family of ion channels, including documented genes from nematodes, insects, mollusks and mammals. Organisation into subfamilies is based on the homology of the amino acid sequences. *Adapted from Kellenberger, Schild, 2002*

cloned from human brain (Yamamura *et al.* 2006; Giraldez *et al.* 2007). Zhao *et al.* (2012) reported cloning of δ_2-isoform from the human bronchial epithelial 16HBE14o- cell line. Combination of alternative transcription starting sites, a reading frame shift and alternative splicing result in a sequence encoding a 704 amino acid protein with a longer intracellular N-terminus than the originally described δ_1-isoform. The C-terminus, on the other hand, is conserved between the two isoforms, as are the transmembrane domains and the extracellular loop.

1.2.3 Delta-ENaC in rodents

For a long time, δ-ENaC was believed to be a pseudogene in mice and rats. Thus, experiments in transgenic mice, as conducted previously for α-, β- and γ-ENaC (Hummler *et al.* 1996; Barker *et al.* 1998; McDonald *et al.* 1999), were not regarded as an option for elucidation of the functional role of δ-ENaC. Hernández-González *et al.* (2006) were the first to report murine expression of δ-ENaC subunit at mRNA and protein levels, in spermatogenic cells and mature sperm. A role in the regulation of the capacitation-associated hyperpolarisation in mouse sperm was suggested for both α- and δ-ENaC. Moreover, mRNA transcripts encoding for two δ-ENaC splicing variants were detected by means of RT-PCR in mouse pleural tissue, in co-expression with α-, β- and γ-subunits (Nie *et al.* 2009a). The same research group demonstrated presence of the longer splicing variant (by RT-PCR) in mouse lung tissue (Nie *et al.* 2009b). However, these are the only studies highlighting δ-ENaC expression in mice up to date. Considering the fact that no full-length cloning of δ-ENaC from a rodent species has been reported so far, the presence of a functional δ-ENaC gene in rodents remains controversial (Giraldez *et al.* 2012).

1.2.4 Expression sites of δ-ENaC, co-expression with canonical ENaC and putative roles

Delta-ENaC is distributed throughout various epithelial and non-epithelial tissues (**Table 1**). However, Northern blot analysis showed the highest transcriptional expression levels of δ-ENaC in non-epithelial tissues, in particular, in brain and pancreas. This fact is probably the most obvious difference to αβγ-ENaC, suggesting that the function and regulation of δ-ENaC may be different from those of classic ENaC subunits and may primarily lie outside epithelia. High mRNA expression levels were

also found in testis and ovary. Low expression levels were observed in heart, lung, kidney, colon and other tissues, and absence for spleen and small intestine (**Figure 5**; Waldmann *et al.* 1995).

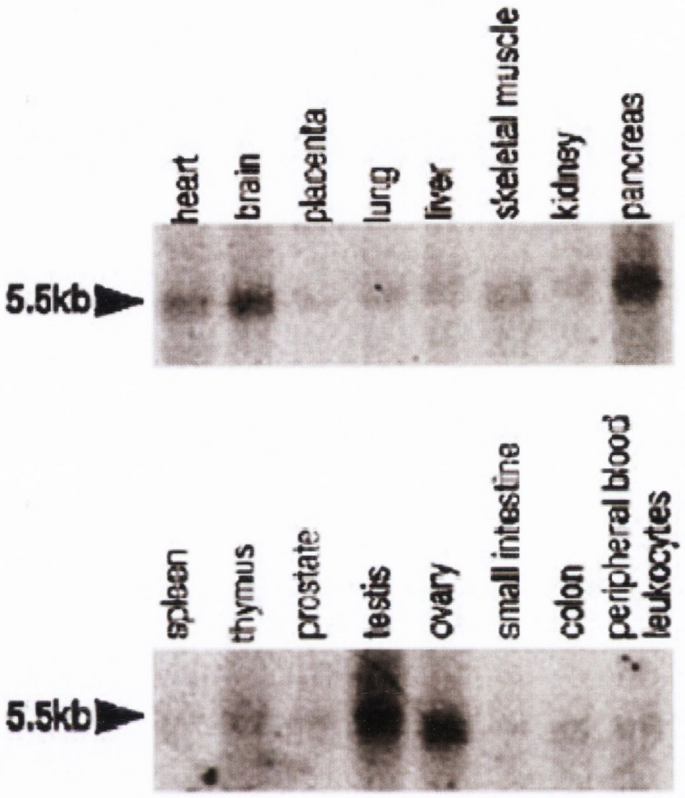

Figure 5. Northern blot showing transcriptional tissue distribution of δ-ENaC. *Adapted from Waldmann et al. 1995*

1.2.4.1 Neuronal δ-ENaC expression sites

Yamamura and colleagues (2004a) investigated expression of δ-ENaC in human brain in more detail and confirmed the presence of δ-ENaC mRNA transcripts in various brain regions such as cerebellum, cerebral cortex, hippocampus and caudate nucleus. *In situ* hybridisation revealed that both δ_1- and δ_2-isoforms were differentially expressed in pyramidal neurons of the cerebral cortex and in different neuronal populations of the subcortical telencephalic centres in human and monkey. Based on the low co-

localisation level between the isoforms (~60% of pyramidal cells expressing δ_1-isoform, ~30% expressing δ_2, merely 10% co-expressing δ1 and δ2), distinct functional roles for the splicing variants and strict regulation of their expression seem likely (Giraldez *et al.* 2007; Wesch *et al.* 2012). Whilst no expression was detected in glial cells in human and monkey brain (Giraldez *et al.* 2007), cultured glioblastoma cells do express δ-ENaC (Berdiev *et al.* 2003), suggesting that δ-subunit may play a role in certain pathological conditions. Considering the fact that δ-ENaC is activated by protons, a role as a transducer of pH stimuli in human brain was postulated (Yamamura *et al.* 2004a; Ji *et al.* 2004). Wesch *et al.* suggested that δ-ENaC, as a voltage-independent, constitutively active Na^+ channel, may be involved in control of membrane resting potential and cell excitability in the CNS.

While, in non-neuronal tissues, δ-ENaC is often co-expressed with α-, β- and γ-subunits (Waldmann *et al.* 1995; Ji *et al.* 2006), there are conflicting reports on expression of αβγ-ENaC in nervous system. Some groups described expression of α- and β-ENaC mRNA in different brain areas (Dyka *et al.* 2005; Amin *et al.* 2005), whilst others failed to detect expression of either of the canonical ENaC subunits (Giraldez *et al.* 2007), pointing towards other ENaC/DEG members as potential interaction partners for both δ-isoforms, e.g., ASIC channels which are known to be expressed in pyramidal neurons of cerebral cortex (Alvarez de la Rosa *et al.* 2003).

1.2.4.2 Non-neuronal δ-ENaC expression sites

Outside neuronal tissues, δ-ENaC mRNA transcripts were detected in pancreas, skeletal muscle and kidney (Giraldez *et al.* 2007), epithelial cell lines of human lung, pancreas and colon origin (A549, H441, CFPAC and Caco-2) (Ji *et al.* 2006), primary human alveolar epithelial type II cells and human lung tissue (Nie *et al.* 2009b) as well as in

human and mouse mesothelial cells (Nie *et al.* 2009a). Yamamura and colleagues (2008b, 2008c) described δ-ENaC mRNA in human oesophageal epithelium as well as in human epidermis and cultured PHK16-0b keratinocytes (here as well at protein level). Transcripts for ENaC α-, β- and γ-subunits were also detected in these tissues confirming previous reports (Awayda *et al.* 2004; Brouard *et al.* 1999). Acidosis-evoked ATP-release in cultured keratinocytes was found to be amiloride-sensitive. Moreover, human oesophageal ENaC complexes (i.e., δβγα-ENaC) generated amiloride-sensitive pH-inducible currents, when expressed in *Xenopus* oocytes. This led Yamamura *et al.* to the conclusion that δ-ENaC was a candidate molecule for pH sensing in the human oesophagus and skin and, therefore, part of a defence mechanism against acidic stress. The same group later reported expression of δ-ENaC in human melanoma G-361 cells (Yamamura *et al.* 2008a).

Brockway *et al.* (2002) demonstrated expression of δ-ENaC mRNA in rabbit retina. Messenger RNA transcripts encoding α-, β- and γ-ENaC subunits as well as ASIC1, 2, 3 and 4 were also shown to be present. In human ocular tissues, δ-ENaC was also found at mRNA level, co-expressed with the classic ENaC subunits, with the highest expression levels detected in cornea, ciliary body, iris and retina (Krueger *et al.* 2012). Moreover, δ-ENaC was reported in taste bud cells of human lingual fungiform papillae at mRNA and protein levels (Huque *et al.* 2009). Interestingly, immunohistochemical staining for δ-ENaC was observed on both apical and basolateral membranes of taste bud cells.

1.2.4.3 Respiratory epithelial expression sites of δ-ENaC

Ji *et al.* (2006) demonstrated δ-ENaC co-expression with α-, β- and γ-ENaC subunits in human epithelial cells *in vitro, inter alia* at mRNA level in alveolar A549 and bronchiolar H441 cell lines. Furthermore, δ-ENaC mRNA transcripts were detected in the human bronchial epithelial 16HBE14o- cell line (Zhao *et al.* 2012), primary epithelial ATII cells and in human, rabbit and mouse lung tissue (Nie *et al.* 2009b). Interestingly, two bands were observed as RT-PCR products and identified as fragments of two δ-ENaC isoforms in human alveolar epithelial A549 and ATII cells as well as in human lung tissue, whereas in rabbit and mouse lung tissue only one band, corresponding to the longer splicing variant (i.e., the δ_2-isoform) was observed. Similarly, only the longer PCR product was detected in H441 cells, suggesting that only one splicing variant of δ-ENaC is expressed in this cell type (Ji *et al.* 2006; Nie *et al.* 2009b). In contrast, Wesch and colleagues (2010, 2012) isolated both δ_1- and δ_2-isoforms from the H441 cell RNA generating the respective plasmids, so that it remains controversial whether one or both splicing variants are present in H441 cells.

At protein level, no antibodies distinguishing between the two δ-isoforms are available to date. Delta-ENaC protein was detected in A549 and H441 cell lines as well as in human lung tissue by Western blot and immunofluorescence microscopy (Ji *et al.* 2006; Nie *et al.* 2009b). Additionally, co-immunoprecipitaton revealed physical interactions between α- and δ- as well as between γ- and δ-ENaC in H441 cells, suggesting that δ-ENaC can form multimeric channels with classic ENaC subunits (Ji *et al.* 2006).

The epithelial sodium channels play an important role in lung fluid homoeostasis, as mentioned above. Several distinct amiloride-sensitive conductances have been detected in alveolar epithelial cells and can be divided into four categories with differences in

unitary conductance, open state probability, cationic selectivity and amiloride sensitivity: highly selective cation channels (HSC), which have a large selectivity for Na^+ over K^+ (4-5 pS), two types of poorly selective cation channels with different unit conductances (8-9 pS and 56 pS), and non-selective cation channels (NSC) with no selectivity for Na^+ over K^+ (19-24 pS). While HSC display almost identical properties to those of αβγ-composed ENaC channels expressed in *Xenopus* oocytes, homomeric α-ENaC channels have been suggested to represent NSC, and combinations of α-subunit with either β- or γ-ENaC the poorly selective channel conductances (reviewed by Matalon *et al.* 2002). However, the molecular basis of poorly and non-selective channels remains debatable. Given the fact that α-, β-, γ- and δ-ENaC are co-expressed in alveolar epithelial cells and, furthermore, biophysical and pharmacological characteristics (ion selectivity, single channel sodium conductance, affinity to amiloride, gating kinetics, etc.) of δαβγ-channels differed from those of αβγ- and δβγ-ENaC in *Xaenopus laevis* oocytes (Ji *et al.* 2006), it is conceivable that δ-ENaC may form different combinations of heteromeric channels with classic ENaC subunits and thus, contribute to the variety of amiloride-sensitive currents across the native (alveolar) epithelia. Presently, however, the contribution of δ-ENaC to the ion transport across epithelial barriers is purely a hypothesis that needs to be confirmed.

Expression and function of δ-ENaC was also characterised in another part of respiratory epithelium. Bangel-Ruland *et al.* (2009) demonstrated that at least the δ_1-isoform was present in primary human nasal epithelial cells (HNE) at both mRNA and protein levels, most likely in co-expression with α-, β- and γ-subunits, since their abundance had been described in this tissue previously (Bangel *et al.* 2008). Transepithelial measurements in modified Ussing chambers revealed that approximately 50% of the amiloride-sensitive sodium current in HNE cells were sensitive to the reported δ-ENaC inhibitor, Evans

blue. Furthermore, δ-ENaC knock-down with siRNA reduced δ-ENaC mRNA and protein abundance and abolished the Evans blue-sensitive component of the short-circuit current, suggesting that δ-ENaC was functionally expressed in human nasal epithelium and made a contribution, equal to that of α-ENaC, to the amiloride-sensitive current in this tissue. To date, this study remains the only published attempt to functionally characterise δ-ENaC in organotypic cells using the reported δ-ENaC inhibitor Evans blue, previously characterised in *X. laevis* oocytes (Yamamura *et al.* 2005b).

Table 1. Overview of the δ-ENaC expression sites, which have been reported to date. Abbreviations: *NB:* Northern blot; *RT-PCR:* reverse transcriptase-PCR; *qPCR:* quantitative real-time PCR; *ISH: in situ* hybridisation; *WB:* Western blot; *IFM*: immunofluorescence microscopy; *ICH:* immunohistochemistry; *ATI:* alveolar epithelial type I cells; *ATII:* alveolar epithelial type II cells

Tissue/Cell type	Species	Co-expressed ENaC subunits	Expression level	Detection method	Reference
Highest levels: testis, ovary, pancreas, brain, heart Moderate to low levels: lung, liver, skeletal muscle, kidney, thymus, prostate, colon, leukocytes, placenta	Human		mRNA	NB	Waldmann, 1995
Wide tissue distribution: Various brain areas, spinal cord, heart, oesophagus, stomach, colon, kidney, skeletal muscle, bone marrow, trachea, lung, placenta, ovary, liver, pancreas, etc.	Human		mRNA	RNA dot-blot analysis	Yamamura, 2004a
Muscle, brain, pancreas Pyramidal cells of cerebral cortex, different neuronal populations of subcortical telencephalic centres	Human Human, monkey		mRNA mRNA	RT-PCR ISH	Giraldez 2007, Wesch, 2010, 2012
Normal temporal lobe tissue, glioblastoma tissue, glioma-derived cell lines	Human	Sample and cell line-dependent	mRNA	RT-PCR	Berdiev, 2003

Tissue/Cell type	Species	Co-expressed ENaC subunits	Expression level	Detection method	Reference
Leptomeninges	Sheep	β-ENaC	Protein	IHC	Filippidis, 2012
Retina	Rabbit	αβγ-ENaC	mRNA	RT-PCR	Brockway, 2002
Wide range of ocular tissues: cornea, ciliary body, iris and retina	Human	αβγ-ENaC	mRNA	qPCR	Krueger, 2012
Epithelial cell lines: respiratory A549 and H441, pancreatic CFPAC, intestinal Caco-2	Human	αβγ-ENaC	mRNA	RT-PCR	Ji, 2006
H441 cells	Human	αβγ-ENaC	Protein	IFM, WB	
Human ATII cells; human, rabbit and mouse lung tissue	Human, rabbit, mouse		mRNA	RT-PCR	Nie, 2009b
ATII cells, human lung tissue	Human		Protein	IFM, WB	
Respiratory epithelial A549 and 16HBE14o- cell lines, lung tissue	Human	α-ENaC	mRNA	qPCR	Zhao, 2012
ATI and ATII cells	Human		mRNA	ISH	
Nasal epithelial cells in primary culture	Human		mRNA Protein	RT-PCR WB, IFM	Bangel-Ruland, 2009

Tissue/Cell type	Species	Co-expressed ENaC subunits	Expression level	Detection method	Reference
Melanoma G-361 cell line	Human	αβγ-ENaC	mRNA Protein	RT-PCR, ISH IHC	Yamamura, 2008a
Skin, cultured keratinocytes (PHK16-0b)	Human	αβγ-ENaC	mRNA Protein	RT-PCR, ISH WB, IFM	Yamamura, 2008b
Oesophagus	Human	αβγ-ENaC	mRNA	RT-PCR, ISH	Yamamura, 2008c
Taste bud cells	Human		mRNA Protein	RT-PCR IHC	Huque, 2009
Spermatogenic cells and mature sperm	Mouse	α-ENaC	mRNA Protein	RT-PCR WB, IFM	Hernández-González, 2006
Pleural mesothelial cells in primary culture, mesothelioma M9K cell line Pleural tissue	Human Mouse	αβγ-ENaC αβγ-ENaC αβγ-ENaC	mRNA Protein mRNA	RT-PCR WB, IFM RT-PCR	Nie, 2009a

1.2.5 Stoichiometry of δ-ENaC containing channels

So far there have been no studies directly investigating the stoichiometry of δ-containing channels. For the classic ENaC, a tetramer (2α/1β/1γ) or, alternatively, the formation of a complex of nine subunits (3α/3β/3γ) has been suggested (Firsov *et al.* 1998; Snyder *et al.* 1998). However, recent reports of the crystal structure of ASIC1a

(Jasti *et al.* 2007) indicate ENaC to be a trimer (1α/1β/1γ) (Stockland *et al.* 2008). Since the conducting subunits may replace each other in the formation of a functional channel, similar stoichiometries are conceivable for δ-ENaC. Nevertheless, it is important to consider that it is the combination of the pore-forming and the accessory subunit/subunits that is determinant factor for the biophysical properties of the resulting channel, less so the exact channel stoichiometry.

1.2.6 Biophysical characteristics of δ-ENaC composed channels

Most electrophysiological studies conducted so far have investigated δ-ENaC heterologously expressed in *Xenopus laevis* oocytes. In these studies, δ-ENaC generated small amiloride-sensitive Na^+ currents, when expressed on its own. Co-expression with accessory β- and γ-subunits increased the magnitude of δ-ENaC induced currents by around 50-fold, without changing its properties, which is similar to previous observations with α-ENaC (Waldmann *et al.* 1995). However, whilst the presence of γ-subunit is sufficient to amplify the amplitude of α-ENaC-mediated current 5-18-fold (Lingueglia *et al.* 1994; Canessa *et al.* 1994), presence of both accessory subunits is required to induce a significant increase in δ-ENaC-mediated currents. In addition, the pharmacological and biophysical properties of δ-ENaC induced currents are clearly distinct, not only from those of α-ENaC generated currents, but also from those of any other known amiloride-sensitive currents (Waldmann *et al.* 1995).

The first major difference is the affinity to the ENaC blocking, potassium-sparing diuretic, amiloride and its analogue benzamil, with sensitivities of δ-channels being around 30-times lower than those of α-channels ($K_{0.5\ (amiloride)}$ = 2.6 μM and 0.08 μM, $K_{0.5\ (benzamil)}$ = 270 and 7 nM for δ- and α-ENaC, respectively). The next difference is the ion selectivity. Whilst both αβγ- and δβγ-channels are virtually impermeable for K^+ and

show comparable permeability for Li^+ ($P_{Li+\ (\delta\text{-ENaC})}$ = 6.8 pS, $P_{Li+\ (\alpha\text{-ENaC})}$ = 7.3 pS), δ-ENaC comprising channels are more permeable for Na^+ than α-channels ($P_{Na+\ (\delta\text{-ENaC})}$ = 11.6 pS, $P_{Na+\ (\alpha\text{-ENaC})}$ = 4.5 pS). This results in δ-ENaC being more selective for Na^+ *versus* Li^+ and α-ENaC more selective for Li^+ *versus* Na^+ (P_{Li+}/P_{Na+} = 0.6 and 1.6 for δ- and α-ENaC, respectively) (Waldmann *et al.* 1995). Furthermore, the base-line open probability of δβγ-ENaC (P_o = 0.5) is significantly higher than that of αβγ-ENaC (P_o = 0.14) (Haerteis *et al.* 2009; Wesch *et al.* 2012). **Table 2** summarises the functional differences between αβγ- and δβγ-channels.

According to Haerteis *et al.* (2009), whole-cell currents generated by δβγ-ENaC (δ_1-isoform) are significantly larger than those of αβγ-ENaC, when heterologously expressed in *X. laevis* oocytes. The authors explained this difference by a higher channel open probability and, thus, a higher overall channel activity of δβγ-ENaC at base-line level. This suggests that the differential expression of either α- or δ-subunit may provide an alternative way of regulating ENaC activity according to the needs of different tissues. In contrast, Giraldez and colleagues (2007, 2012) reported αβγ-ENaC to generate higher whole-cell currents than δβγ-channels due to the less efficient insertion of δ-ENaC containing channels into the plasma membrane.

Table 2. Functional differences between αβγ- and δβγ-composed ENaC channels, expressed in heterologous expression systems. All data from Waldmann *et al.* 1995 except for [a] Haerteis *et al.* 2009.

Channel	Conductance (P_{Li+}; pS)	Conductance (P_{Na+}; pS)	Ion selectivity (P_{Li+}/P_{Na+})	P_o (uncleaved) / P_o (cleaved)	Amiloride (IC_{50}; µM)	Benzamil (IC_{50}; µM)
αβγ	7.3	4.8	2	0.14 / 0.9 [a]	0.1	0.01
δβγ	6.8	11.6	0.6	0.5 / 0.9 [a]	2.6	0.27

The different biophysical properties of δ_1- and δ_2-isoforms also remain controversial. The transmembrane domains as well as the extracellular loop, which are the structural elements responsible for most biophysical and pharmacological characteristics of ENaC, are conserved between the splicing variants. Indeed, similar single channel properties, in particular, single channel current magnitude, open probability, mean open and closed times as well as affinity to amiloride and activation by protons, were observed for both isoforms (Yamamura *et al.* 2006; Wesch *et al.* 2012). Whilst, according to Yamamura and colleagues, macroscopic currents of comparable magnitude were generated by δ_1- and δ_2-channels expressed in *X. laevis* oocytes, Wesch *et al.* (2012) observed approximately 2.5-fold higher whole-cell currents in case of the δ_1-isoform, regardless of the chosen heterologous expression system and the co-expression with accessory β- and γ-ENaC subunits. Further investigation showed that the insertion rates of newly synthesised or recycled channels into the plasma membrane were lower for δ_2-isoform, leading to lower channel abundance in the plasma membrane and, thus, smaller whole-cell currents. Two amino acid sequences in the N-terminus of the δ_2-protein ($\delta_2\Delta$25-45 and Δ66-86) were identified as motifs responsible for the differences in channel trafficking to the membrane. The endocytosis rates, on the other hand, were similar for both isoforms. In contrast to these findings, Zhao and colleagues (2012) reported diverse whole-cell and single channel characteristics for $\delta_2\beta\gamma$- and $\delta_1\beta\gamma$-ENaC in *X. laevis* oocytes. Significantly increased whole-cell currents were measured in $\delta_2\beta\gamma$-expressing oocytes, most likely resulting from larger single channel currents and higher open probability of $\delta_2\beta\gamma$-ENaC. Furthermore, significant differences in affinity to amiloride, EC_{50} for capsazepine as well as in gating kinetics of proton activation were

detected between $\delta_2\beta\gamma$- and $\delta_1\beta\gamma$-channels by this research group. The reasons for these discrepancies are unknown.

1.2.7 Pharmacological profile of δ-ENaC

The pharmacological profile of the δ-subunit has been barely characterised. Amiloride, as *bona fide* inhibitor of the ENaC/DEG family, blocks both α- and δ-ENaC-mediated currents and, therefore, only allows distinguishing between the channel complexes on the basis of its ~30-fold higher affinity to α-subunit. More selective modulators of δ-ENaC function have been identified only recently. Yamamura *et al.* characterised Evans blue as a specific inhibitor (2005b) and both capsazepine (2004b) and icilin (2005a) as activators of the human δ-ENaC in heterologous *X. laevis* oocytes expression system. The chemical structures of the compounds are shown in **Figure 6**.

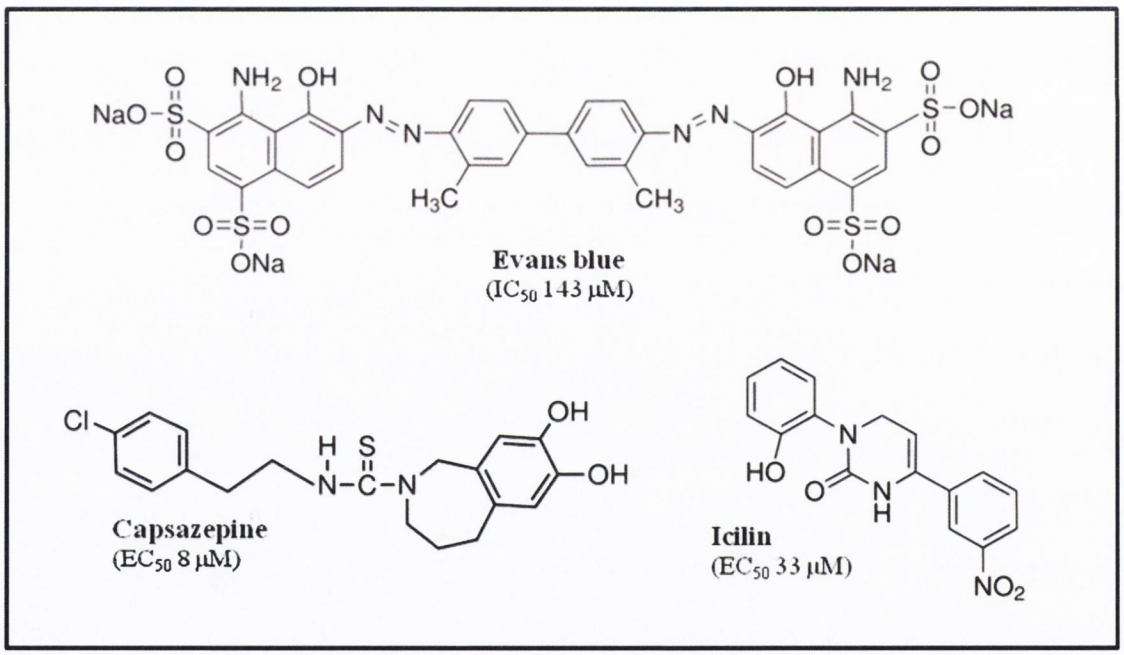

Figure 6. Chemical structures and respective IC_{50} and EC_{50} values of δ-ENaC inhibitor Evans blue as well as of activators capsazepine and icilin, respectively. All compounds have been characterised as δ-ENaC modulators in *X. laevis* expression system (Yamamura *et al.* 2005b, 2004b, 2005a).

1.2.7.1 Inhibitor of δ-ENaC function: Evans blue

Evans blue is an azo dye commonly used as a diagnostic tool for the determination of blood volume and vascular permeability, due to its strong affinity to albumin (Patterson *et al.* 1992). Furthermore, the compound has been reported to inhibit P_2X-purinergic receptors (Bultmann and Starke, 1993), the glutamate transporter (Roseth *et al.* 1995) and to activate large-conductance, Ca^{2+}-activated K^+ channels (Hollywood *et al.* 1998). Unlike amiloride, which inhibits both αβγ- and δβγ-channel complexes, Evans blue inhibited the inward Na^+ currents only in human δβγ-ENaC expressing oocytes. This happened in a concentration-dependent manner with an IC_{50} value of 143 μM. Whilst currents mediated by δ-ENaC homomers could also be inhibited, Evans blue failed to produce an inhibitory effect on α-ENaC and, surprisingly, slightly increased the amiloride-sensitive currents in αβγ-ENaC-expressing oocytes (Yamamura *et al.* 2005b).

1.2.7.2 Activators of δ-ENaC function: capsazepine and icilin

Capsazepine is a competitive antagonist of the transient receptor potential vanilloid subfamily 1 (TRPV1) (Bevan *et al.* 1992) that also inhibits voltage-dependent Ca^{2+} and K^+ channels (Docherty *et al.* 1997; Kuenzi *et al.* 1996), nicotinic acetylcholine receptors (Liu, Simon 1997) and acts as a competitive antagonist for the transient receptor potential melastatin subfamily 8 (TRPM8) (Behrendt *et al.* 2004). Icilin, which is structurally unrelated to capsazepine, activates TRPM8 and ankyrin-like subfamily 1 (Andersson *et al.* 2004; Story *et al.* 2003). Both compounds activated the inward Na^+ currents in δβγ-ENaC-expressing oocytes in a concentration-dependent manner with EC_{50} values of 8 μM and 33 μM for capsazepine and icilin, respectively. The increases in δ-ENaC currents were also significant. All capsazepine and icilin-evoked currents were sensitive to 100 μM amiloride. Once again, no effect was shown on α-ENaC-

mediated currents. The inward currents in αβγ-ENaC-expressing oocytes were slightly decreased by both compounds. These finding were in accordance with data obtained with Evans blue in the *X. laevis* oocytes expression system (Yamamura *et al.* 2004b, 2005a).

As these compounds selectively influence δ-ENaC-mediated currents without having an effect on α-ENaC - at least in heterologous expression systems - their identification has promise for functional characterisation of δ-ENaC and determination of its physiological role in organotypic models. Thus far, however, only one publication uses these compounds as modulators of δ-ENaC function in this context (Bangel-Ruland *et al.* 2009).

1.2.8 Activation of δ-ENaC by protons and its potential role in acid sensing

A number of conflicting studies report on how ENaC activity is affected by protons. Whilst, rat αβγ-ENaC-mediated currents were blocked by intracellular but not affected by extracellular acidification (Chalfant *et al.* 1999), currents generated by human αβγ-ENaC were decreased by a decrease in extracellular pH (Ji, Benos, 2004). According to other reports, however, extracellular protons activated human αβγ-ENaC-mediated currents (Collier, Snyder, 2009). On the other hand, activation of δ- and δβγ-ENaC-mediated currents by extracellular acidification, with a half-maximal pH for activation in the range of pH 5.0 to 6.0, has been consistently reported by several labs (Yamamura *et al.* 2004a; Ji, Benos, 2004; Wesch *et al.* 2012). In contrast, intracellular acidification decreased both basal and proton-evoked δ-ENaC currents. Acidic metabolites (i.e., lactate, pyruvate and formate) potentiated proton-evoked currents, as did a decrease in extracellular osmolarity. Combination of hypotonic and lactate stimuli enhanced proton-activation of δβγ-ENaC. As possible mechanism for current activation, an increase in

channel open probability and recruitment of silent channel populations at the plasma membrane were suggested (Ji, Benos, 2004).

Activation by drop in extracellular pH, together with the predominant expression of δ-ENaC in heart and brain, suggests δ-ENaC to play a role as pH sensor and mediator of ischemic signals in these (and possibly other) tissues. Interestingly, ASIC, another channel involved in pH sensing in neuronal tissues, is characterised by millisecond activation and fast (< 1 s) desensitisation in response to acidic stimuli (Waldmann et al. 1999), whereas activation and desensitisation of δ-ENaC is much slower (Ji, Benos, 2006). Since the accumulation of acidic metabolites during cardiac and brain ischemia may require several minutes to produce a significant decrease in extracellular pH, the efficiency of ASIC as pH sensor may be compromised. Thus, it is conceivable that δ-ENaC could act as a pH/ischemic sensor, complementary to ASIC, by itself or as a part of a proton receptor complex.

1.2.9 Activation of δ-ENaC by shear stress and its potential role as a mechanosensor molecule

Abi-Antoun *et al.* (2011) demonstrated that δβγ-ENaC, similar to αβγ-ENaC, was activated in respond to laminar shear stress, a feature especially important in the distal nephron where Na^+ absorption and K^+ secretion are modulated by the tubular flow rate (Satlin *et al.* 2001; Malnic *et al.* 1989). Although both time course and magnitude of activation were remarkably different from those of αβγ-channels, this report indicated that δ-ENaC may be involved in mechanotransduction at the renal epithelium and other tissues such as, for instance, muscle spindles, as suggested by Simon *et al.* (2010).

1.2.10 Regulation of δ-ENaC abundance and activity in the plasma membrane

Sodium re-absorption mediated by classic αβγ-ENaC is regulated by the combination of two mechanisms: firstly, by alternation of ENaC surface expression by controlled insertion of the channel into the apical membrane and by its internalisation and, secondly, by change of channel gating kinetics and resulting increase in open probability (P_o) of ENaC (reviewed by Butterworth, 2010). Not much is known about the endogenous regulation of δ-ENaC. Parallels to the regulation of the classic αβγ-ENaC are not necessarily given, however, possible.

1.2.10.1 Trafficking to the plasma membrane and activation by proteolytic cleavage

Trafficking of δ-ENaC protein to the cell surface was shown to be independent from co-expression with accessory subunits. However, it differs between δ_1 and δ_2-isoforms, with the δ_2-isoform showing lower membrane insertion rates than δ_1, probably caused by the differential N-termini of the isoforms (Wesch *et al.* 2012).

In the case of classic αβγ-ENaC, electrically silent as well as constitutively active channel populations are present at the cell surface. Channels composed of uncleaved subunits have low channel open probabilities ($P_o \sim 0.1$) and constitute the electrically silent ENaC population. For the channel complex to reach its constitutively active state with high open probability ($P_o \sim 0.9$), both α- and γ-ENaC subunits need to be cleaved, to release 26- and 43-residue inhibitory peptides, respectively. Most likely, proteolytic cleavage leads to an increase in P_o and, therefore, current stimulation via a conformational change of the channel. Whilst several cleavage sites have been described in the extracellular loops of α- and γ-subunits, no cleavage site has yet been reported for β-ENaC (reviewed by Kleyman *et al.* 2009). Haerteis and colleagues (2009) were the first to report that δ-ENaC also undergoes proteolytic cleavage.

Exposure to chymotrypsin resulted in the elevation of whole-cell currents and appearance of δ-ENaC cleavage products at the plasma membrane of δβγ-injected oocytes (N-terminal 20 kDa and C-terminal 65 kDa δ-fragments, schematically presented in **Figure 7**). However, current stimulation by treatment with chymotrypsin was smaller for δβγ- than for αβγ-ENaC, due to higher base-line activity of δβγ-ENaC with channel open probability of ~ 0.5, as opposed to base-line P_o of 0.1 for αβγ-ENaC. Thus, substitution of α- by δ-subunit in the heteromeric channel complex was suggested as an alternative route of ENaC regulation, improving overall channel activity.

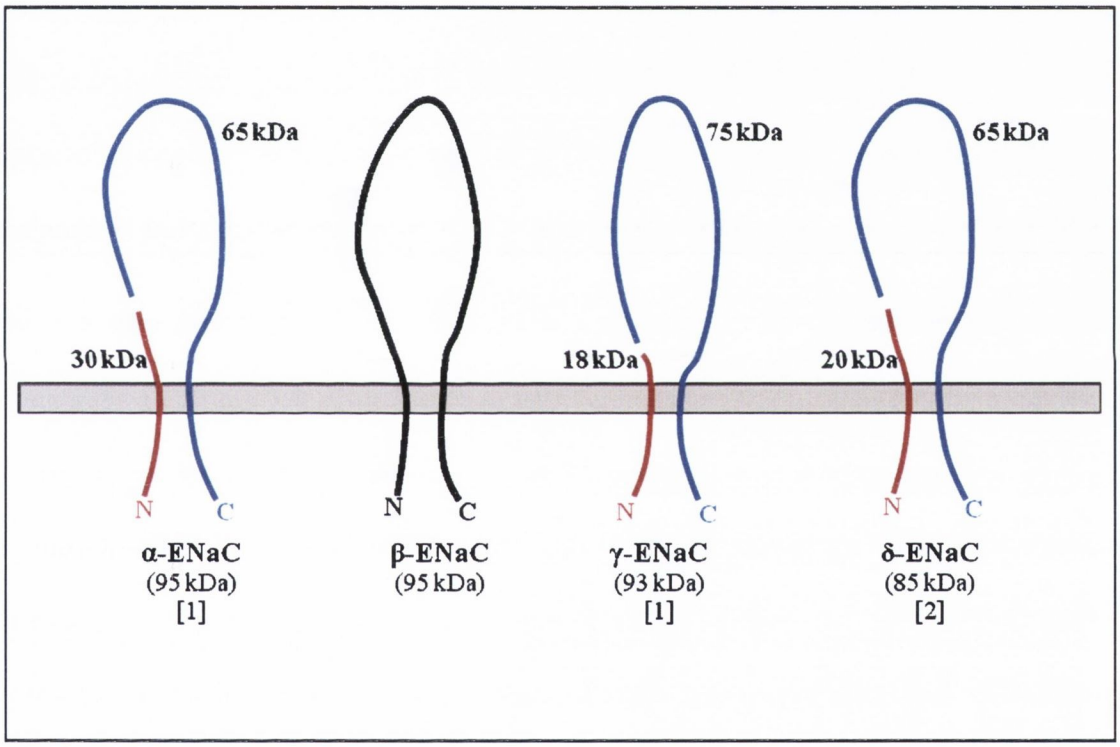

Figure 7. ENaC channels at the cell surface are converted from electrically silent to constitutively active state by proteolytic cleavage of the subunits by extracellular proteases. Cleaved α-, γ- and δ-ENaC are schematically presented as reported by [1] Hughey *et al.* 2003 and [2] Haerteis *et al.* 2009. N-terminal cleaved fragments are labelled in red; C-terminal fragments are blue. Molecular weights of the full-length protein and of the respective cleavage products are indicated. No proteolytic cleavage sites have been reported for β-ENaC.

1.2.10.2 Internalisation and recycling

Ubiquitination of N-terminal lysine residues of ENaC subunits is the signal for internalisation of the αβγ-channel from the cell surface (Zhou *et al.* 2007). Nedd4-2, an E3 ubiquitin ligase, catalyses the ubiquitination by binding to the C-terminal *PPPxY* (PY) region, a motif conserved in α-, β- and γ-ENaC. Ubiquitination and following internalisation of the channel is independent of the cleavage state of ENaC subunits (Kabra *et al.* 2008). The internalisation occurs via clathrin-mediated pathways, with internalised channels being delivered to the early endosomes (Shimkets *et al.* 1997). There, ubiquitin residues may be removed. Deubiquitinated ENaC can then be trafficked directly back to the apical surface or to the recycling endosomes, a storage pool from which ENaC can be released to the cell surface in response to elevation of cAMP (Butterworth *et al.* 2005, 2007). ENaC that remains ubiquitinated is transported to the late endosomes/lysosomes for degradation (Wiemuth *et al.* 2007).

Ubiquitination of ENaC subunits by Nedd4-2 is an essential step for down-regulation of ENaC activity. Agents inactivating Nedd4-2 enhance ENaC stability in the cell membrane and, therefore, increase the net channel activity. The serum and glucocorticoid kinase, SGK1, is one example of such an agent. SGK1 expression is induced by aldosterone. SGK1 phosphorylates Nedd4-2 and prevents its interaction with ENaC, leading to an increase of steady-state surface population of ENaC (Debonneville *et al.* 2001). Thus, the stimulation of αβγ-ENaC-mediated currents by SGK1 depends on the presence of C-terminal PY motif.

Since the C-terminus of δ-ENaC is lacking the *PPPxY* motif (Waldmann *et al.* 1995), which is required for binding to Nedd4-2 and subsequent ubiquitination and internalisation of the ion channel, a regulation pathway independent from Nedd4-2 and

SGK1 would appear likely. However, Wesch *et al.* (2010) demonstrated that homomeric as well as heteromeric δ-channels are regulated by SGK1.1, a SGK1 splice isoform abundantly present in CNS. Co-expression with SGK1.1 increased δ-ENaC-mediated sodium currents in *X. laevis* oocytes expression system by increasing channel abundance in the plasma membrane. This stimulating effect was independent from co-expression of accessory β or γ-ENaC subunits, indicating that SGK1.1 activated δ-ENaC via an alternative mechanism, independent from PY-motifs. Therefore, although no direct evidence for PY-motif independent regulation of δ-ENaC by Nedd4-2 is available to date, this possibility may not be ruled out.

Additionally, ubiquitination of δ-ENaC can also be promoted, despite the absence of the PY-domain. Interaction with COMMD1 protein (copper metabolism Murr1 domain 1) leads to ubiquitination of δ-ENaC, which is associated with an increase in channel internalisation and subsequent trafficking of δ-ENaC to the endosomal recycling and storage pool. Down-regulation of δ-ENaC surface population and activity are the result of binding to COMMD1 (Biasio *et al.* 2004; Chang *et al.* 2011). However, COMMD1 does not regulate δ-ENaC exclusively, as it was also shown to bind to β- and γ-ENaC, albeit not to α-ENaC, and to inhibit αβγ-ENaC-mediated currents by increasing ubiquitination and internalisation of the channel via interaction with SGK1/Akt1-Nedd4-2 pathway (Biasio *et al.* 2004; Ke *et al.* 2010).

Despite the differences in trafficking efficiency to the membrane mentioned above, endocytosis rates are comparable for both δ-ENaC isoforms, albeit, half of what has been reported for αβγ-ENaC. Furthermore, δ-ENaC follows an alternative endocytosis pathway, the exact mechanism of which is yet unknown, as opposed to the dynamin-dependent clathrin-mediated endocytosis typical for αβγ-subunits (Wesch *et al.* 2012).

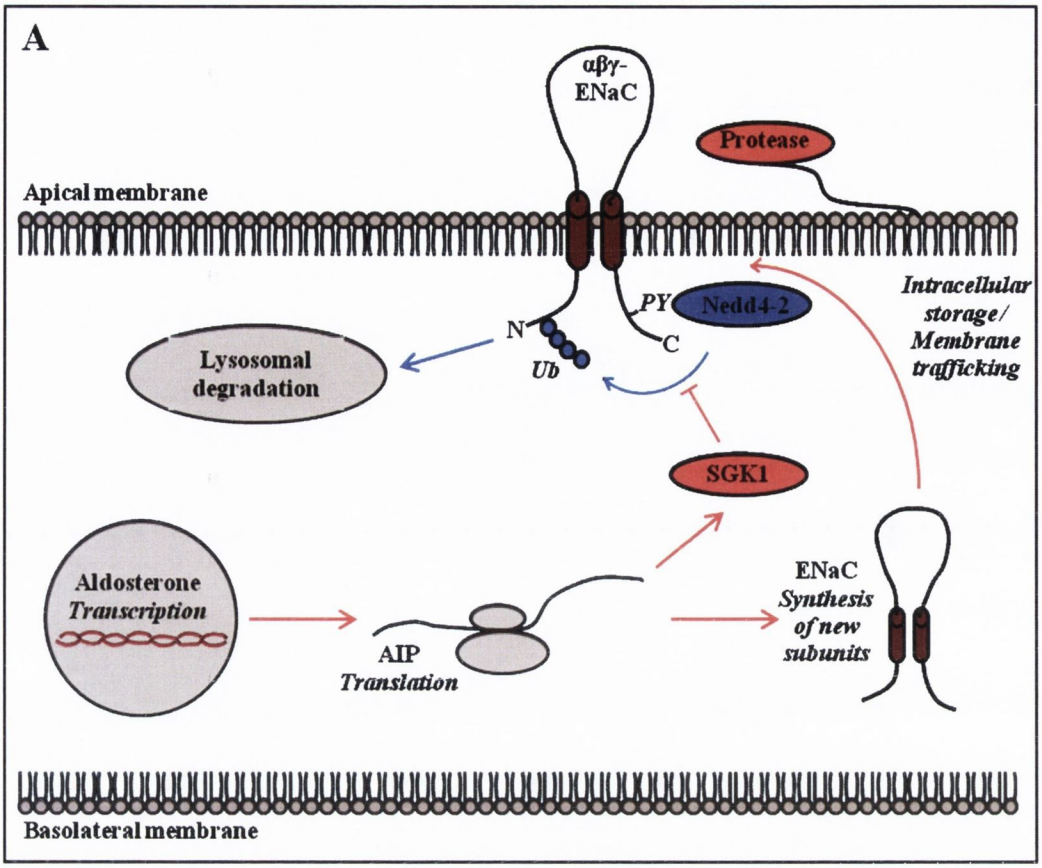
A
αβγ-
ENaC
Protease
Apical membrane
Intracellular
storage/
Membrane
trafficking
PY
Nedd4-2
N
C
Ub
Lysosomal
degradation
SGK1
Aldosterone
Transcription
AIP
Translation
ENaC
Synthesis
of new
subunits
Basolateral membrane

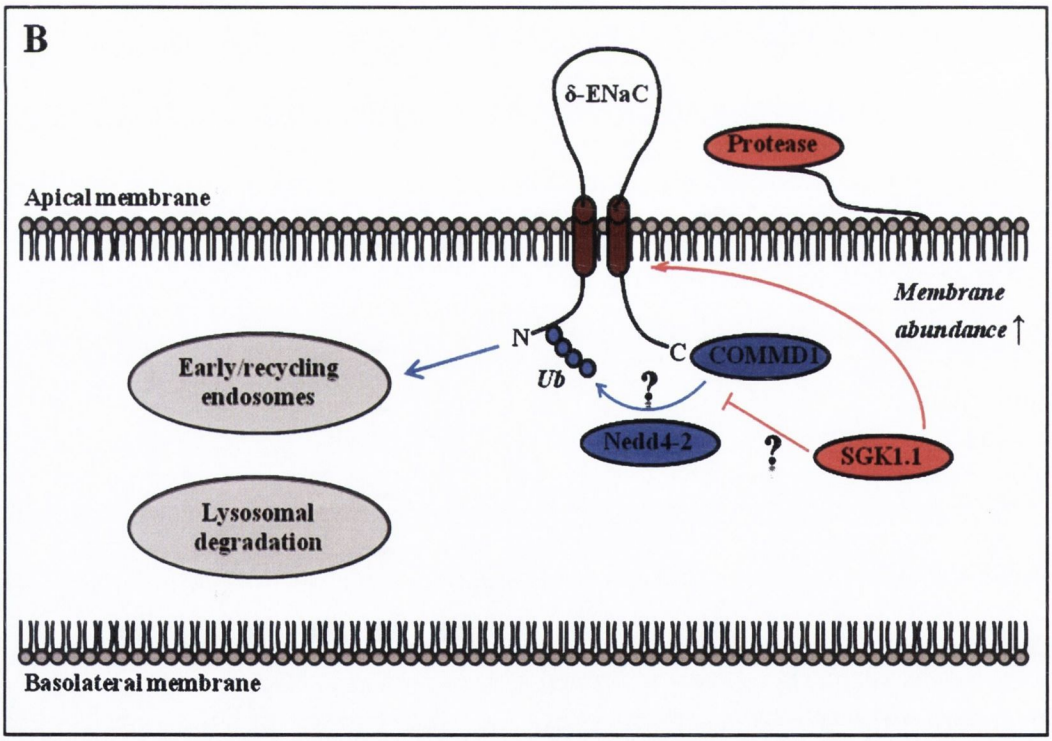
B
δ-ENaC
Protease
Apical membrane
Membrane
abundance ↑
N
C
COMMD1
Ub
?
Early/recycling
endosomes
Nedd4-2
?
SGK1.1
Lysosomal
degradation
Basolateral membrane

Figure 8. Regulation of abundance in the apical membrane and activity of classic αβγ-ENaC **(A)** and of δ-subunit containing channels **(B)**. Extracellular proteases cleave and activate ENaC channels at the cell surface. **(A)** Nedd4-2 binds to the C-terminal PY-motifs of αβγ-subunits, promoting ubiquitination of N-terminal lysine residues and internalisation of ENaC and, therefore, down-regulation of ENaC activity. Aldosterone triggers *de novo* synthesis of aldosterone-induced proteins (AIP), *inter alia* ENaC and SGK1 (serum and glucocorticoid kinase 1). SGK1 phosphorylates and inactivates Nedd4-2, increasing αβγ-ENaC population at the cell surface and thus, ENaC activity. *Modified from Alvarez de la Rosa et al. 2000.* **(B)** Exposure to the extracellular protease chymotrypsin results in appearance of cleaved δ-ENaC fragments in the membrane and stimulation of ENaC activity in δβγ-ENaC expressing *X. laevis* oocytes (Haerteis *et al.* 2009). COMMD1, copper metabolism Murr1 domain 1 protein, interacts with the C-terminus of δ-ENaC, leading to increased ubiquitination and internalisation of δ-subunit and down-regulation of δ-ENaC activity. Hereby, translocation to the early/recycling endosomes is promoted rather than to the lysosomal degradation pathway (Biasio *et al.* 2004, Chang *et al.* 2011). Co-expression with SGK1.1 in *X. laevis* increases δ-ENaC population in the apical membrane, stimulating δ-ENaC mediated whole-cell currents (Wesch *et al.* 2010). The exact molecular mechanism for interaction of δ-ENaC with both COMMD1 and SGK1.1 is unknown. It is, however, independent of the C-terminal PY-motif and may involve interaction with Nedd4-2, albeit direct evidence is presently missing.

1.2.11 Conclusions

The epithelial sodium channel δ-subunit is widely distributed throughout various tissues of the human body. Strikingly, its highest expression levels are found in non-epithelial tissues, such as heart, pancreas and brain. This is in contrast to α-, β- and γ-ENaC subunits that are expressed mainly in Na^+ transporting epithelia of kidney, colon and lung. Biophysical and pharmacological features as well as some regulatory pathways of δ-ENaC comprising channels also differ from classic ENaC. One of the suggested physiological roles of δ-ENaC is the mediation of persistent Na^+ currents in the CNS, which have been detected in several neuronal cell types and are involved in the regulation of neuron excitability (Bean, 2007; Giraldez *et al.* 2012). Furthermore, due to

stimulation of δ-ENaC-mediated currents by extracellular protons and the kinetics of this activation, a role of δ-ENaC as pH sensor in oesophageal epithelium and skin as well as a transducer of ischemic and hypoxic signals in neuronal tissues is conceivable. In epithelia, where δ-ENaC is also expressed, albeit at lower levels, δ-ENaC may combine with α-, β-, γ-subunits and, thus, contribute to the variety of amiloride-sensitive Na^+ conductances, which have been detected in absorptive epithelial, in particular, alveolar epithelial cells. The molecular basis of this contribution, however, remains unclear.

It is noteworthy that most of the evidence in support of the hypothesised physiological roles of δ-ENaC is based on expression studies *in vitro* combined with functional analysis in heterologous expression systems (i.e., *Xenopus laevis* oocytes). To date, the only report of Na^+ transport activity mediated by δ-ENaC in organotypic cells is that of Evans blue-sensitive Na^+ currents in human nasal epithelial cells *in vitro* (Bangel-Ruland *et al.* 2009). In addition to apparent difficulties in finding a good cell model and limited pharmacological tools, the absence of δ-ENaC gene expression in mice and rats hinders the development of experimental animal models. Therefore, the physiological role of δ-ENaC still remains controversial.

1.3 Aims of the study

Keeping in mind the importance of the alveolar fluid clearance, it is crucial to understand the array of the ion channels involved in this process, as these may act as drug targets in the pharmacotherapy of diseases such as lung oedema. Ji *et al.* (2006) demonstrated co-expression of four homologuos ENaC subunits in human bronchiolar epithelial H441 cells as well as the distinct biophysical properties of δαβγ-, αβγ- and δβγ-ENaC channels in *X. laevis* oocytes expression system. Due to these findings, the hypothesis has been postulated that δ-ENaC contributes to the diversity of amiloride-sensitive Na^+ conductances and, thus, to the net Na^+ transport in the human respiratory epithelium. The objective of this work was to confirm this hypothesis and to further improve our understanding of the processes and mechanisms underlying the ion and fluid transport in the lung, however, using organotypic epithelial cells rather than heterologous expression systems as models. The systematic approach was three-fold.

Firstly, the expression of δ-ENaC at transcriptional and protein levels was to be confirmed in both continuously growing respiratory epithelial cell lines (alveolar A549, bronchiolar H441 as well as bronchial Calu-3 and 16HBE14o-) and human alveolar epithelial cells in primary culture.

Secondly, the contribution of δ-ENaC to Na^+ transport across the respiratory epithelium was to be investigated, using presently available pharmacological tools. To this end, effects of the reported modulators of δ-ENaC activity, Evans blue, capsazepine and icilin (Yamamura *et al.* 2004b, 2005a, 2005b), on the ion currents across respiratory epithelial cell monolayers were to be studied, using standard four-electrode voltage-clamp technique in modified Ussing chambers.

Thirdly, knockdown and/or over-expression studies were to confirm the specificity of the effects observed in transepithelial measurements and, thus, the functional expression of δ-ENaC in the cell models tested.

CHAPTER 2

Materials and methods

2.1 Materials

Polyclonal rabbit anti-δ-ENaC antibodies were either commercially available, i.e., purchased from Santa Cruz Biotechnology (SC-21015, Heidelberg, Germany) and Thermo Scientific Pierce (OSR00100W, Medical Supply Company, Dublin, Ireland) or kindly provided by Dr. Diego Alvarez de la Rosa (Universidad de La Laguna, La Laguna, Spain). Polyclonal goat anti-α-ENaC (SC-22239) and anti-γ-ENaC (SC-22245) as well as monoclonal mouse anti-β-ENaC (SC-25354) antibodies were purchased from Santa Cruz Biotechnology. Monoclonal mouse anti-Na^+-K^+-ATPase α-1, clone C464.6 (05-369) antibody and δ-ENaC control peptide (AG981) were obtained from Millipore (Carrigtwohill, Ireland). Monoclonal mouse anti-ZO-1 antibody (610966) was purchased from BD Biosciences (Oxford, UK). Monoclonal mouse anti-β-actin (A1978) and anti-pan-cytokeratin (C2562) antibodies were purchased from Sigma-Aldrich (Dublin, Ireland). Relevant secondary antibodies for Western blot (i.e., goat anti-rabbit IgG-peroxidase antibody and rabbit anti-goat IgG-peroxidase antibody) were obtained from Sigma-Aldrich with the exception of the goat anti-mouse IgG HRP conjugate from Promega (Medical Supply Company, Dublin, Ireland). For immunofluorescence microscopy (IFM) relevant Alexa Fluor-488-labelled $F(ab')_2$ fragments were purchased from Invitrogen (Biosciences, Dun Laoghaire, Ireland). Unless mentioned otherwise, the reagents for polymerase chain reaction were purchased from Bioline (London, UK) and Applied Biosystems (Branchburg, NJ). All cell culture plastics were obtained from Greiner BioOne (Frickenhausen, Germany), with the exception of Lab-Tek chamber slides (Nunc, Roskilde, Denmark) and Corning Transwell Clear permeable filter inserts (VWR, Dublin, Ireland). All cell culture media and reagents were from Sigma-Aldrich, apart from RPMI 1640 medium (Invitrogen) and Small Airway Growth Medium

(SAGM, Lonza, Verviers, Belgium). All other chemicals used were of the highest commercially available grade.

2.2 Cell culture

All cells were cultured in humidified atmosphere at 37°C in 5% CO_2. The medium was changed every other day. Cells cultured on Transwell Clear permeable filter inserts were grown under liquid-covered culture (LCC) conditions. The transepithelial electrical resistance (TEER) of cell monolayers grown on Transwell Clear inserts was measured over time, using a Millicell ERS Volt-Ohm Meter with STX-2 chopstick electrodes (Millipore, Carrigtwohill, Ireland), and corrected for the background value contributed by the Transwell Clear filter and medium. Unless mentioned otherwise, experiments were conducted using cells from at least three different passages.

2.2.1 A549 (American Type Culture Collection, ATCC CCL-185)

The human alveolar epithelial A549 cell line, obtained from the European Collection of Animal Cell Cultures (ECACC, Salisbury, UK), was derived from an alveolar adenocarcinoma (Giard *et al.* 1973) and has been shown to have not only some morphologic but also metabolic (Lieber *et al.* 1976) and transport properties (Foster *et al.* 1998) consistent with those of alveolar epithelial type II cells. Due to this fact, the cell line has often been used as a model to study the function of the alveolar epithelium (Sporty *et al.* 2008). Moreover, presence of mRNA transcripts for α-, β-, and γ-ENaC subunits in A549 cells was shown by RT-PCR (Lazrak *et al.* 2000). Their functional expression was proven by identification of amiloride-sensitive currents in patch-clamp studies (Lazrak *et al.* 2000). Unfortunately, A549 cells lack the ability to form functional tight junctions and, therefore, polarised monolayers, as evaluated by

measurements of transepithelial electrical resistance (TEER) values of filter-grown A549 cells (Foster *et al.* 1998). This renders the cell line unsuitable for Ussing chamber studies. A549 cells were seeded at 40,000 cells/cm^2 and cultured in Dulbecco's modified Eagle's medium:Ham's F-12 (1:1 mix), supplemented with 5% FBS, 100 U/ml penicillin and 100 µM/ml streptomycin. Experiments were carried out after A549 cell layers reached confluence (i.e., on day 5 in culture).

2.2.2 Calu-3 (ATCC HTB-55)

The human bronchial epithelial cell line, Calu-3 (obtained from ECACC, Salisbury, UK) was derived from an adenocarcinoma of the lung (Fogh, Trempe 1975) and has been shown to form polarised cell monolayers consisting of mixed cell phenotypes, *inter alia* ciliated and secretory cells (Shen *et al.* 1994). The ability to form tight junctions and develop high TEER (>1000 Ω·cm^2 under LCC conditions, Grainger *et al.* 2006) makes this cell line a suitable model for drug and ion transport across the bronchial epithelium. For transepithelial Ussing chamber measurements, Calu-3 cells were seeded at a density of 100,000/cm^2 on Transwell Clear permeable filter inserts. In all other cases Calu-3 cells were seeded at 75,000/cm^2 and grown in Eagle's minimum essential medium (EMEM), supplemented with 10% FBS, 100 U/ml penicillin, 100 µM/ml streptomycin, 1 mM sodium pyruvate, 0.1 mM non-essential amino acids and 15 mM glucose. Ussing chamber studies were carried out on days 14-21 in culture, all other experiments on day 12.

2.2.3 16HBE14o-

The generation of 16HBE14o- cell line was accomplished by transformation of normal human bronchial epithelial cells with SV40 large T-antigen (Cozens et *al.* 1994). 16HBE14o- exhibit a non-serous, non-ciliated phenotype and form polarised cell layers

with functional tight junctions when grown under LCC conditions, as opposed to AIC conditions where 16HBE14o- fail to polarise and form cell layers of 10-16 cells in thickness (Ehrhardt *et al.* 2002). The cell line was a gift from Dr. Dieter C. Gruenert (University of California, San Francisco, CA). Cells were seeded at a density of 100,000/cm^2 and grown in EMEM, supplemented with 10% FBS, 100 U/ml penicillin, 100 µM/ml streptomycin, 1 mM sodium pyruvate, 0.1 mM non-essential amino acids and 15 mM glucose for 8 days.

2.2.4 NCI-H441 (ATCC HTB-174)

The human bronchiolar epithelial H441 cell line (purchased from LGC Standards, Teddington, UK) was derived from a pulmonary adenocarcinoma (Brower *et al.* 1986) and exhibits characteristics of both alveolar type II (O'Reilly *et al.* 1988) and bronchiolar Clara epithelial cells (Zhang *et al.* 1997). H441 cells express all four mammalian homologous ENaC subunits (Ji *et al.* 2006) and are a popular model to study amiloride-sensitive currents using both patch-clamp and Ussing chamber techniques (Itani *et al.* 2002; Althaus *et al.* 2011). H441 cells were seeded at a density of 250,000/cm^2 on Transwell Clear permeable filter inserts and at 75,000/cm^2 on tissue culture plastics. Cells were cultured in RPMI 1640 medium, supplemented with 10% FBS, 100 U/ml penicillin, 100 µM/ml streptomycin, 1 mM sodium pyruvate, 5 µg/ml insulin, 5 µg/ml human transferrin, 5 ng/ml sodium selenite and 200 nM dexamethasone. Experiments with H441 cells were carried out on day 8 in culture.

2.2.5 HEK-293 (ATCC CRL-1573)

Human embryonic kidney HEK-293 cells (obtained from the ECACC, Salisbury, UK) were used as an established model for heterogeneous protein expression. Cells were

grown in Dulbecco's modified Eagle's medium (DMEM), supplemented with 10% FBS, 100 U/ml penicillin and 100 µM/ml streptomycin.

2.2.6 Human alveolar epithelial cells (hAEpC)

Human type II alveolar epithelial cells (ATII) were freshly isolated from non-tumour lung tissue obtained from patients undergoing lung resection and kindly provided by Dr. Claus-Michael Lehr's lab (Saarland University, Saarbrücken, Germany). The use of human material was approved by Saarland State Medical Board, Germany. Isolation of ATII was performed as described in detail by Ehrhardt *et al.* (2005). Briefly, the minced tissue was digested using 150 mg trypsin type I (Sigma, Deisenhofen, Germany) and 0.641 mg elastase (CellSystems, St. Katharinen, Germany) in 30 ml HEPES-buffered balanced salt solution containing 137 mM NaCl, 5 mM KCl, 0.7 mM $Na_2HPO_4 \times 7\ H_2O$, 10 mM HEPES, 5.5 mM glucose, pH 7.4 for 40 min at 37°C. Combination of differential cell attachment, Percoll density-gradient centrifugation, and magnetic cell sorting (HEA MicroBeads, Miltenyi Biotec, Bergisch-Gladbach, Germany) was used for purification of the ATII cell population. Purified ATII were seeded at a density of 600,000 cells/cm^2 on collagen/fibronectin-coated plastics using SAGM supplemented with 100 U/ml penicillin, 100 µM/ml streptomycin and 1% FBS. Under the chosen culture conditions, ATII transdifferentiated into monolayers of type I-like phenotype (ATI-like) (Fuchs *et al.* 2003, Demling *et al.* 2005) and were used for experiments on days 8-10 in culture. Cell culture plastics were coated with a solution of 100 µl collagen type I solution (5 mg/ml) and 100 µl fibronectin solution (1 mg/ml) in 10 ml ice-cold SAGM.

2.3 Polymerase chain reaction (PCR)

2.3.1 Primers

Primers were preferably designed within an exon. The sequences of the relevant ENaC subunits were identified with CHIP Bioinformatics Tools (http://snpper.chip.org/). Taking existing transcription variants into account, exons suitable for primer design (sufficient length of 150-250 bp, presence in all transcription variants etc.) were chosen and validated using Primer3 (http://frodo.wi.mit.edu/). Primers designed against these sequences (**Table 1**) were aligned with Nucleotide Blast (http://www.ncbi.nlm.nih.gov/Blast.cgi?PROGRAM=blastn&BLAST_PROGRAMS=megaBlast&PAGE_TYPE=BlastSearch&SHOW_DEFAULTS=on&LINK_LOC=blasthome) in order to confirm their unique presence within the human genome. Optimisation of the primers (Eurofins, Ebersberg, Germany) was carried out using genomic DNA (Bioline) at varying temperatures, with or without DMSO as an additive.

Table 1. Primer sequences for RT-PCR analysis. All primers were derived from GenBank, using the displayed accession numbers. Where more than one transcript variant exists, accession number for variant 1 is displayed. Other variants can be accessed through this record.

ENaC subunit	Gene	GenBank accession number	Primer sequence (5' to 3')	[bp]	Optimised conditions
α	*SCNN1A*	NM_001038	f: CAG CCC ATA CCA GGT CTC AT r: ATG GTG GTG TTG TTG CAG AA	221	58°C 5% DMSO
β	*SCNN1B*	NM_000336	f: TCC TAC CCT CGT CCC TAC CT r: CCA GGA AGG AGA AAA CCA CA	151	58°C 5% DMSO
γ	*SCNN1G*	NM_001039	f: AGA CAG AGC TGA CCC TTC CA r: TGC AGT CCC CTA TGC TAACC	207	58°C 5% DMSO
δ	*SCNN1D*	NM_001130413	f: CCC CTT GAG ACT CTG GAC AC r: CCA GGC AGT GTA GGT GGT TT	202	60°C 5% DMSO
β-actin	*ACTB*	NM_001101	f: AAA CTG GAA CGG TGA AGG TG r: TTT TCG GTG GGG TGA AGA GA	171	all conditions

2.3.2 RNA isolation

Messenger RNA was isolated from cell layers using an RNeasy Mini kit (Qiagen, Crawley, UK) according to manufacturer's instructions (protocol for purification of total RNA from animal cells using spin technology). To eliminate potential genomic DNA contamination of the samples, on-column digestion of DNA was performed with an RNase-free DNase kit (Qiagen). The concentration of RNA was quantified by UV absorption at 260 nm (NanoDrop ND 1000 spectrophotometer, Labtech International, Ringmer, UK).

2.3.3 Reverse transcription

For the reverse transcription to cDNA, $Pd(N)_6$ random hexamers 5'-phosphate, diethylpyrocarbonate-treated water, dNTP Mix, Bioscript and RNAse inhibitor were used (all from Bioline). Two µg of template RNA, 4 µl random hexamers and water up to a total volume of 12 µl were incubated in the PCR block (Primus 96 Advanced Gradient thermocycler, Peqlab, Erlangen, Germany) for 5 min at 70°C. After 1 µl 10 mM dNTP mix, 4 µl 5x reaction buffer, 1.5 µl DEPC-treated water, 1 µl Bioscript and 0.5 µl RNase inhibitor were added (total volume of 20 µl), the samples were incubated 10 min at 25°C, then 60 min at 42°C, before the reaction was stopped by heating at 70°C for 10 min.

2.3.4 Semi-quantitative PCR

Polymerase chain reaction was carried out with the generated cDNA (40 ng per sample) using a BIOTAQ Core kit (Bioline) including 0.75 µl 25 mM $MgCl_2$, 1 µl 2.5 mM dNTP mix, 1.25 µl Taq buffer, 0.1 µl Taq polymerase, 0.5 µl 10 pmol/µl of each primer, forward and reverse, 0.625 µl 5% DMSO and DEPC-treated water up to a total volume of 12.5 µl. The initial reaction step was incubation at 94°C for 5 min, followed by 35

amplification cycles (30 s at 94°C, 45 s at 58 or 60°C and 45 s at 72°C), after which the reaction was terminated by a final extension step at 72°C for 10 min. DNA fragments were separated by gel electrophoresis (2% agarose) and visualised using ethidium bromide staining. A HyperLadder IV size marker (Bioline) was run in parallel.

2.3.5 Real-time PCR

Reverse transcription was performed as described above. The generated cDNA was used in a 1:3 dilution for the subsequent real-time PCR assay which was carried out on a Mastercycler ep realplex^2 S (Eppendorf, Hamburg, Germany). Amplification (all samples in triplicate) was performed in a 20 µl reaction mixture containing 1 µl of the relevant TaqMan gene expression assay (*SCNN1A*: Hs00168906_m1; *SCNN1B*: Hs00165722_m1; *SCNN1G*: Hs00168918_m1 and *SCNN1D*: Hs00161595_ml; Applied Biosystems), 10 µl TaqMan Universal PCR Master Mix (Applied Biosystems), 3 µl cDNA and 6 µl RNase-free water. Reaction was started with incubation for 10 min at 95°C, followed by 40 two-step cycles of 15 s at 95°C and 60 s at 60°C. As housekeeping gene, β-actin was used in all cases (TaqMan endogenous control, human ACTB, Vic/MGB). Threshold cycles (C_t) were calculated by instrument's software. Normalisation of C_t values to β-actin (ΔC_t) as well as calculations of fold variation values (R) was carried out with Microsoft Excel as followed:

$$\Delta C_t = C_{t\ \text{ENaC subunit}} - C_{t\ \beta\text{-actin}}$$

$$R = 2^{-\Delta Ct}$$

2.4 Western blot

Cell cultures were lysed with cell extraction buffer (Invitrogen) supplemented with protease-inhibitor cocktail (Sigma-Aldrich) on ice and briefly sonicated. Protein sample concentrations were determined using a standard protein assay (Bio-Rad, Hemel Hempstead, UK) according to the manufacturer's instructions. Samples were separated by sodium dodecyl sulphate polyacrylamide gel electrophoresis (SDS-PAGE) and transferred to immunoblot polyvinylidene fluoride membranes (Bio-Rad). Membranes were blocked in 5% bovine serum albumin (BSA) in phosphate-buffered saline with 0.2% Tween 20 (pH 7.4) at 4°C overnight. Incubation with the dilution of the respective primary antibody for 2 h at room temperature (α-ENaC, β-ENaC, γ-ENaC and δ-ENaC (Santa Cruz) 1:250; Na^+-K^+-ATPase and δ-ENaC (D Alvarez de la Rosa) 1:5000; β-actin 1:8000) was followed by 1 h incubation with HRP-conjugated secondary antibody at room temperature. Peroxidase activity was detected with Immobilon Western Chemiluminescent HRP substrate (Millipore). Relative levels of protein expression were quantified by densitometric analysis of the immunoblot using a ChemiDoc documentation system (Bio-Rad). To ensure equal loading, protein was normalised to β-actin.

2.5 Cell surface biotinylation

Sulfo-NHS-biotin (0.5 mg/ml) was applied to the apical or basolateral membranes of confluent filter-grown cell monolayers and incubated at 4°C for 20 min. To prevent biotinylation of basolateral or apical membrane proteins, respectively, BSA (10%) in PBS, supplemented with 2.0 mM Ca^{2+}, was applied to the respective opposite membrane. Subsequently, cell monolayers were incubated with 10% BSA in PBS in

both apical and basolateral compartments to stop the biotinylation reaction. Following cell lysis, protein concentration of the whole cell lysates was determined by Bradford assay and equal amounts of protein were loaded onto streptavidin-agarose beads (500 μg whole cell protein/100 μl streptavidin-agarose beads) for overnight incubation at 4°C. The next day, biotinylated membrane proteins, now bound onto beads, were separated from non-biotinylated proteins by centrifugation, washed, resuspended in protein loading buffer and used for Western blot.

2.6 Protein deglycosylation

GlycoProfile II, Enzymatic In-Solution N-Deglycosylation kit (Sigma-Aldrich) was used according to manufacturer's instructions. Briefly, protein samples were denaturated by incubation with denaturant solution containing 2% octyl-β-D-glucopyranoside and 100 mM β-mercaptoethanol at 100°C for 10 min and diluted to the final protein concentration of 1 mg/ml. Peptide N-glycosidase F (PNGase F) was added at the concentration of 50 units/ml. Equal volume of water was added to the untreated control sample. After 6 h of incubation at 37°C, reaction was stopped by heating at 100°C for 10 min. Aliquots of PNGase F treated samples and untreated controls were used for subsequent analysis by Western blot. Supplied solution of RNAse B was used as glycoprotein standard and positive control.

2.7 Immunofluorescence microscopy (IFM)

Lab-Tek chamber slide or Transwell filter grown cell monolayers were fixed by 10 min incubation with ice-cold methanol, followed by 8 min permeabilisation with 0.1% Triton X-100. Unspecific binding sites were blocked by incubation with PBS containing

5% BSA at 37°C for 30 min. After a 60 min incubation with 200 µl dilution of the respective primary antibody (α-ENaC, β-ENaC, γ-ENaC, δ-ENaC (Santa Cruz), δ-ENaC (D Alvarez de la Rosa) 1:50; δ-ENaC (Pierce) 1:100, Na^+-K^+-ATPase, cytokeratin, ZO-1 1:300) in PBS containing 1% BSA, the cell layers were washed three times with PBS (1% BSA), before incubation with 200 µl of a 1:1000 dilution of the relevant Alexa Fluor-488-labelled $F(ab')_2$ fragment in PBS containing 1% BSA. To counterstain cell nuclei, propidium iodide (1 µg/ml in PBS) was used. After 30 min of incubation, the specimens were again washed three times with PBS (1% BSA) and embedded in FluorSave anti-fade medium (Merck, Nottingham, UK). Images were obtained using a confocal laser scanning microscope (CLSM, Zeiss LSM 510, Göttingen, Germany) and processed using LSM Image Browser software (Zeiss). Cell monolayers stained with the respective secondary antibodies only were used as background controls. To be able to compare the immunofluorescent signal obtained in different cell models, i.e. in H441, Calu-3 and ATI-like cells as well as in the wild-type and δ-ENaC over-expressing H441 cells, identical conditions of imaging, illumination intensity, and photomultiplier settings (pinhole settings, detector gains and offset levels) were used to detect the respective protein of interest.

2.8 Transepithelial measurements

Transwell filter grown cell monolayers were regarded as suitable for the transepithelial measurements when the net TEER values exceeded 300 $\Omega \cdot cm^2$. Confluent cell monolayers, grown for 15-21 (Calu-3), 8-14 (H441) or 8-10 (ATI-like) days, were then mounted into modified Ussing chambers (custom-built or Physiologic Instruments, San Diego, CA). Cells were incubated with Krebs-Ringer-Buffer pH 7.4 on both sides (composition of KRB: 116.4 mM NaCl, 5.4 mM KCl, 0.78 mM NaH_2PO_4, 25 mM

$NaHCO_3$, 5.55 mM glucose, 15 mM HEPES, 1.8 mM $CaCl_2$, 0.81 mM $MgSO_4$). Sodium-free solutions contained equivalent amounts of KCl, KH_2PO_4 and $KHCO_3$, respectively, whereas in Cl^--free solutions, equivalent amounts of the relevant gluconate salts were used. Chambers and bathing solutions were maintained at 37°C and were continuously stirred. For the measurements, the transepithelial potential difference (PD) was clamped to 0.0 mV using a standard four-electrode voltage clamp (DVC-1000, World Precision Instruments, Sarasota, FL or VCC MC6, Physiologic Instruments, San Diego, CA) and the short-circuit current (I_{SC}) was measured. Subsequently, voltage impulses of 0.5 mV were given every 50 s in order to monitor the transepithelial electrical resistance (TEER) of cell monolayers. The short-circuit current was continuously recorded using Chart5 for Windows (ADInstruments, Oxfordshire, UK) or WinDAQ for Windows software (Dataq Instruments, Akron, OH). Cell monolayers were allowed to reach steady state basal I_{SC} before the actual measurement was conducted (after approx 10-15 min). Then, the compound of interest was added. The used stock solutions were 50 mM Evans blue, 5 mM capsazepine, 10 mM icilin, 2.5 mM $CFTR(inh)_{172}$, 50 mM amiloride and 100 mM ouabain (all in DMSO; all from Sigma-Aldrich). *Note: Usage of different sets of instruments (Ussing chambers, voltage clamp as well as data acquisition software) was due to the fact that a part of the measurements was performed at Children's Hospital Oakland Research Institute, Oakland, CA (Dr. Horst Fischer's Lab).*

2.9 Delta-ENaC knockdown studies

2.9.1 Transient transfection with siRNA

To transiently down-regulate δ-ENaC, a commercially available GeneSolution siRNA kit (1027416, Qiagen, Crawley, UK) containing four siRNAs complementary to the δ-ENaC subunit (siRNA sequences given in **Table 2)** was used. As negative control, non-silencing scrambled siRNA was used (AllStars Negative Control siRNA, Qiagen). Calu-3 cells were transfected using HiPerfect Transfection reagent (Qiagen). The general transfection procedure was carried out according to manufacturer's protocol. For optimisation of the method, different conditions were tested. In particular, transfections were carried out with cells at different time in culture (1-9 days) grown on plastics as well as on Transwell filter inserts. Small interfering RNA amounts from 5 to 50 nM as well as different volumes of transfection reagent were used per well. The HiPerfect transfection reagent/siRNA complexes remained on the cells for 24 h. Isolation of protein samples was carried out at various time points (24, 48 and 72 h after transfection).

Table 2. Nucleotide sequences of δ-ENaC siRNA constructs contained in the GeneSolution siRNA kit (1027416, Qiagen, Crawley, UK) according to manufacturer's product information.

siRNA	Target sequence (5' to 3')
Hs_SCNN1D_5	CGGCATCAGGGTCATGGTTCA
Hs_SCNN1D_6	CTGGCGGGAGTCTCAGCCGAA
Hs_SCNN1D_1	CACACTTGGGCTGCTCTGAAA
Hs_SCNN1D_2	CCGCAATGGCTGAGCACCGAA

2.9.2 Transfection with dominant negative cDNA constructs

To transiently down-regulate functional δ-ENaC, dominant negative cDNA constructs, kindly provided by Dr. Catherine M Fuller (University of Alabama, Birmingham, AL) were used. Generation and amplification of the plasmid are described in section 2.11 of this chapter. H441 cells were transfected using Lipofectamine 2000 transfection reagent (Invitrogen) following the manufacturer's protocol. Briefly, cells were seeded at 150,000/cm^2 into 24-well plates 24 h prior to transfection, in order to reach approximately 90% confluence the following day. The transfection mixture included 0.8 to 1.6 μg plasmid cDNA per well in 1:2.5 to 1:5 ratio to Lipofectamine 2000 (2 and 4 μl Lipofectamine 2000 for 0.8 μg cDNA and 4 and 8 μl Lipofectamine 2000 for 1.6 μg cDNA, respectively). The Lipofectamine 2000/plasmid cDNA complexes remained on the cells for 24 h. Protein samples to assess the down-regulation of δ-ENaC were collected 24, 48 and 72 h after transfection.

2.9.3 Stable transfection with shRNA

To stably down-regulate δ-ENaC expression in H441 and Calu-3 cells, commercially available δ-ENaC shRNA lentiviral particles (SC-42421-V, Santa Cruz Biotechnology) were used. The particle pool consisted of transduction-ready viral particles carrying three different constructs, each encoding for a 19 nt shRNA (shRNA sequences given in **Table 3)**, designed to knockdown δ-ENaC gene expression, and a puromycin resistance gene. As negative control, control shRNA lentiviral particles (SC-108080, Santa Cruz Biotechnology), carrying constructs encoding for negative scrambled shRNA and puromycin resistance gene, were used. Cells (H441 passage 59, Calu-3 passage 38) were seeded at 100,000/cm^2 in 24-well plates 24 h prior to lentiviral infection. The next day, medium was replaced with medium containing 5 μg/ml Polybrene (Santa Cruz Biotechnology), a polycation, neutralising membrane charges and, therefore, enhancing

the interaction between the cell membrane and the viral capsid. Subsequently, lentiviral particles were added onto the cells (7.5×10^3 infectious units of virus (IFU) per well). Forty eight hours after the transduction, cells were split at a 1:3 ratio. Following overnight incubation in complete medium, puromycin containing medium was applied onto the cells to select shRNA expressing puromycin-resistant cells. Subsequently, selected puromycin-resistant cells were expanded. The puromycin concentration suitable for selection was determined previously as the lowest concentration to kill 100% of wild-type cells in 3-5 days from the start of the puromycin selection and was 2.5 μg/ml puromycin for H441 and 7.5 μg/ml for Calu-3 cells.

Table 3. Nucleotide sequences of δ-ENaC shRNA constructs in δ-ENaC shRNA lentiviral particles (SC-42421-V, Santa Cruz Biotechnology, Heidelberg, Germany) according to the manufacturer's product information.

shRNA	shRNA sequence (5' to 3')	
	sense	antisense
A	GUG ACG AAG CUG UGA UUC Att	UGA AUC ACA GCU UCG UCA Ctt
B	CAC CUU CUU CUG CAC CAA Utt	AUU GGU GCA GAA GAA GGU Gtt
C	GGU ACC ACU UCC ACU AUG Utt	ACA UAG UGG AAG UGG UAC Ctt

2.10 Delta-ENaC over-expression studies

2.10.1 Transient δ-ENaC over-expression

For transient over-expression, plasmid construct encoding human full-length δ_1-ENaC protein, subcloned in pcDNA3.1(+) vector, was kindly provided by Dr. Diego Alvarez de la Rosa (Universidad de La Laguna, La Laguna, Spain). Details on the generation

and amplification of the plasmid are given below. H441 and HEK-293 cells were transfected using Lipofectamine 2000 transfection reagent following the manufacturer's protocol. Briefly, approximately 90% confluent cell monolayers were transfected 24 h after seeding with a transfection mixture of 0.8 μg plasmid cDNA and 0.4, 2 and 4 μl Lipofectamine 2000 transfection reagent (1:0.5, 1:2.5 and 1:5 ratio of μg cDNA to μl Lipofectamine 2000) to optimise the transfection conditions. The Lipofectamine 2000/plasmid cDNA complexes remained on the cells for 24 h. Two hours after transfection, the ENaC inhibitor benzamil was added to the medium at a concentration of 10 μM, in order to prevent adverse effects of increased Na^+ influx on cell viability. Protein samples to assess δ-ENaC over-expression were collected 24, 48 and 72 h after transfection, quantified and analysed by Western blot. The transfection mixture with 1:5 ratio of μl cDNA to μl Lipofectamine 2000 was shown to result in the highest δ-ENaC over-expression levels and was used for all subsequent experiments as well as for generation of stably transfected, δ-ENaC over-expressing cell lines.

2.10.2 Stable δ-ENaC over-expression

H441 (passage 68) cells were transfected with a transfection mixture of 0.8 μg δ_1-ENaC plasmid cDNA and 4 μl Lipofectamine 2000. Two hours after transfection, 10 μM benzamil was added to the medium. Cells were split into medium containing 600 μg/ml of the aminoglycoside antibiotic, geneticin (G418, Sigma-Aldrich), and 10 μM benzamil in ratios of 1:5 to 1:100, 48 hours after transfection. The G418 concentration of 600 μg/ml was previously shown to be suitable for selection. Subsequently, several G418-resistant colonies were picked, expanded and assessed for δ-ENaC expression by Western blot. Colonies stably expressing δ-ENaC were kept in culture and used for subsequent expression and functional studies.

2.11 cDNA constructs

Delta-ENaC dominant negative cDNA as well as δ_1-ENaC encoding construct, used in this work, were kindly provided by Dr. Catherine M Fuller (University of Alabama, Birmingham, AL) and Dr. Diego Alvarez de la Rosa (Universidad de La Laguna, La Laguna, Spain), respectively. Delta-ENaC dominant negative construct was generated as described by Kapoor *et al.* (2009) by introducing a premature stop codon in human δ-ENaC cDNA at Ser-35 during PCR and integration of the PCR product into pEYFP-C1 vector. The encoded premature δ-ENaC protein (E35X) is schematically described in **Figure 1**. Plasmid construct coding for the full-length δ_1-ENaC protein was generated as described by Wesch *et al.* (2010) by restriction enzyme subcloning of human δ_1-ENaC cDNA in pcDNA3.1(+) vector. Both plasmids were amplified by transformation in *Escherichia coli*. Briefly, 25 µl *E. coli* (Invitrogen) were transformed with 200 ng of the relevant plasmid cDNA and, following 1 h incubation in 200 µl SOC medium (Invitrogen) at 37°C, plated on Luria Bertani (LB) plates containing 30 µg/ml kanamycin or 50 µg/ml ampicillin (for E35X or δ_1-ENaC plasmids, respectively). After overnight incubation at 37°C, 5 ml LB medium containing 30 µg/ml kanamycin or 50 µg/ml ampicillin were inoculated with transformed *E. coli* and incubated for 12-16 h at 37°C with constant shaking. Subsequently, DNA was isolated using QIAprep Spin Miniprep Kit (Qiagen, Crawley, UK) and quantified with a NanoDrop ND 1000 spectrophotometer (Labtech International, Ringmer, UK).

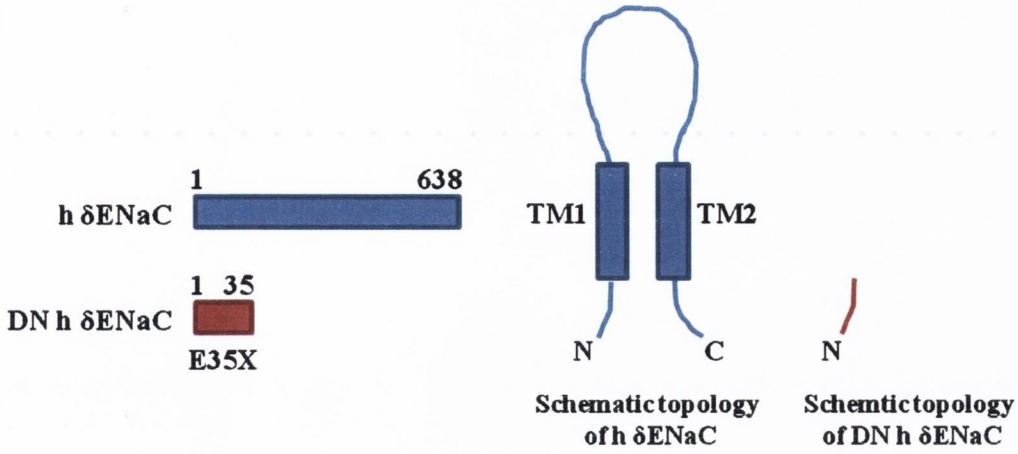

Figure 1. Schematic diagram of δ-ENaC dominant negative construct (E35X). *Modified from Kapoor et al. (2009).*

2.12 Statistical analysis

All experiments were carried out at least in triplicate using cells from at least three different passages. Results, all given as means ± SD, were compared using one-way analysis of variance (ANOVA), followed by the Student-Newman-Keuls post-hoc test. $P < 0.05$ was considered as significant.

CHAPTER 3

Expression and localisation of δ-ENaC in human respiratory epithelial cells

3.1 Expression of ENaC subunits in human respiratory epithelial cells

Epithelial sodium channel α-, β- and γ-subunits are known to be expressed in alveolar epithelial cells (Matsushita *et al.* 1996, Smith *et al.* 2000). Recently, expression of δ-ENaC was shown in respiratory epithelial A549, H441 and 16HBE14o- cell lines as well as in human lung tissue (Zhao *et al.* 2012; Ji *et al.* 2006). Against this background, the aim of the first set of experiments was to investigate and to confirm the expression of the four ENaC subunits at mRNA and protein levels in bronchial and alveolar organotypic cell models available in our laboratory.

3.1.1 Gene expression

The RT-PCR studies were performed by Aurélie Guery, Trinity College Dublin, Ireland.

In a preliminary study, reverse transcriptase-PCR experiments were carried out in the alveolar and bronchial epithelial A549 and Calu-3 cell lines, respectively. Messenger RNA for all studied ENaC subunits was found to be expressed in these cells as shown in **Figure 1**. These data were the basis for further studies in which mRNA levels were quantified by means of real-time PCR in these two cells lines, as well as in 16HBE14o- cells.

For quantitative PCR, mRNA samples were isolated from four different cell passages and experiments were run in triplicates. Positive and negative controls were included. Beta-actin was used as housekeeping gene in all cases. Results obtained by q-PCR confirmed the RT-PCR findings, i.e., mRNA encoding all four ENaC subunits were expressed in respiratory epithelial cells. **Figure 2 (A)** shows mRNA expression of the

relevant ENaC subunits as fold variations of β-actin expression in human respiratory cell lines. **Figure 2 (B)** presents the expression pattern for ENaC subunits in individual cell lines. The abundance of mRNA was highest for α-ENaC, followed by moderate levels for β- and rather low signal intensities for γ- and δ-subunits. In general, mRNA expression patterns were similar in all investigated cell lines showing no major difference between the alveolar and the bronchial cell types.

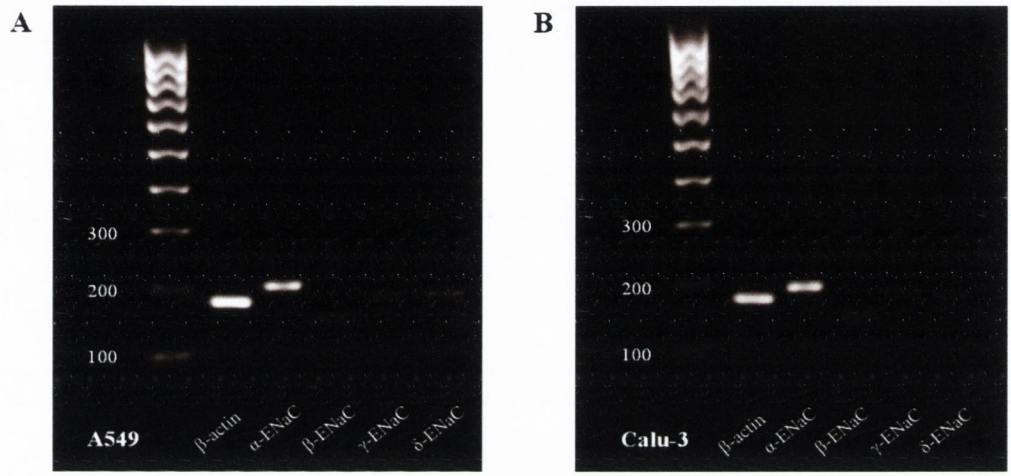

Figure 1. Representative agarose gel images obtained after performing RT-PCR in A549 (**A**) and in Calu-3 (**B**) cells. These data indicate the presence of all the investigated ENaC subunits in both cell lines. Alpha-ENaC showed the relatively highest mRNA abundance with signal intensities being comparable to β-actin. Messenger RNA encoding β-, γ- and δ-subunits was also detected, but the expression levels were comparatively weaker.

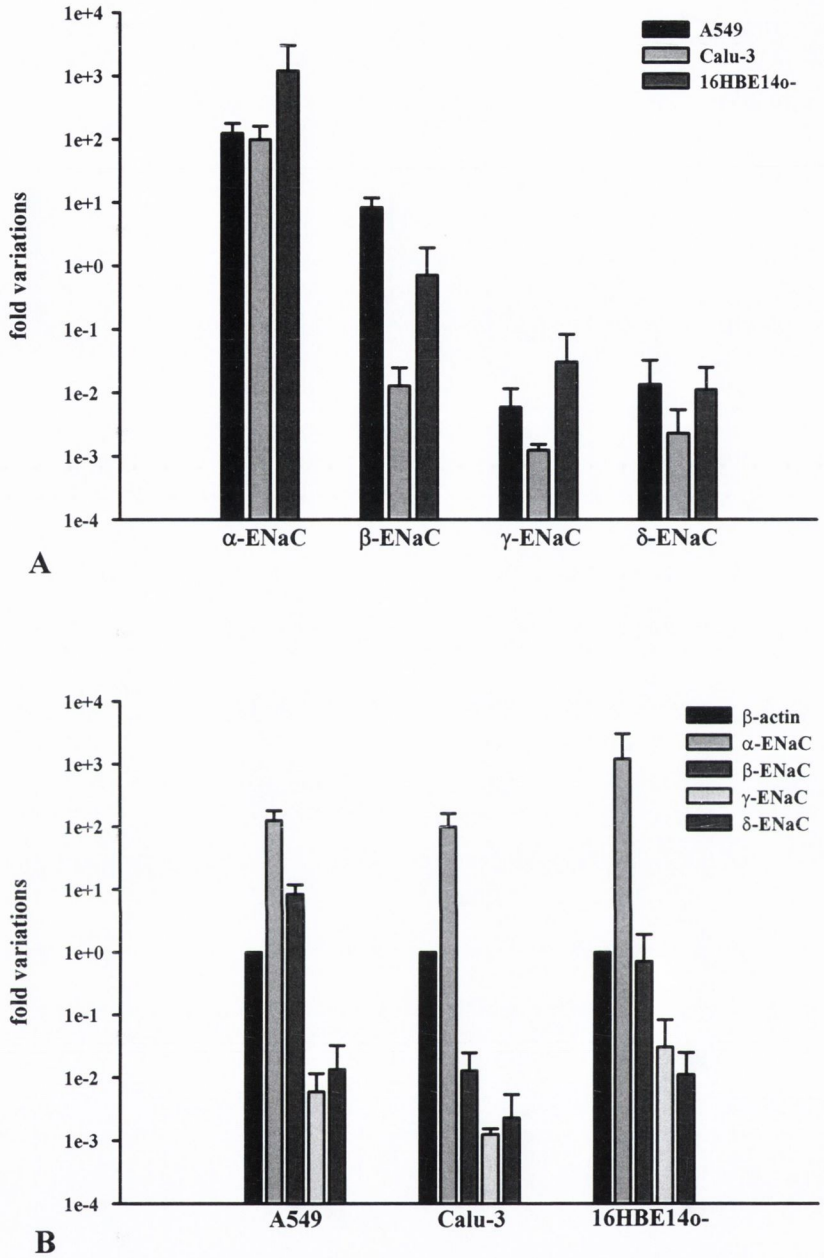

Figure 2. (A) Expression levels of mRNA transcripts encoding ENaC subunits relative to β-actin in A549, Calu-3 and 16HBE14o- respiratory epithelial cells (means ± SD, $n = 4$) as obtained by q-PCR. **(B)** The same data set arranged by cell type.

3.1.2 Protein expression and localisation

3.1.2.1 Western blot

To confirm the presence of ENaC subunits at protein level in human respiratory epithelial cells *in vitro*, Western blot analyses were carried out. All experiments were performed in triplicate. Representative immunoblots are shown in **Figure 3.**

All four homologous ENaC subunits were found to be expressed in the cell lines tested. In general, the expression pattern of α-, β- and γ-ENaC subunits was comparable between A549, Calu-3 and 16HBE14o- cell lines. In all cases, multiple bands were observed for α-ENaC. Whilst the 90 kDa band corresponds to the *N*-glycosylated full-length α-ENaC, 65 and 62 kDa bands represent *N*-glycosylated C-terminal protein fragments originating from proteolytic cleavage (Hughey *et al.* 2004). A full-length 95 kDa band was observed for β-ENaC. In the case of γ-ENaC, only the cleaved protein could be detected (75 kDa band as opposed to the glycosylated full-length form of 93 kDa). The observed protein bands for α-, β- and γ-ENaC subunits were consistent with previous reports (Hughey *et al.* 2003, 2004; Tan *et al.* 2011). Bands at higher molecular weights (190 kDa bands for α- and β-ENaC) are likely to represent dimers or multimers formed by, presumably glycosylated, subunit proteins and their fragments. Since proteolytic cleavage mediates activation of ENaC (Hughey *et al.* 2004; Carattino *et al.* 2008), detection of cleaved forms of α- and γ-subunits suggests presence of active ENaC in all three cell types tested.

For δ-ENaC, multiple bands (140, 100 and 85 kDa) were observed in A549, Calu-3 as well as in 16HBE14o- cells. An additional band of 130 kDa was detected in Calu-3 cell lysates. Haerteis *et al.* (2009) reported the existence of two prominent bands of 86 and 75 kDa in δ-hENaC injected *X. laevis* oocytes, with the larger size band being a

glycosylated form of the smaller sized protein. According to this, the 85 kDa band in our case could be the one corresponding to the glycosylated full-length protein. Bands observed at higher molecular weights (i.e., 100, 130 and 140 kDa) could as well be glycosylated forms of δ-ENaC and/or their dimers. Delta-ENaC immunoblots are discussed in more detail in sections 3.2.1 and 3.2.2 of this chapter.

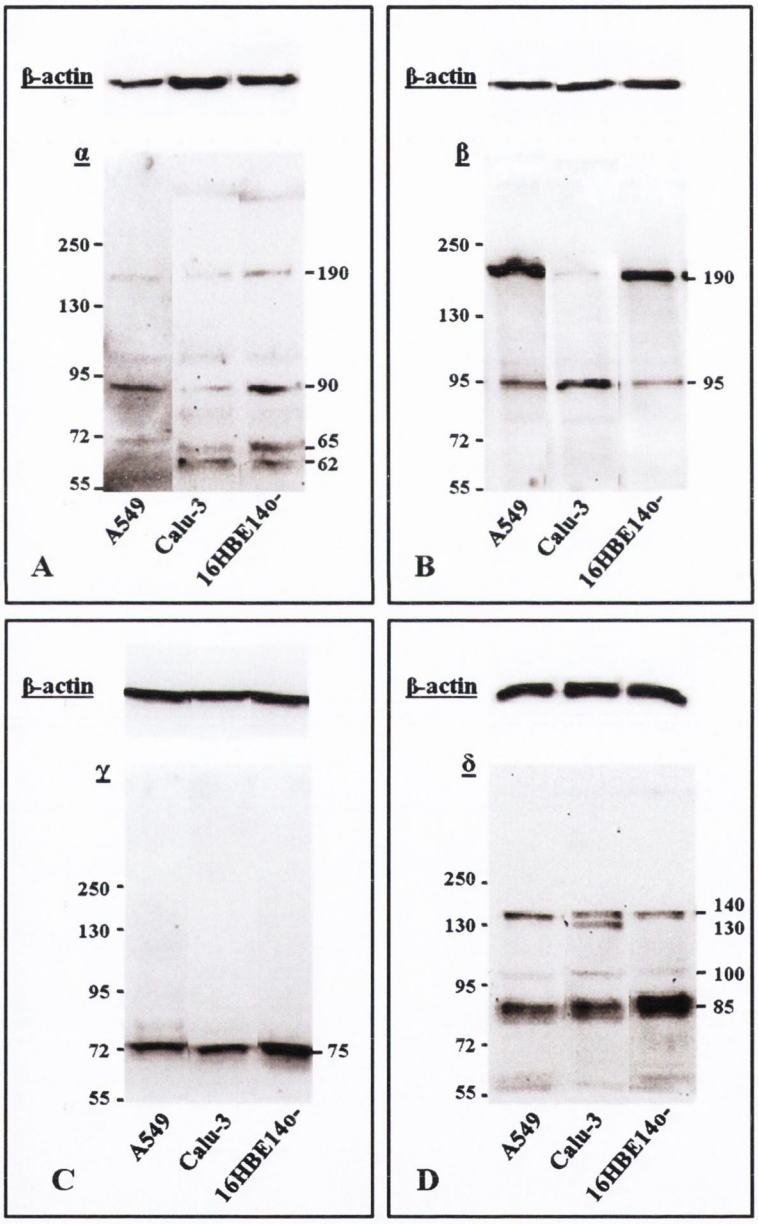

Figure 3. Representative Western blots for ENaC α-, β-, γ- and δ-subunits (**A**, **B**, **C** and **D**, respectively) in A549, Calu-3 and 16HBE14o- cells. Beta-actin was used as loading control in all cases.

3.1.2.2 Immunofluorescence microscopy

Although Western blot revealed presence of all four homologous subunits at protein level in the cell lines tested, only their expression in Calu-3 cells was confirmed by immunofluorescence confocal laser scanning microscopy, with comparable signal intensities obtained for α-, β-, γ- and δ-ENaC. In A549 as well as in 16HBE14o- cells, β-ENaC signal showed nuclear localisation and only low signals of α-, γ- and δ-ENaC protein were detected. The respective images are shown in **Figure 4**. The green signal represents the relevant ENaC subunit and the red signal propidium iodide counterstained cell nuclei.

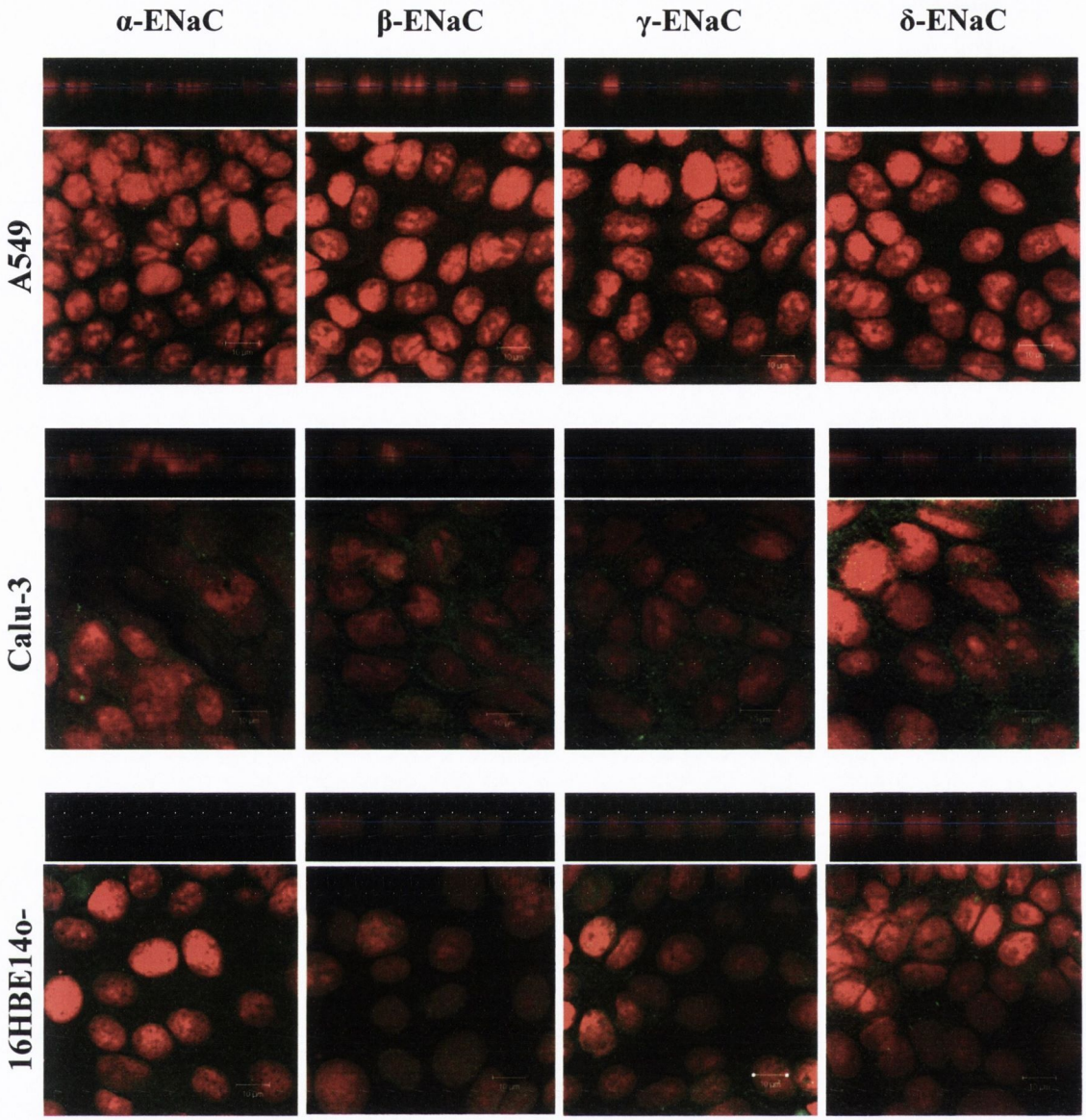

Figure 4. Immunofluorescence microscopy of ENaC α-, β-, γ- and δ-subunits in human respiratory epithelial cell lines (green). Cells were grown on Lab-Tek Chamber slides. Cell nuclei were counterstained with propidium iodide (red).

3.2 Delta-ENaC expression and localisation in human respiratory epithelial cells

According to our initial experiments as well as to a number of publications by other labs (Ji *et al.* 2006; Bangel-Ruland *et al.* 2010; Zhao *et al.* 2012), human respiratory epithelial cells endogenously express δ-ENaC. In order to gain a more detailed insight into its expression, another set of experiments addressing the subcellular localisation of δ-subunit was performed. These investigations focused on bronchial Calu-3 as well as bronchiolar H441 epithelial cell lines. Moreover, δ-ENaC expression and localisation in freshly isolated human alveolar epithelial cells in primary culture were studied.

3.2.1 Characterisation of polyclonal anti-δ-ENaC antibodies

Several rabbit polyclonal anti-δ-ENaC antibodies were used for the experiments described below. **Figure 5** schematically shows a map of the binding sites of the respective antibodies as well as the localisation of the reported cleavage site within the δ-ENaC protein. Two of the antibodies were commercially available. The polyclonal anti-δ-ENaC antibody purchased from Santa Cruz Biotechnology (H-230, SC-21015) was raised against amino acids 81-310 near the N-terminus of human δ-ENaC and recognises both δ_1- and δ_2-isoform. This antibody has been used in several publications by different labs (references given in **Figure 5**) and is referred to as anti-δ-ENaC (SC) in the further course of this work. The second commercially available anti-δ-ENaC antibody was obtained from Pierce (Thermo Fisher, OSR00100W). It was raised against amino acid region 400-500 and, therefore, recognises the extracellular loop of both δ-ENaC isoforms. This antibody is further referred to as anti-δ-ENaC (TF). To our knowledge, no data generated using this antibody has yet been published. Lastly, an antibody was kindly provided to us by Dr. Diego Alvarez de la Rosa (Universidad de La

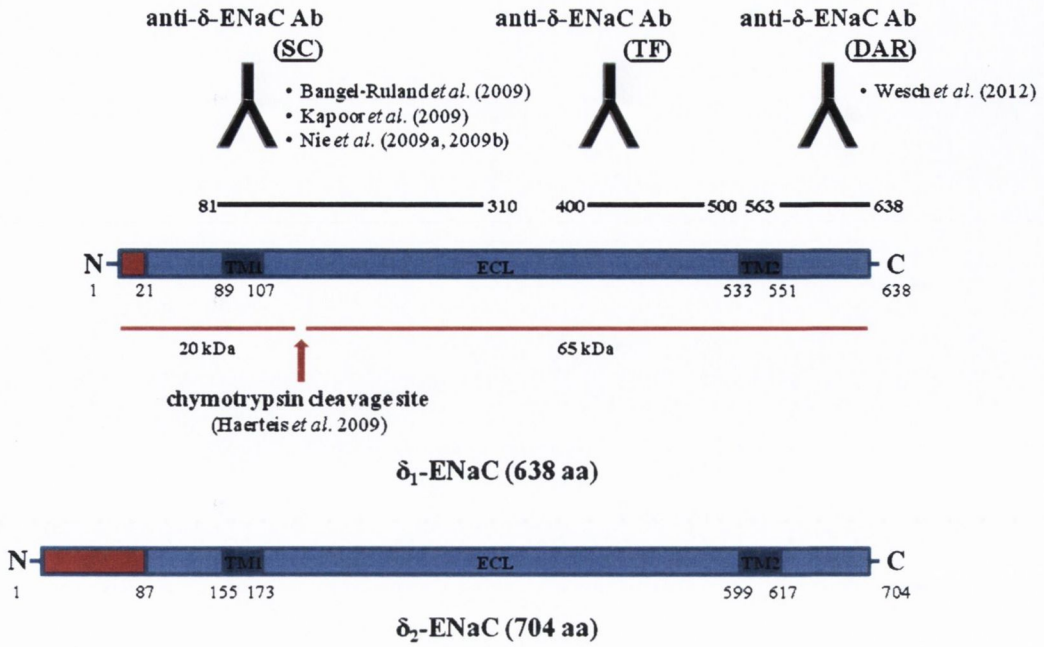

Figure 5. Localisation of the binding sites of the anti-δ-ENaC antibodies within the δ-ENaC protein as well as the structural difference between two δ-ENaC isoforms. The blue bars represent amino acid regions shared by both, δ_1- and δ_2-isoforms. Amino acid sequences different in the two isoforms are marked red. Black lines indicate the epitopes of the respective antibodies. Also, the reported chymotrypsin cleavage site as well as the resulting δ-ENaC cleavage products are indicated. *Abbreviations: N: N-terminus; C: C-terminus; TM1 and TM2: transmembrane domains 1 and 2; ECL: extracellular loop; aa: amino acid.*

Laguna, La Laguna, Spain). This rabbit polyclonal anti-δ-ENaC antibody was raised against the C-terminus of the δ-ENaC protein (amino acids 563-638) (Wesch *et al.* 2012). It recognises both δ_1- and δ_2-isoform and is referred to as anti-δ-ENaC (DAR). The anti-δ-ENaC (TF) antibody could not be optimised for the Western blot application. For that reason, this antibody was only used for immunofluorescence microscopy. For characterisation of the polyclonal anti-δ-ENaC SC and DAR antibodies, immunoblots with negative and the positive controls as well as Calu-3 and H441 cell lysates were probed with the respective anti-δ-ENaC antibodies. The results are presented in **Figure 6**. Lysates of the wild-type and the mock-transfected HEK-293 cells were used as negative controls. Positive controls were HEK-293 cells transiently transfected with δ_1-

ENaC plasmid and a commercially available δ-ENaC control peptide purchased from Millipore (AG981). According to manufacturer's information, the control peptide is a δ-ENaC protein fragment, the sequence of which includes the amino acid region 171-189. More information, however, was not provided.

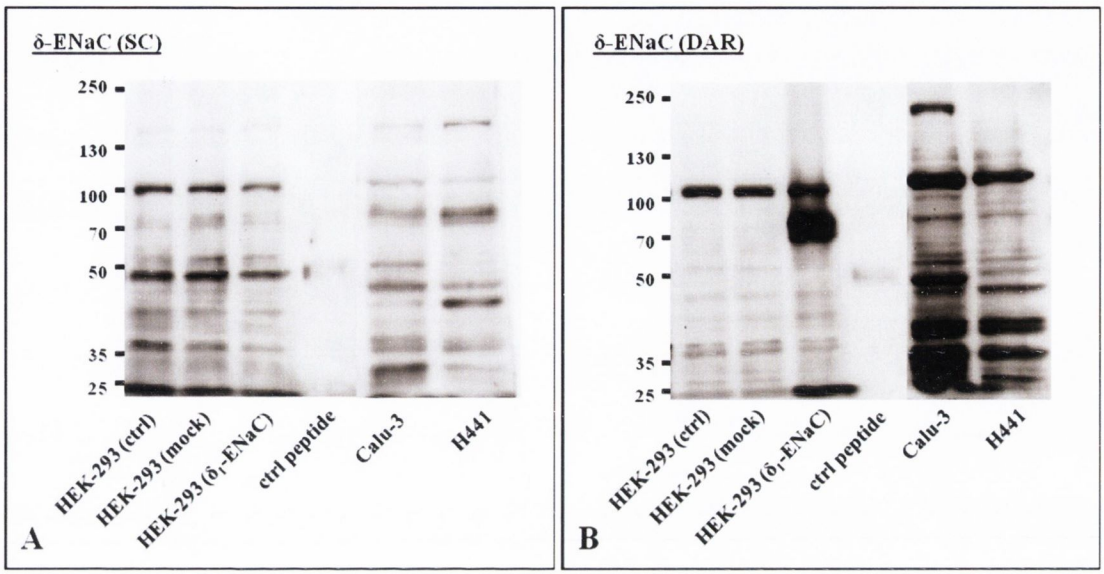

Figure 6. Characterisation of polyclonal anti-δ-ENaC antibodies: **(A)** SC, **(B)** DAR. Western blots of non-transfected (ctrl), mock-transfected (mock) HEK-293 as negative controls, δ_1-ENaC-transfected (δ_1-ENaC) HEK-293 cells and δ-ENaC control peptide (AG981, Millipore) as positive controls as well as Calu-3 and H441 cell lysates were probed with the respective anti-δ-ENaC antibody.

The anti-δ-ENaC antibody SC (**Figure 6 (A)**) revealed identical band patterns for the non-transfected, mock-transfected and δ_1-ENaC expressing HEK-293 cells. High intensity bands were detected at the molecular weights of 48 and 100 kDa and, additionally, several bands of lower intensity (140, 80, 55, 36 kDa). No additional band was observed for the HEK-293 (δ_1-ENaC) cell lysate, suggesting that the antibody did not recognise the heterologously expressed δ_1-ENaC protein. The δ-ENaC control peptide, however, was detected showing a molecular weight of approximately 50 kDa. In the lysates of respiratory epithelial cells, multiple bands were observed (at 140, 130,

100, 85, 55, 48, 36 and 30 kDa for Calu-3 and at 140, 100, 85, 48, 44, 36 and 30 kDa for H441 cells). The bands at 48 and 100 kDa could be identified as unspecific, as they were observed throughout all the samples and negative controls. The prominent band at approximately 80-85 kDa, observed in the respiratory epithelial cell lysates, could potentially represent the full-length δ-ENaC protein, consistent with the previous reports using this antibody (Nie *et al.* 2009a, 2009b; Kapoor *et al.* 2010). However, the overall picture was rather inconclusive, since the SC antibody failed to recognise the over-expressed δ_1-ENaC protein, raising doubts in the specificity of the bands observed in Calu-3 and H441 cell lysates and, therefore, questioning our initial findings regarding the presence of δ-ENaC in these cells.

The corresponding immunoblot for anti-δ-ENaC antibody DAR is shown in **Figure 6 (B)**. Again, an unspecific band at 100 kDa was observed throughout the control and the respiratory epithelial cell lysates. However, a strong band at approximately 70-85 kDa appeared in δ_1-ENaC transfected HEK-293 cells, supporting the fact that the DAR antibody indeed recognises the δ_1-ENaC protein. This band could potentially represent a merged double band of δ-ENaC protein at 75 kDa and its glycosylated form at 86 kDa (Haerteis *et al.* 2009). The synthetic control peptide was also detected by the DAR antibody. In Calu-3 and H441 cell lysates, multiple bands were observed, *inter alia* a band of rather low intensity at approximately 75 kDa, corresponding to the δ_1-ENaC band in HEK-293 (δ_1-ENaC) cell lysate and, therefore, confirming δ-ENaC expression in these cell lines.

In the further course of this work, the anti-δ-ENaC antibody DAR was used due to the encouraging results of the control experiment. Albeit, in our hands, the SC antibody was of questionable specificity, it was used continuously as an additional control, considering the fact that some of the published data on δ-ENaC was generated using this

antibody. However, the results obtained with the SC antibody were examined critically. Furthermore, the TF antibody was used for immunofluorescence microscopy.

3.2.2 Expression of δ-ENaC in human respiratory epithelial cells

Immunoblots of cell lysates of bronchial Calu-3, bronchiolar H441 cells as well as of human primary epithelial type I-like cells were probed with SC and DAR anti-δ-ENaC antibodies and are shown in **Figure 7** in direct comparison. Due to extremely low protein yield, ATII cell lysate was probed with SC antibody only. However, the resulting immunoblot was of very poor quality as seen in **Figure 7 (D)**. Both antibodies revealed multiple bands in all cell lysates tested. Bands detected by the SC antibody were at 140, 100, 75-85, 55, 50 kDa as well as at lower molecular weights and common in Calu-3, H441 and ATI-like cells. The 60 kDa band present in Calu-3 and ATI-like cells was not detected in H441 cells. The DAR antibody detected the following bands:

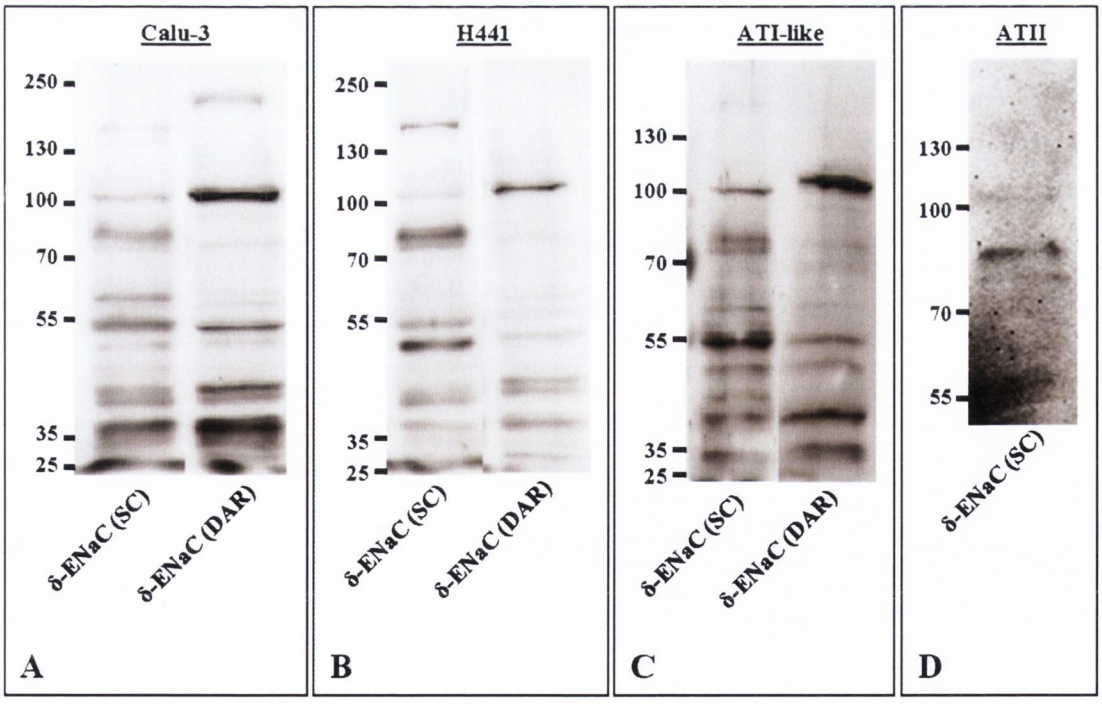

Figure 7. Representative Western blots for δ-ENaC in Calu-3 **(A)** and H441 **(B)** cell lines as well as in human primary alveolar epithelial type I-like **(C)** and type II **(D)** cells obtained with anti-δ-ENaC SC antibody compared to those obtained with anti-δ-ENaC DAR antibody.

200 (Calu-3 only), 100, 75, 55 (very weak in H441) and 50 kDa (very weak Calu-3) as well as further protein bands of lower molecular weights. Several bands were detected by both antibodies, among them the band at 100 kDa, previously confirmed to be unspecific. More importantly, both SC and DAR antibodies recognised the band at ~75 kDa, which, in case of DAR antibody, was very weak, but δ-ENaC-specific, as shown in the control experiment described earlier. Moreover, bands at 55 and 50 kDa were obtained with both antibodies.

3.2.3 Deglycosylation assay

Epithelial sodium channel subunits are thought to undergo *N*-linked glycosylation during their assembly in the endoplasmatic reticulum, whereas the *N*-glycans are modified later, during the transit through the Golgi network (Hughey *et al.* 2004). To examine whether any of the bands detected with the anti-δ-ENaC antibodies result from the glycosylation of the protein core, samples were treated with PNGase F to remove *N*-linked oligosaccharides and then analysed by Western blotting. Untreated control samples were run in parallel. As a control for the efficiency of the PNGase F treatment, RNase B, a glycoprotein of a high mannose type, was used. As shown in **Figure 8**, none of the bands in Calu-3 and H441 cell lysates showed migration to a lower molecular weight following PNGase F treatment, indicating that none of the bands represented an *N*-glycosylated protein. This result was obtained with both SC and DAR anti-δ-ENaC antibodies and is, in the case of the SC antibody, another argument against our initial assumption that the 85 kDa band detected with this antibody represented a glycosylated form of δ-ENaC as reported by Haerteis *et al.* (2009). As RNase B, treated under the same conditions, showed a shift in the molecular weight from 15 to 13 kDa, PNGase F treatment was performed correctly.

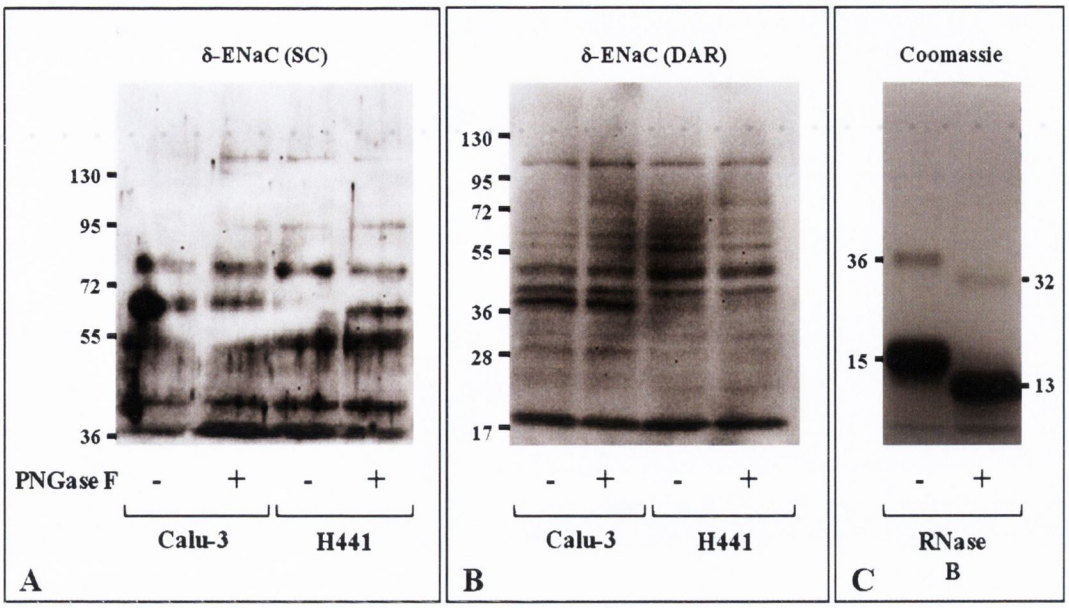

Figure 8. State of glycosylation of proteins detected by SC **(A)** and DAR **(B)** anti-δ-ENaC antibodies in Calu-3 and H441 cell lysates. Untreated controls were run in parallel to PNGase F treated samples. **(C)** Coomassie staining of RNase B, a standard *N*-glycosylated protein, used as positive control.

3.2.4 Cell surface biotinylation

To determine whether any of the proteins detected with the anti-δ-ENaC antibodies were localised in the plasma membrane, apical and basolateral surface proteins of confluent cell monolayers grown on Transwell filter inserts were biotinylated, recovered from the cell lysates on streptavidin-agarose beads and analysed by Western blot with anti-δ-ENaC SC and DAR antibodies. Beta-actin was used as control to exclude the contamination of the biotinylated samples with the intracellular protein. Na^+/K^+-ATPase was used as a marker for the basolateral membrane samples and also to identify contamination of the apical membrane samples with basolateral protein. **Figure 9** shows representative immunoblots of the whole cell lysates as well as the apically and basolaterally biotinylated membrane protein fractions. The SC antibody revealed 60 and 55 kDa protein fragments in the biotinylated samples of Calu-3, H441 and ATI-like cells for both apical and basolateral membranes. The DAR antibody detected a 36 kDa

band in the apical and basolateral membrane fractions of Calu-3 cells only. No bands, potentially corresponding to the full-length δ-ENaC protein, were detected in the biotinylated membrane fractions by either of the antibodies. This indicates absence of the full-length δ-ENaC from the plasma membrane of Calu-3, H441 and ATI-like cells. The proteins detected in the respective membrane fractions could potentially represent 60 and 55 kDa cleavage products of the full-length protein (in all cell models tested) as well as the C-terminal 36 kDa δ-ENaC protein fragment (in Calu-3 cells). So far, only C-terminal 65 kDa and N-terminal 20 kDa cleavage products have been reported in literature (Haerteis *et al.* 2009). However, novel, yet unreported cleavage sites cannot be excluded as a potential explanation for the observed bands. Another issue that remains debatable is the detection of δ-ENaC fragments in both, i.e., apical and basolateral membranes. Although expression of δ-ENaC on both cellular aspects has been reported previously in human taste bud cells (Huque *et al.* 2009), ENaC proteins are generally thought to be exclusively localised to the apical membrane in respiratory epithelium. Unfortunately, no antigen suitable as an apical marker could be successfully optimised in this work, so that contamination of the basolaterally biotinylated samples with apical protein cannot be excluded and abundance of δ-ENaC in both membranes of respiratory epithelial cells remains uncertain.

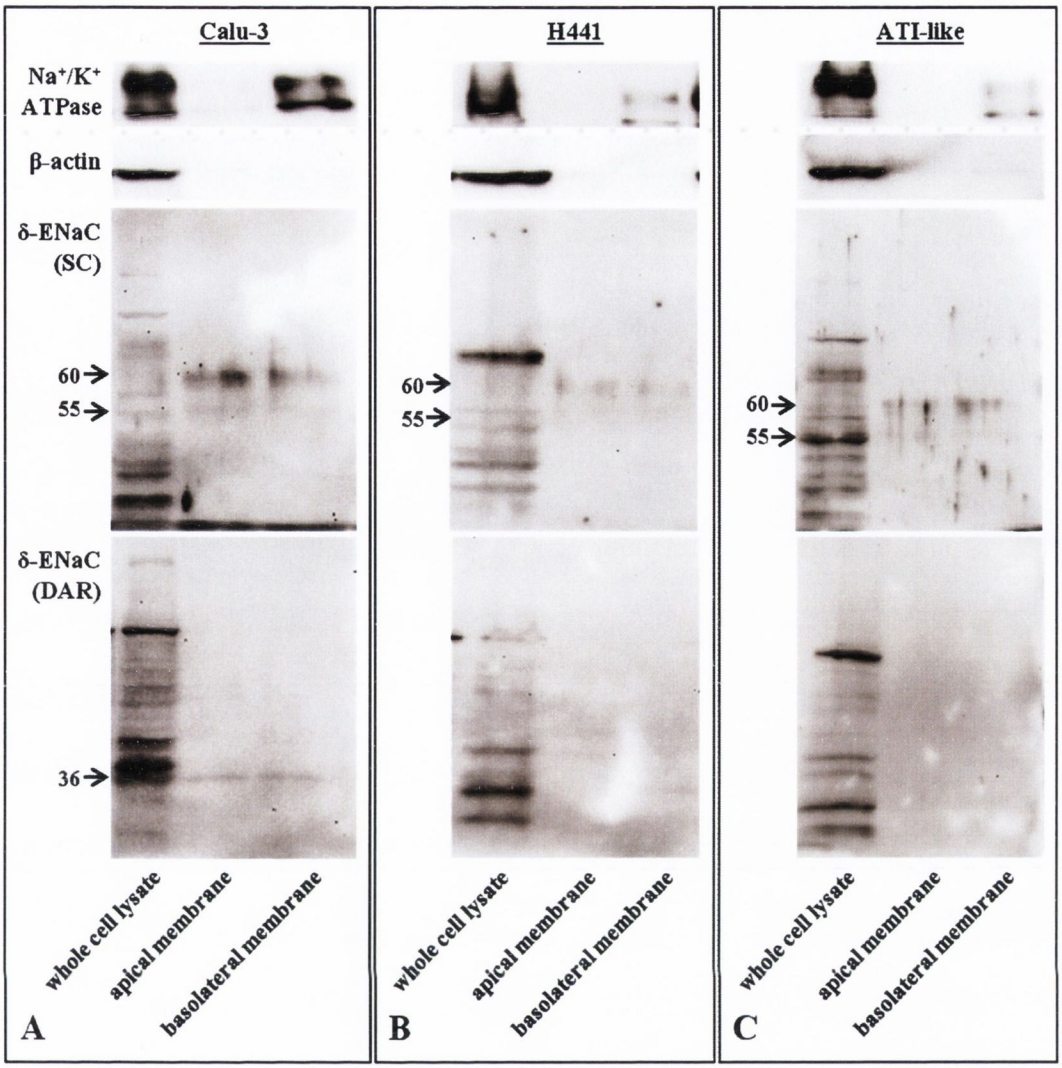

Figure 9. Representative Western blots of the whole cell lysates as well as of the apically and basolaterally biotinylated surface protein fractions from Calu-3 **(A)**, H441 **(B)** and human primary alveolar epithelial type I-like **(C)** cells obtained with anti-δ-ENaC SC and DAR antibodies, respectively. Arrows indicate the molecular weights of the protein bands detected in the biotinylated samples. Beta-actin and Na^+/K^+-ATPase were used as controls to exclude potential contamination of the biotinylated samples with intracellular non-biotinylated protein and contamination of the apical protein fraction with basolateral protein, respectively.

3.2.5 Localisation of δ-ENaC in human respiratory epithelial cells

According to the results of the cell surface biotinylation and subsequent Western blot analysis using both SC and DAR anti-δ-ENaC antibodies, no full-length δ-ENaC protein was present in the cell membranes of Calu-3, H441 or primary ATI-like cells. To obtain a more detailed insight into the subcellular localisation of the protein and its fragments, the respective cells were grown on Transwell Clear filter inserts and immunostained using SC, DAR and TF anti-δ-ENaC antibodies. To ensure that the formed cell monolayers were confluent and polarised, TEER values were measured prior to the fixation and permeabilisation procedure. Further, cells were stained for Na^+/K^+-ATPase, as a marker for the basolateral membrane, for zonula occludens ZO-1 protein, to demonstrate presence of functional tight junctions, and for cytokeratin, as a cytoskeletal element. Unfortunately, no antibody suitable as an apical control could be successfully optimised. Cell nuclei were counterstained with propidium iodide. The obtained immunofluorescence images of Calu-3, H441 and ATI-like cells are shown in **Figure 10, 11 and 12**, respectively.

Transepithelial electrical resistance values were > 1300 $\Omega \cdot cm^2$ for both Calu-3 and H441 cells and > 2000 $\Omega \cdot cm^2$ for ATI-like cell monolayers. Additionally, staining for the tight junction protein ZO-1, found mostly along intercellular contacts, was intact and of high intensity and, therefore, confirmed the confluence of the respective cell monolayers as well as the presence of intact cell-to-cell contacts. Na^+/K^+-ATPase was shown to be localised in the basolateral membrane and in intracellular storage vesicles. Moreover, staining for cytokeratin revealed organised arrangement of the filaments underneath the cell membranes. Thus, cells, used to investigate cellular localisation of δ-ENaC, were confirmed to form well-defined, tight polarised cell monolayers with well-developed cellular contacts.

Signals obtained with the anti-δ-ENaC SC antibody were of rather low intensity and dot-like appearance in all cell types tested. The signal was mainly diffusely distributed in the cytoplasm, although slightly stronger staining was observed in the perinuclear region. This could be possibly due to the detected protein being localised in intracellular storage vesicles. No membrane localisation of δ-ENaC could be detected with the SC antibody in either cell type.

Staining with the anti-δ-ENaC DAR antibody showed similar punctate pattern as with the SC antibody, thus, localisation of δ-ENaC protein in the vesicular storage pool appears likely. However, the obtained fluorescent signals were of higher intensity and more defined than in the case of the SC antibody. For H441 and ATI-like cells, the staining was mainly perinuclear, whereas accumulation of the signal along the cell borders, but most likely not in the cell membrane, was observed in Calu-3 cells. These findings were consistent with the results of the cell surface biotinylation, where no δ-ENaC protein or protein fragments were found in the membranes of H441 cells and merely a 36 kDa protein fragment was detected in the membranes of Calu-3 cells using the DAR antibody.

Whilst optimisation of the anti-δ-ENaC antibody TF for the Western blot application was not successful, the antibody proved to be suitable for immunofluorescence microscopy. The TF staining was of a less punctate character than in the cases of SC and DAR antibodies. The localisation of the fluorescent signal, however, was similar to that obtained with the DAR antibody. In H441 and ATI-like cells, δ-ENaC signals were perinuclear with little or no signal detected along the cell borders. In Calu-3 cells, in contrast, staining was localised along the cell membranes, however, most likely not in the cell membranes.

In summary, immunofluorescence staining with DAR and TF anti-δ-ENaC antibodies revealed distinct localisation of δ-ENaC in H441 and ATI-like *versus* Calu-3 cells. The fluorescent signals were mainly perinuclear in H441 and ATI-like cells, but mostly perimembranous in Calu-3 cells. Consistent with the results of the cell surface biotinylation, no δ-ENaC protein was detected in the cell membranes. Due to the punctate character of the staining, vesicular localisation of the detected protein seems likely. In the case of SC antibody, the staining was rather diffuse and, therefore, inconclusive in all cell types tested.

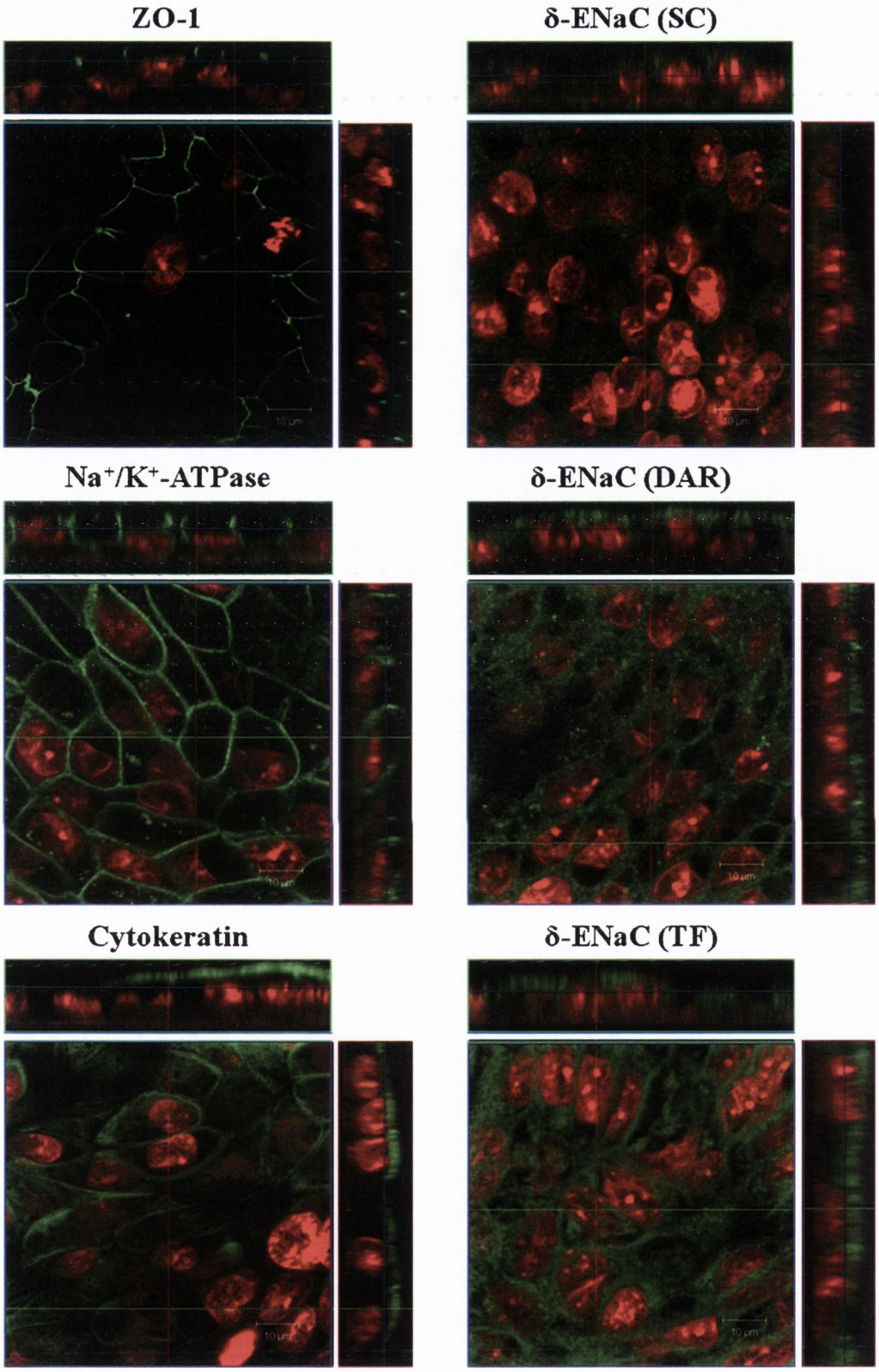

Figure 10. Immunofluorescence microscopy for δ-ENaC as well as for ZO-1, Na^+/K^+-ATPase and cytokeratin (all green) as cellular markers in human bronchial epithelial Calu-3 cells grown on Transwell Clear filter inserts. Delta-ENaC signals were detected using anti-δ-ENaC SC, DAR and TF antibodies (green). Cell nuclei were counterstained with propidium iodide (red).

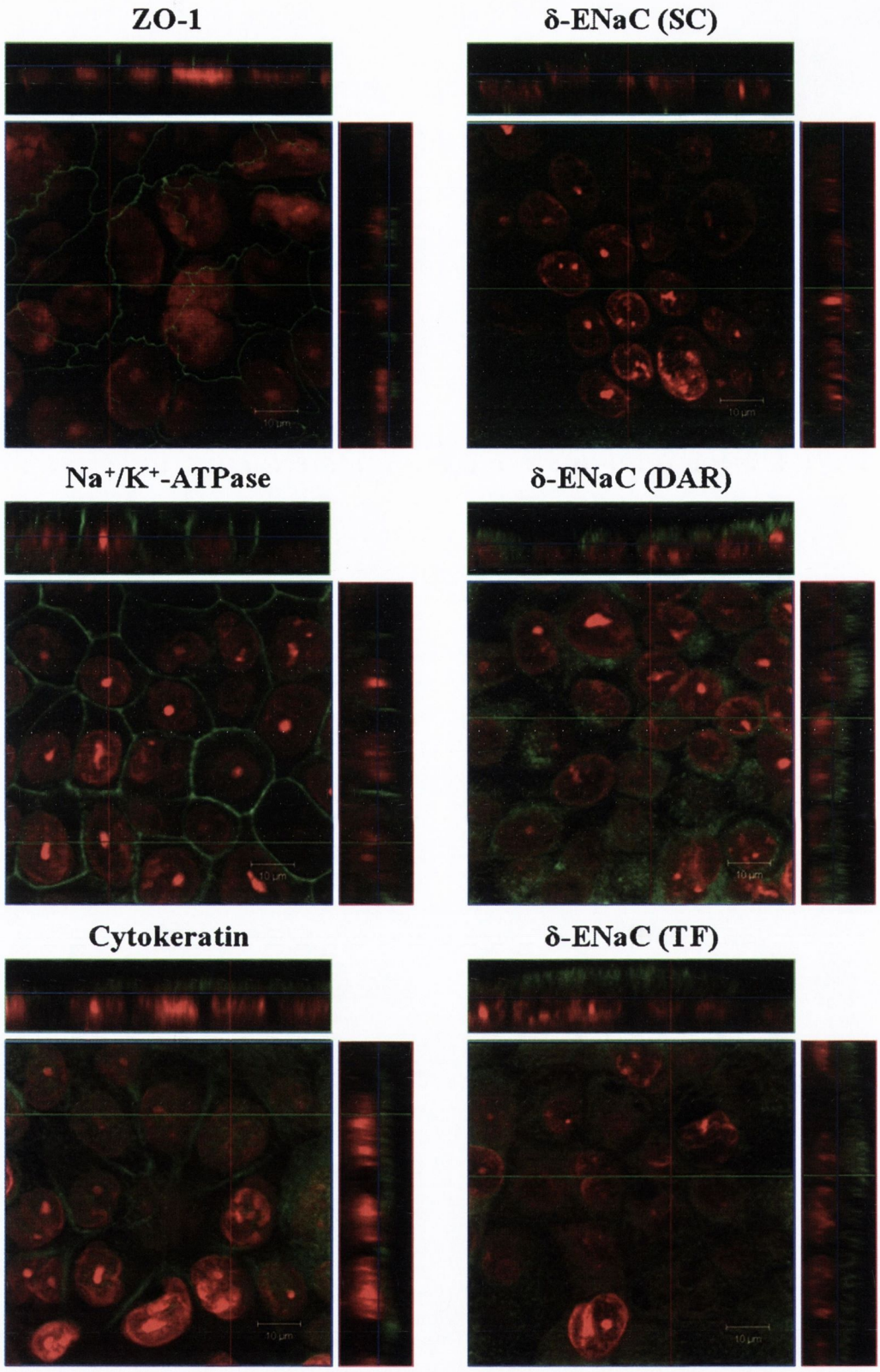

Figure 11. Immunofluorescence microscopy for δ-ENaC as well as for ZO-1, Na^+/K^+-ATPase and cytokeratin (all green) as cellular markers in human bronchiolar epithelial H441 cells grown on Transwell Clear filter inserts. Delta-ENaC signals were detected using anti-δ-ENaC SC, DAR and TF antibodies (green). Cell nuclei were counterstained with propidium iodide (red).

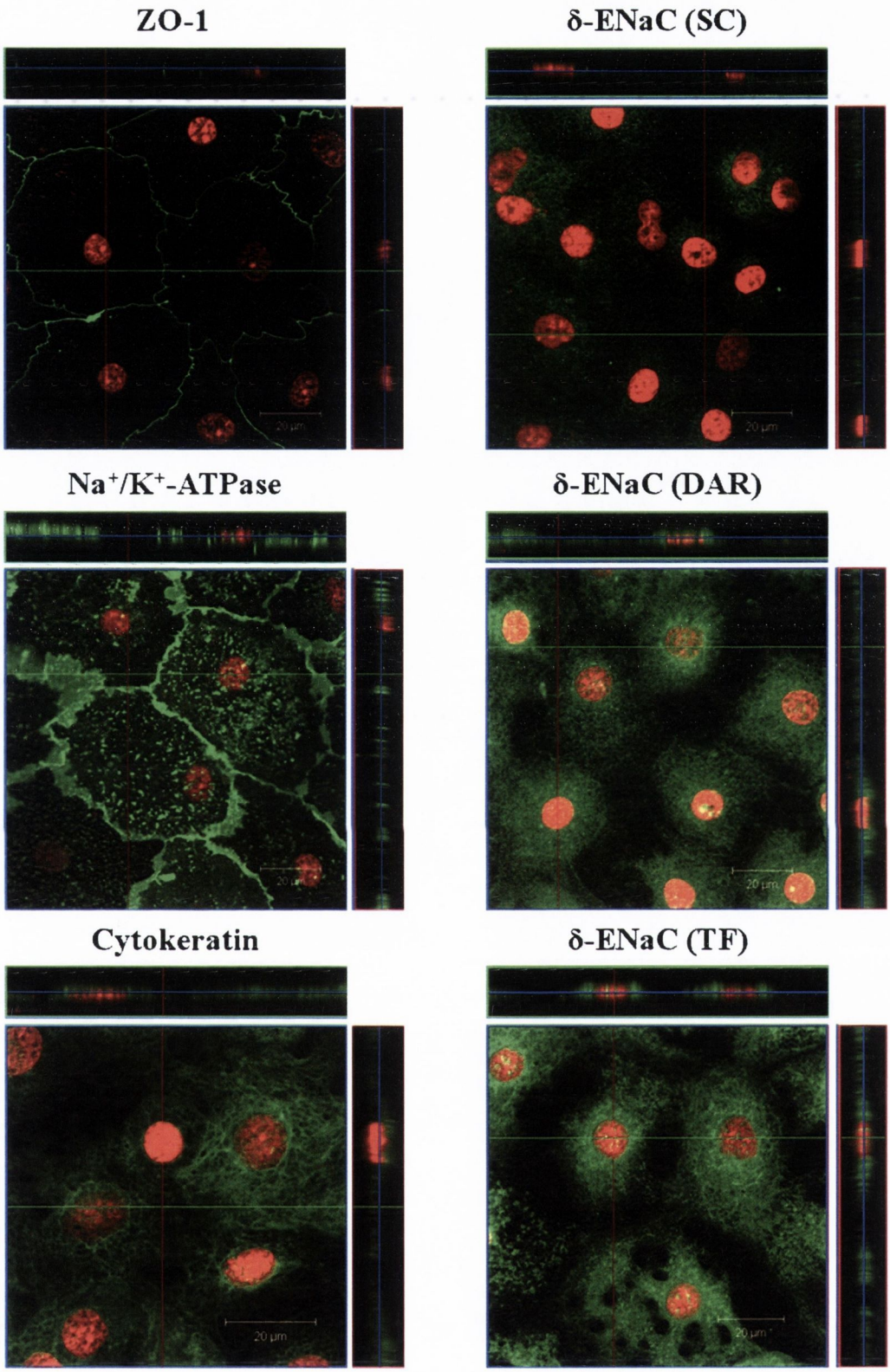

Figure 12. Immunofluorescence microscopy for δ-ENaC as well as for ZO-1, Na^+/K^+-ATPase and cytokeratin (all green) as cellular markers in primary human alveolar epithelial type I-like cells grown on Transwell Clear filter inserts. Delta-ENaC signals were detected using anti-δ-ENaC SC, DAR and TF antibodies (green). Cell nuclei were counterstained with propidium iodide (red).

CHAPTER 4

Functional analysis of δ-ENaC in human respiratory epithelial cells

To answer the question, whether δ-ENaC subunits, present in respiratory epithelial Calu-3, H441 and ATI-like cells, assemble to functional channels (together with α-, β-, and γ- subunits or on their own), functional transepithelial measurements in modified Ussing chambers were performed, using confluent cell monolayers of the respective cell type. To date, only a small number of pharmacological tools have been characterised for their interaction with δ-ENaC. The potassium sparing diuretic, amiloride, as well as its analogue, benzamil, block δ-ENaC-mediated currents ($K_{0.5(amiloride)}$ = 2.6 μM; $K_{0.5(benzamil)}$ = 0.27 μM). They also inhibit α-ENaC-mediated currents at about 30-fold lower concentrations ($K_{0.5(amiloride)}$ = 80 nM; $K_{0.5(benzamil)}$ = 7 nM; Waldmann *et al.* 1995) and, therefore, do not allow a selective analysis of δ-ENaC function in systems expressing more than one subunit. Yamamura and colleagues suggested that Evans blue was a selective inhibitor ($K_{0.5(Evans\ blue)}$ = 143 μM; Yamamura et al. 2005). The same group also published icilin and capsazepine as selective activators ($K_{0.5(icilin)}$ = 33 μM; $K_{0.5(capsazepine)}$ = 8 μM; Yamamura et al. 2005a, 2004) of δ-ENaC function. In *Xenopus laevis* oocytes injected with either δ-, δβγ- or α-, αβγ-cRNA, these substances were reported to modulate δ-, but not α-ENaC-mediated currents. Although known to be pharmacological modulators of other targets in more complex *in vitro* and *in situ* models (Bultmann and Starke, 1993; Bevan *et al.* 1992; Behrendt *et al.* 2004; Andersson *et al.* 2004), these three compounds were used for functional assessment of δ-ENaC in this work, due to the lack of more suitable pharmacological tools.

4.1 Basal currents' characteristics in human respiratory epithelial cells

For Ussing chamber studies, bronchial Calu-3 and bronchiolar H441 epithelial cells as well as human primary alveolar epithelial type I-like cells were grown on permeable filter supports and usually developed TEER values >200 $\Omega \cdot cm^2$ by day 7 in culture, as shown in **Figure 1**. **Table 1** summarises typical bioelectrical characteristics of the cell monolayers used for the transepithelial measurements.

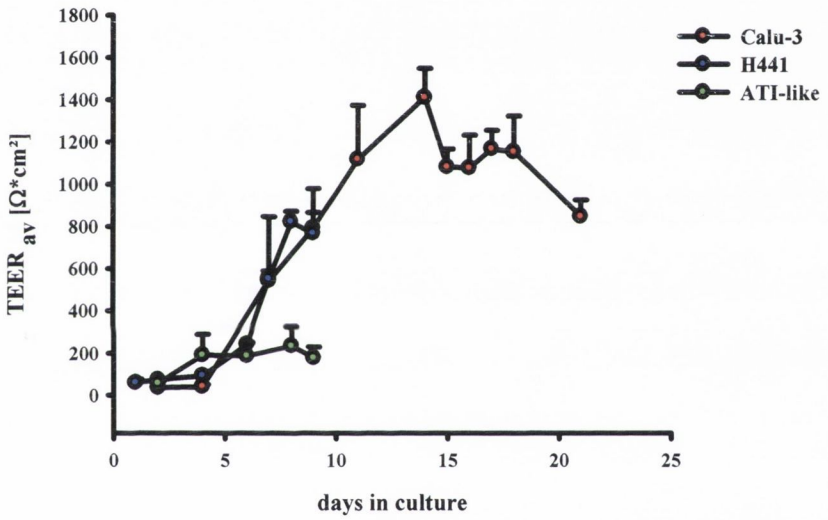

Figure 1. Development of transepithelial electrical resistances over time in Calu-3, H441 and ATI-like cell monolayers grown on permeable filter inserts.

Table 1. Transepithelial potential difference (PD) and basal short-circuit current (I_{SC}) values as electrophysiological characteristics of human respiratory epithelial cell monolayers used for Ussing chamber experiments. Values are given as means ± SD (n = 12 - 124).

	Calu-3	H441	ATI-like cells
PD [mV]	-3.7 ± 1.9	-7.3 ± 3.2	-0.8 ± 0.3
basal I_{SC} [µA/cm²]	6.5 ± 1.9	8.9 ± 4.0	7.3 ± 3.1

Prior to the testing of the δ-ENaC modulators, the function of the key ion channels involved in pulmonary fluid homoeostasis was studied in Calu-3 and H441 monolayers. Results of this characterisation are presented in **Figure 2**.

In Calu-3 monolayers, removal of Na^+ ions from the bathing solution resulted in a decrease of the basal short-circuit current from 6.3 ± 2.7 μA/cm^2 (n = 7) to -4.4 ± 3.7 μA/cm^2 (n = 17). However, the basal currents were amiloride-insensitive, with the apical administration of 10 μM amiloride leading to only a marginal decrease in I_{SC} (5.6 ± 2.4 μA/cm^2; n = 7). This suggests that the basal I_{SC} of Calu-3 monolayers was Na^+-dependent, but not primarily mediated through amiloride-sensitive αβγ-ENaC. Removal of Cl^- ions also led to a decrease of basal I_{SC} levels (1.9 ± 2.8 μA/cm^2, n = 17). Additionally, 69.8 ± 16.7% of the basal current were blocked by 10 μM $CFTR(inh)_{172}$. Short-circuit currents after application of the CFTR-inhibitor (2.0 ± 1.3 μA/cm^2, n = 20) were not significantly different from those measured in Cl^--free KRB, indicating that the basal currents in Calu-3 cell monolayers were mostly Cl^- dependent and mediated by CFTR.

In H441 monolayers, the basal I_{SC} was significantly ($P < 0.01$) reduced from 8.8 ± 3.3 μA/cm^2 (n = 8) to 0.0 ± 0.6 μA/cm^2 (n = 7) by Na^+ removal from the bathing solution. In addition, 88.9 ± 6.1% (n = 8) of the basal short-circuit current were blocked by 10 μM amiloride, reducing the I_{SC} to 0.8 ± 0.4 μA/cm^2 (n = 8) and indicating that the basal currents in H441 cells were amiloride-sensitive Na^+ currents, mostly mediated by αβγ-ENaC.

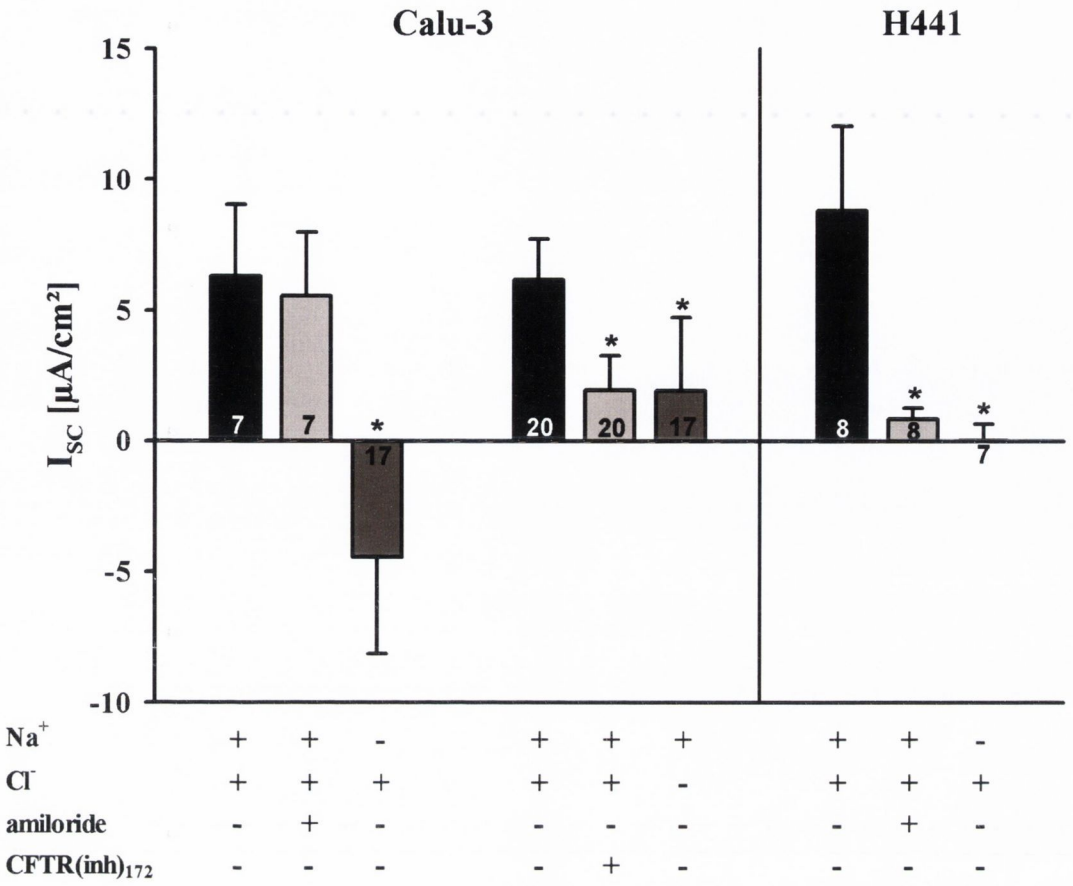

Figure 2. Characterisation of the basal short-circuit currents in Calu-3 and H441 cell monolayers. Na^+- and Cl^--dependencies were assessed as well as amiloride-sensitivity and mediation by CFTR. Results are expressed as means ± SD (n = 7-20). The statistical significance of the difference is expressed as *, $P < 0.01$ versus basal I_{SC}.

4.2 Effects of Evans blue in human respiratory epithelial cells

Surprisingly, Evans blue (EB) which had been suggested to be a selective inhibitor of δ-ENaC function increased I_{SC}, when added apically to Calu-3 cell monolayers. After removal of the EB-containing solution, short-circuit currents recovered and returned to the basal levels. The increase produced by EB was concentration-dependent. **Figure 3** shows representative I_{SC} traces obtained at low to high concentrations of EB (50, 100 and 300 μM) **(A)** as well as the concentration-response curves at different time points (15 and 30 min, n = 3-14), after adding the compound **(B)**. The EC_{50} values for the respective time points were determined and were 70.7 ± 38.4 μM at 15 min and 84.6 ± 37.0 μM at 30 min after addition of EB to the apical compartment.

Whilst activating I_{SC} in bronchial Calu-3 cells, EB decreased I_{SC} in H441 cells in a concentration-dependent manner, with 55.7 ± 5.7% and 73.4 ± 10.7% of the basal I_{SC} being sensitive to 100 and 300 μM EB (n = 3-12) **(C)**, respectively. In primary alveolar epithelial type I-like cells, 62.5 ± 10.0% and 76.3 ± 4.2% of the basal I_{SC} were blocked by 100 and 300 μM Evans blue (n = 3). These effects were fully reversible after removal of EB from the apical compartment. The quantification of the EB effects in human respiratory epithelial cells is shown in **Figure 3 (D)**.

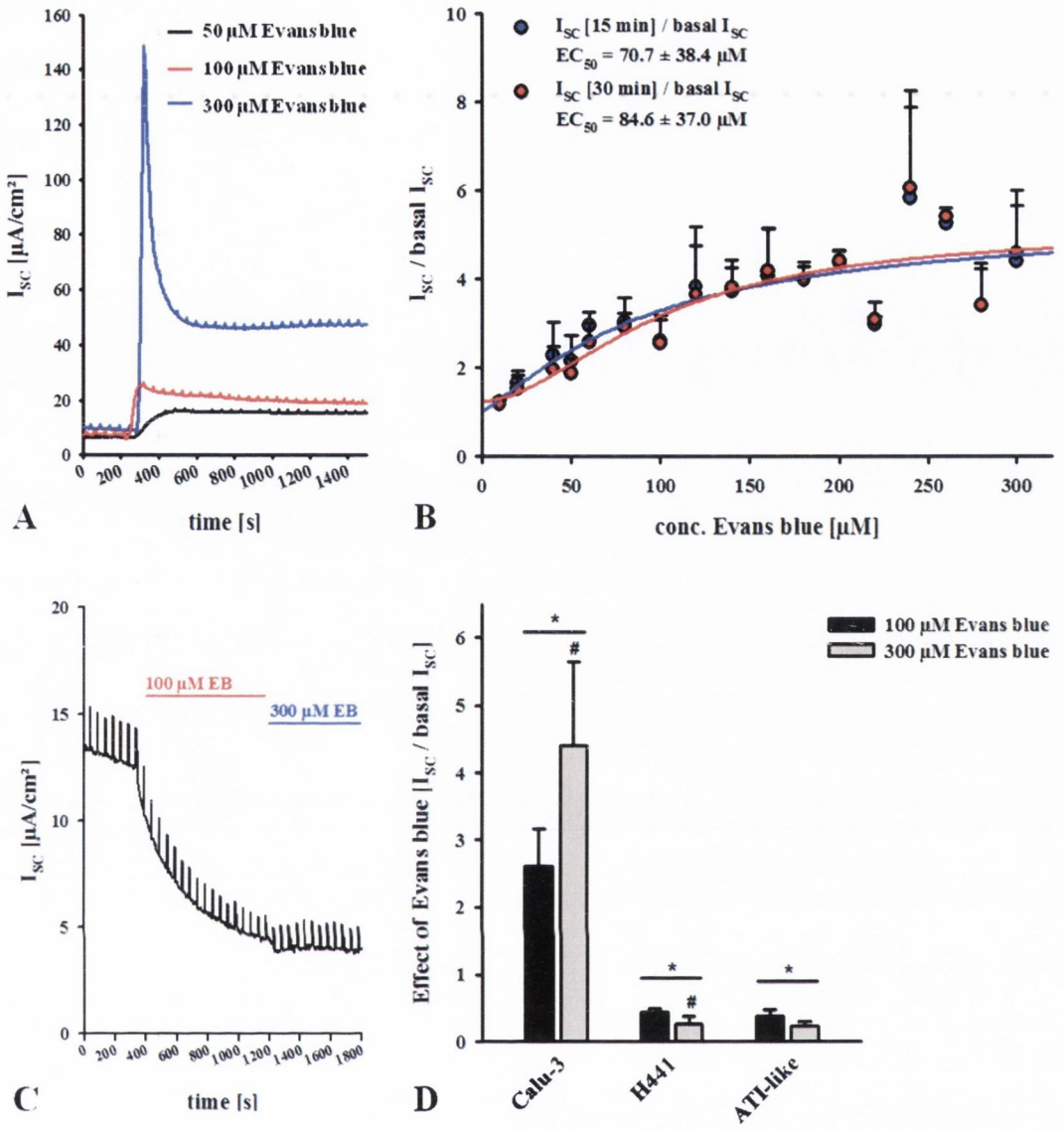

Figure 3. Delta-ENaC inhibitor Evans blue (EB) increased I_{SC} of Calu-3 cell monolayers, when added apically, but had an inhibiting effect on I_{SC} in H441 and ATI-like cells. **(A)** Overlay of the representative current traces of the responses to 50, 100 and 300 µM EB in Calu-3 cells. Short-circuit currents were measured at 15 and 30 min, after adding the compound and normalised by the basal I_{SC} in the absence of EB. The concentration-response curves and the resulting EC_{50} values (70.7 ± 38.4 µM and 84.6 ± 37.0 µM after 15 and 30 min, respectively) are shown in **(B)**. **(C)** Sample current trace of the responses to subsequent addition of 100 and 300 µM EB in H441 cells. **(D)** Quantification of the 15 min response to 100 and 300 µM EB in Calu-3, H441 and ATI-like cells. Results expressed as means ± SD (n = 3-14). The statistical significance of the effect versus basal I_{SC} is expressed as *, $P < 0.01$, versus I_{SC} in response to 100 µM EB as #, $P < 0.01$.

The dependence of the observed currents on the presence of sodium and chloride ions was also investigated. The effects of Na^+ and Cl^- removal as well as of the inhibition of amiloride-sensitive and CFTR-mediated currents on Evans blue-evoked responses in Calu-3 cell monolayers are summarised in **Figure 4**.

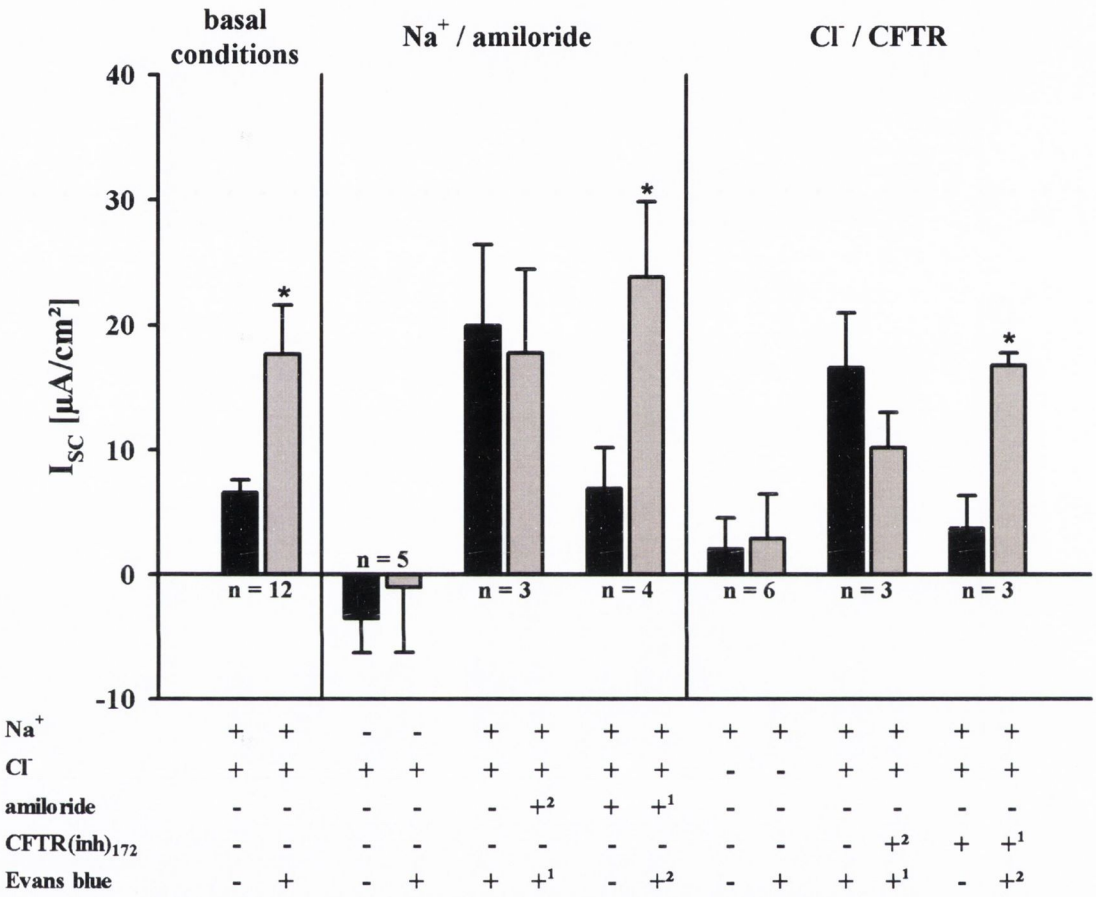

Figure 4. Sodium and chloride-dependence of the apical response to 100 µM EB in Calu-3 cell monolayers. I_{SC} values measured 15 min after addition of the compounds are shown. Results are expressed as means ± SD (n = 3-12). The statistical significance of the differences is expressed as *, $P < 0.01$ versus basal I_{SC}, I_{SC} in the presence of 10 µM amiloride or 10 µM $CFTR(inh)_{172}$, respectively.

[1]: substance was added first

[2]: substance was added 30 min after the first compound

When added apically to Calu-3 cell monolayers in KRB, EB significantly increased I_{SC} from 6.6 ± 1.0 to 17.7 ± 3.9 μA/cm^2 (n = 12, measured 15 min after adding the compound). In Na^+-free KRB, EB led to a non-significant increase of I_{SC} from -3.6 ± 2.8 to -1.0 ± 5.2 μA/cm^2 (n = 5, 15 min after addition of EB), with the amplitude of the increase being significantly lower than under standard conditions ($P < 0.01$). In the presence of 10 μM amiloride, EB increased the short-circuit currents to the level of 23.8 ± 6.0 μA/cm^2 (n = 4) after 15 min, showing no significant difference in the resulting I_{SC} or the amplitude of the increase to the currents induced by EB in the absence of amiloride. In addition, 10 μM amiloride had no significant effect on the EB-stimulated currents, merely reducing the I_{SC} from 20.0 ± 6.5 to 17.8 ± 6.7 μA/cm^2 (n = 3).

In Cl^--free medium, no significant activation of the short-circuit currents was observed 15 min after addition of EB (n = 6). The presence of $CFTR(inh)_{172}$ did not abolish the increase in current by EB. When added after the CFTR-inhibitor, EB increased the I_{SC} to 16.8 ± 1.0 μA/cm^2 (n = 3, response after 15 min). Both the resulting I_{SC} as well as the amplitude of the current activation were not significantly different from the values in the absence of $CFTR(inh)_{172}$. When $CFTR(inh)_{172}$ was added after EB, the decrease in the I_{SC} was not significant (from 16.6 ± 4.4 to 10.2 ± 2.8 μA/cm^2; n = 3).

In summary, these measurements indicate that currents induced by EB in Calu-3 cell monolayers were both Na^+ and Cl^--dependent, however, amiloride-insensitive and not mediated by CFTR channels.

As shown in **Figure 5**, in H441 cells, 300 μM EB inhibited the I_{SC} by 72.5 ± 11.2%, significantly decreasing the short-circuit current from 8.2 ± 3.5 to 2.4 ± 1.4 μA/cm² (n = 9). Addition of 10 μM amiloride led to a further significant reduction of I_{SC} to the level of 7.5 ± 11.1% of the basal I_{SC} (0.5 ± 0.5 μA/cm^2; n = 8). The I_{SC} resulting from

application of both EB and amiloride was not significantly different from the I_{SC} reduced by amiloride alone. In Na^+-free bathing solution, administration of EB did not lead to a significant effect on the I_{SC} (-0.5 ± 0.4 and -0.5 ± 0.6 μA/cm^2 prior and after the administration of EB, respectively; n = 3). All in all, currents inhibited by EB in H441 cells were amiloride-sensitive Na^+ currents.

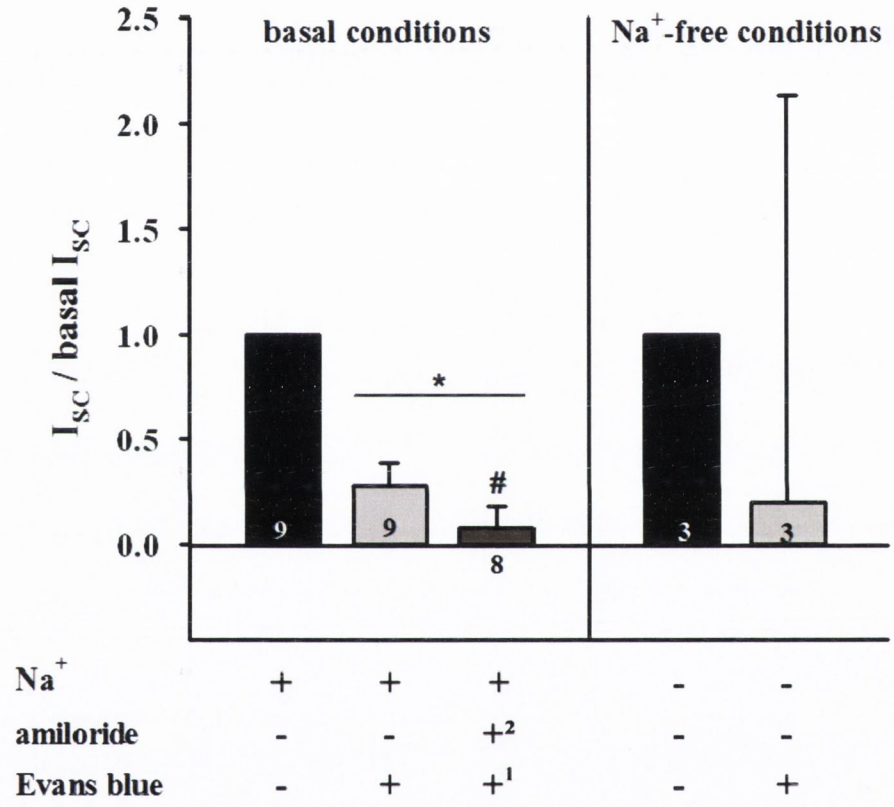

Figure 5. Sodium-dependence of the apical response to 300 μM EB in H441 cells. Results are expressed as means ± SD (n = 3-9). The statistical significance of the differences is expressed as *, $P < 0.01$ versus the basal I_{SC} and as #, $P < 0.01$ versus the I_{SC} in the presence of 300 μM EB.

[1]: substance was added first

[2]: substance was added 30 min after the first compound

4.3 Effects of capsazepine in human respiratory epithelial cells

In our hands, the assumed activator of δ-ENaC function, capsazepine, inhibited I_{SC} in Calu-3 cell monolayers in a concentration-dependent manner, when added apically, with an estimated IC_{50} of 20.2 ± 3.2 μM (**Figure 6 (B)**). Short-circuit currents in H441 and ATI-like cells were also inhibited. The effects of 20 μM capsazepine added to the apical compartments of the respective cell monolayers were quantified and summarised in **Figure 6 (C)**. The inhibition values accounted for 38.6 ± 12.3% in Calu-3 (n = 12), 32.3 ± 9.9 and 43.5 ± 21.3% in H441 (n = 9) and ATI-like cells (n = 4), respectively.

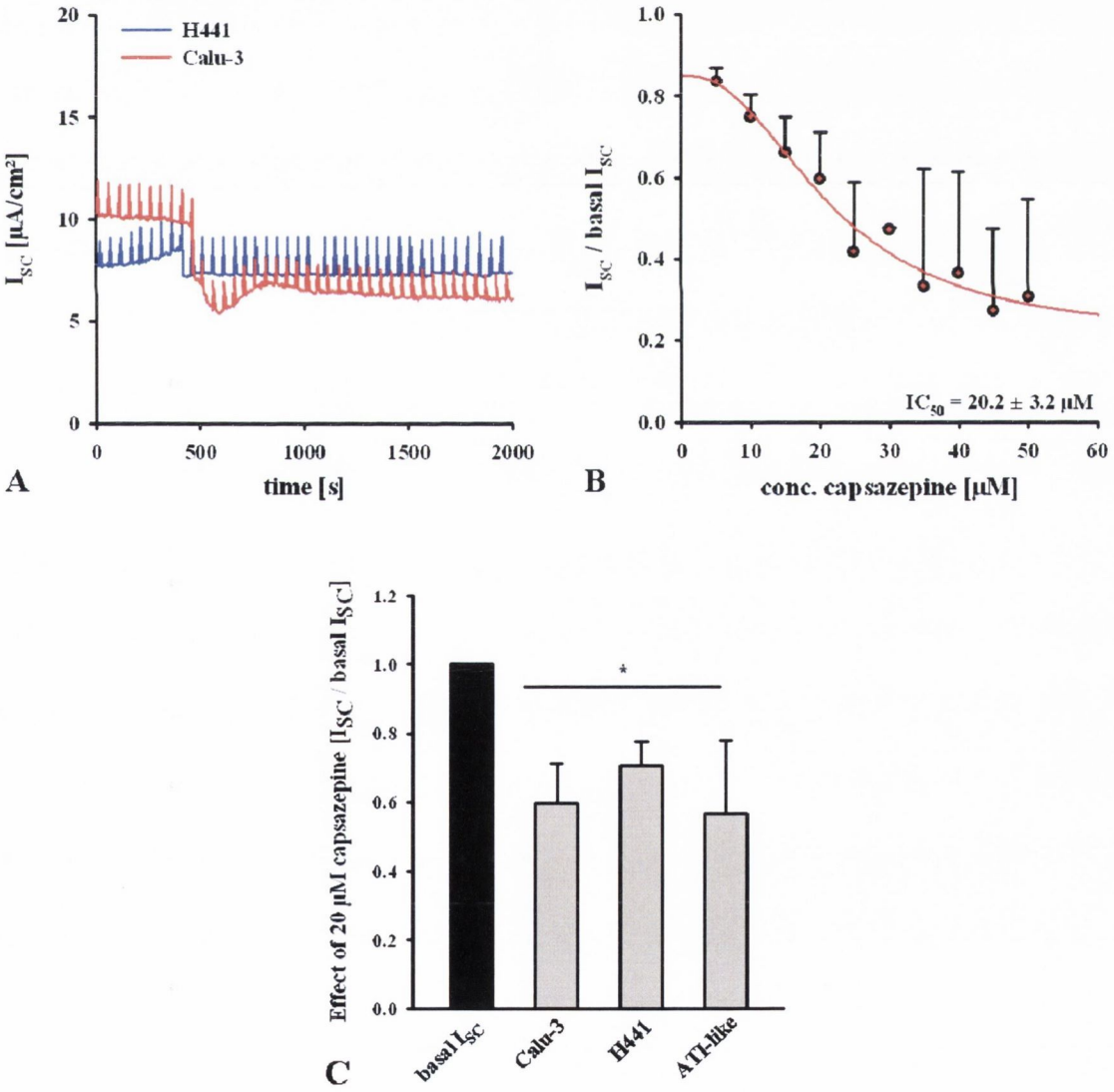

Figure 6. The alleged δ-ENaC activator, capsazepine, decreased I_{SC} in human respiratory epithelial cell monolayers. Representative current traces in response to 20 μM capsazepine in H441 and Calu-3 cells are shown in **(A)**. **(B)** Concentration-response curve for capsazepine in Calu-3 cells (IC_{50} = 20.2 ± 3.2 μM). Short-circuit current values were measured 5 min after adding the compound and normalised against basal I_{SC}. **(C)** Quantification of the responses to 20 μM capsazepine in Calu-3, H441 and ATI-like cells. Results are expressed as means ± SD (n = 4-12). The statistical significance of the effect versus basal I_{SC} is expressed as *, $P < 0.01$.

The dependence of the capsazepine-induced decrease in I_{SC} in Calu-3 cells on the ion composition of the bathing medium is shown in **Figure 7**. When Na^+ was removed from the bathing solution, apical response to 20 μM capsazepine changed from a significant decrease (from 6.8 ± 1.4 to 4.2 ± 1.2 μA/cm^2; n = 12) to a significant, albeit a transient, increase in short-circuit current (from -4.2 ± 3.3 to 3.5 ± 1.5 μA/cm^2; n = 4). In the presence of capsazepine, no additional inhibition of I_{SC} by amiloride was observed. On the other hand, capsazepine, added in the presence of 10 μM amiloride, decreased I_{SC} levels with an amplitude comparable to that in absence of amiloride (from 5.0 ± 1.6 down to 2.6 ± 2.0 μA/cm^2, n = 3). Additionally, the resulting I_{SC} were not significantly different from the short-circuit currents diminished by capsazepine alone.

Removal of Cl^- ions from the bathing solution did not abolish the capsazepine-induced decrease in I_{SC}, although this did not quite reach significance. The short-circuit currents were reduced from 0.2 ± 1.4 to -1.9 ± 1.3 μA/cm^2 (n = 5). The resulting I_{SC} was significantly different from the I_{SC} in response to capsazepine under standard conditions (from 6.8 ± 1.4 to 4.2 ± 1.2 μA/cm^2; n = 12) which was due to significantly different basal currents. The amplitudes of the responses, however, were not significantly different. $CFTR(inh)_{172}$ decreased the short-circuit current by the same amplitude in the presence and absence of capsazepine (-3.6 ± 0.6 μA/cm^2 (n = 3) and -4.2 ± 1.1 μA/cm^2

(n = 20), respectively). Capsazepine, added in the presence of CFTR(inh)$_{172}$, led to a further decrease in I_{SC} from 1.3 ± 0.5 to 0.1 ± 0.6 μA/cm^2 (n = 3).

These data in summary indicate that the decrease in short-circuit current, induced by capsazepine in Calu-3 cells, was dependent on the presence of Na^+, however, Cl^- and CFTR-independent and amiloride-insensitive.

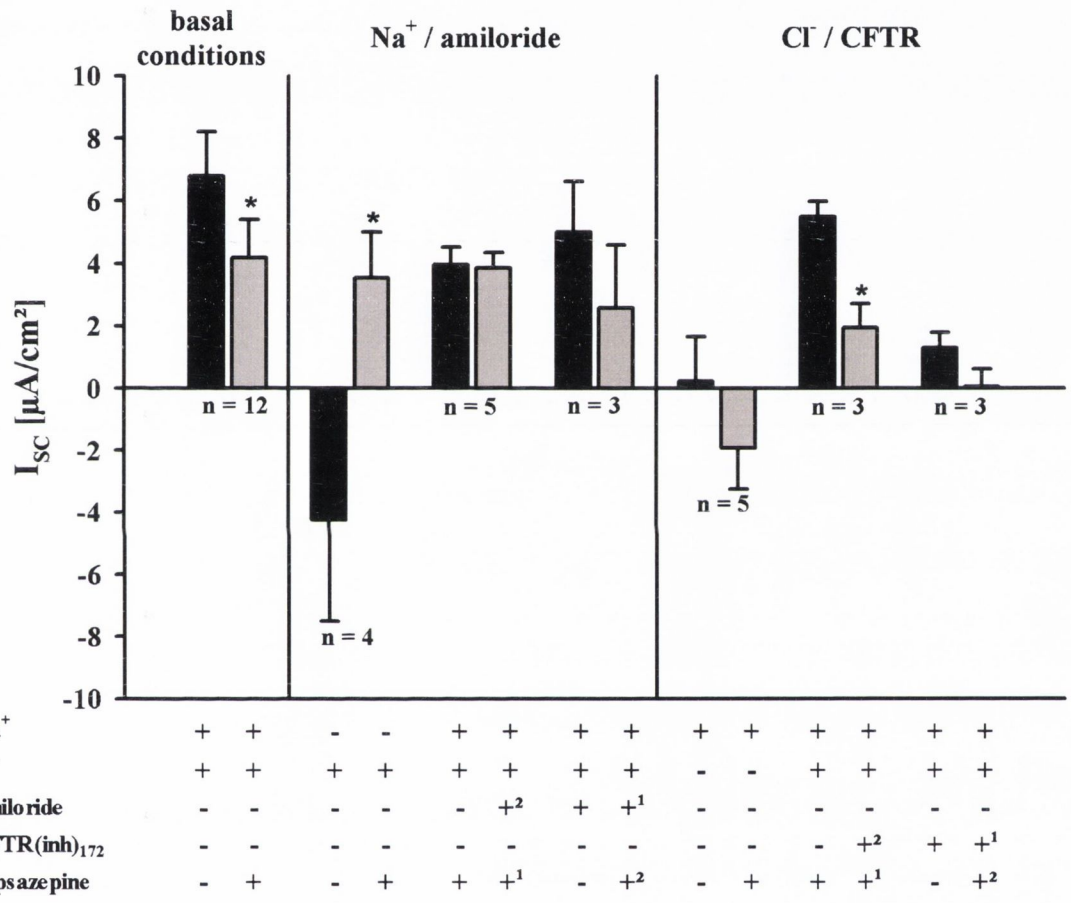

Figure 7. Effects of Na^+ and Cl^- removal as well as of the inhibition of the amiloride-sensitive and CFTR-mediated currents on the apical response to 20 μM capsazepine in Calu-3 cell monolayers. Results expressed as means ± SD (n = 3-12). The statistical significance of the differences is expressed as *, $P < 0.01$ versus the basal I_{SC}, I_{SC} in Na^+-free KRB as well as the I_{SC} in the presence of 20 μM capsazepine, respectively.

[1]: substance was added first

[2]: substance was added 30 min after the first compound

In H441 cells (**Figure 8**), 20 μM capsazepine decreased the short-circuit currents by 32.3 ± 9.9% (n = 9) under standard conditions. Addition of 10 μM amiloride reduced the I_{SC} further to 5.9 ± 7.6% of the basal I_{SC} (n = 7), a level comparable with the I_{SC} resulting from addition of amiloride alone. In the absence of Na^+, no significant capsazepine effect was observed (I_{SC} values of -0.1 ± 0.4 and -0.1 ± 0.3 μA/cm^2 were measured at the basal level and in the presence of capsazepine, n = 3), suggesting that the currents inhibited by capsazepine in H441 cells were Na^+-dependent and amiloride-sensitive.

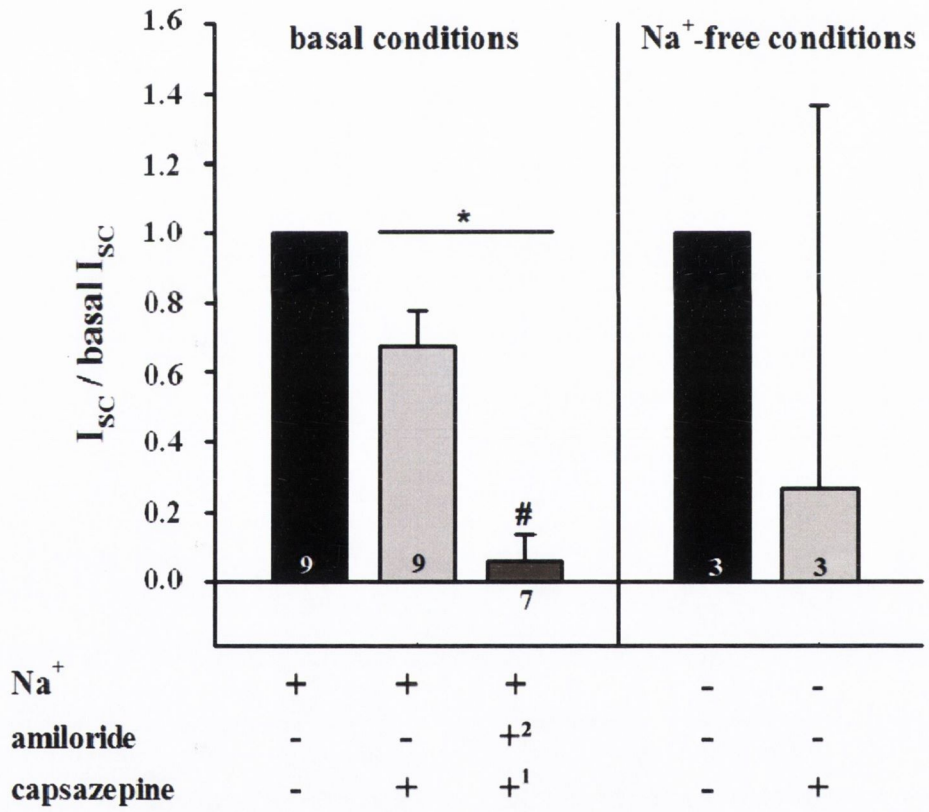

Figure 8. Sodium-dependence of the apical response to 20 μM capsazepine in H441 cells. Results expressed as means ± SD (n = 3-9). The statistical significance of the differences is expressed as *, $P < 0.01$ versus the basal I_{SC} and as #, $P < 0.01$ versus the I_{SC} in the presence of 20 μM capsazepine.

[1]: substance was added first

[2]: substance was added 30 min after the first compound

4.4 Effects of icilin in human respiratory epithelial cells

Apical administration of icilin, another activator of δ-ENaC suggested by Yamamura *et al.* (2005a), to Calu-3 cell monolayers resulted in a concentration-dependent increase of I_{SC} (EC_{50} = 41.0 ± 9.2 μM and 41.4 ± 8.4 μM; I_{SC} measured at 8 and 30 min after adding icilin, respectively; **Figure 9 (B)**). Short-circuit current was stimulated by 79.0 ± 29.5% (n = 15) by 60 μM icilin. This response was fully reversible after removal of the compound from the apical compartment. In H441 and ATI-like cells, however, an inhibitory effect on I_{SC} was observed with 21.4 ± 4.8 and 43.6 ± 12.8% of basal I_{SC} being inhibited by 60 μM icilin, respectively (n = 4-8) **(Figure 9 (C))**.

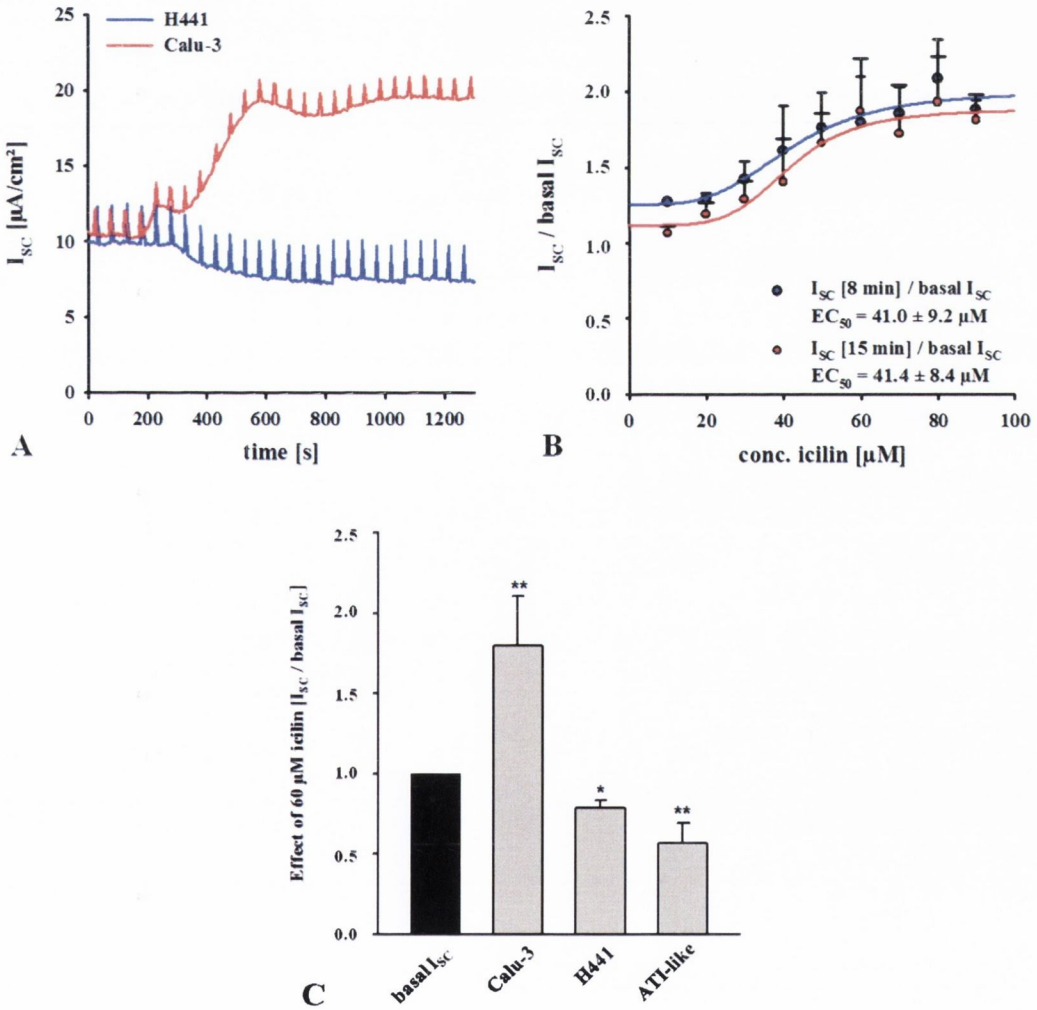

Figure 9. Whilst exhibiting inhibitory effects in H441 and ATI-like cells, icilin stimulated currents in Calu-3 cell monolayers. **(A)** Overlay of representative current traces in response to 60 μM icilin in H441 and Calu-3 cells. In Calu-3 cells, I_{SC} values were measured at 8 and 30 min after adding the compound and normalised against the basal I_{SC} in the absence of icilin. The concentration-response curves and the resulting EC_{50} values (41.0 ± 9.2 μM and 41.4 ± 8.4 μM after 8 and 30 min, respectively) are shown in **(B)**. **(C)** Quantification of the responses to 60 μM in Calu-3, H441 and ATI-like cells. Results are expressed as means ± SD (n = 4-14). The statistical significance of the effect versus the basal I_{SC} is expressed as **, $P < 0.01$ and as *, $P < 0.05$, respectively.

In Calu-3 cell monolayers, the short-circuit currents were elevated by 60 μM icilin under standard conditions, from 7.2 ± 2.2 μA/cm^2 to 12.6 ± 3.1 μA/cm^2 (delta I_{SC} = 5.4 ± 1.8 μA/cm^2, n = 15) at 8 min after adding the compound **(Figure 10)**. The resulting I_{SC} as well as the amplitude of the induced increase was not significantly different from those in the presence of 10 μM amiloride (from 4.3 ± 1.9 up to 10.7 ± 3.1 μA/cm^2, delta I_{SC} = 6.3 ± 1.2 μA/cm^2, n = 3). Moreover, 10 μM amiloride did not have a significant effect on the icilin-stimulated currents. After removal of Na^+ from the bathing solution, merely a transient icilin-induced increase was observed (I_{SC} increased from -7.1 ± 4.6 to 31.5 ± 5 μA/cm^2, n = 3).

Icilin decreased the I_{SC} in Cl^--free medium (from 4.4 ± 2.5 to 0.4 ± 3.9 μA/cm^2, n = 3). Although this effect did not quite reach significance, it was contrary to the I_{SC} increase in complete KRB. In the presence of CFTR-inhibitor, icilin increased the short-circuit current from 1.3 ± 0.9 to 3.1 ± 1.3 μA/cm^2 (n = 4), however, the resulting I_{SC} as well as the amplitude of the increase were significantly lower than in absence of CFTR-inhibitior (delta I_{SC} = 1.8 ± 1.3 μA/cm^2 (n = 4) and 5.4 ± 1.8 μA/cm^2 (n = 15) in the presence and absence of CFTR-inhibitor, respectively). Furthermore, when added after icilin, $CFTR(inh)_{172}$ completely abolished the increase induced by icilin. The resulting

I_{SC} of 2.9 ± 0.1 μA/cm^2 (n = 4) was significantly smaller than the basal current in Calu-3 cells and comparable with the I_{SC} levels in the presence of CFTR-inhibitor alone (2.0 ± 1.3 μA/cm^2, n = 20).

In summary, icilin-induced elevation of I_{SC} in Calu-3 cells was due to Na^+ and Cl^--dependent, CFTR-mediated, but amiloride-insensitive currents.

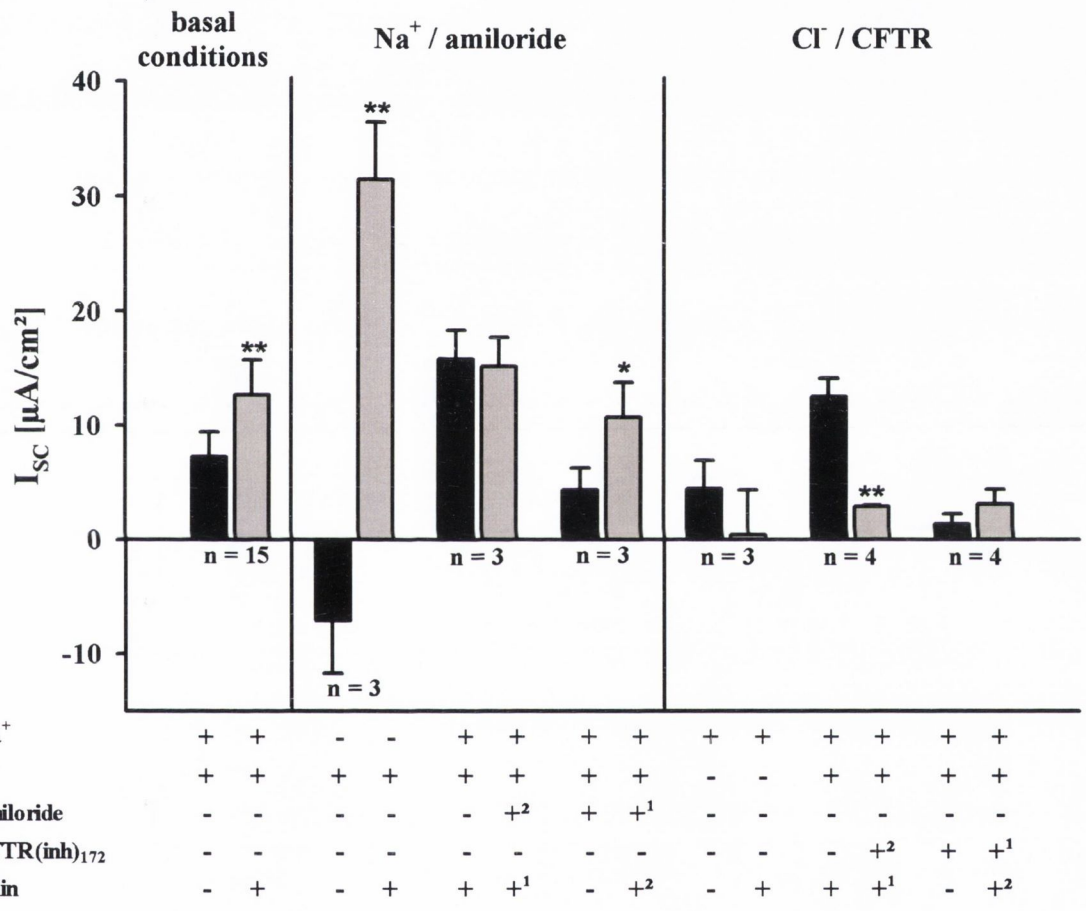

Figure 10. Sodium and chloride-dependence of the apical response to 60 μM icilin in Calu-3 cell monolayers. I_{SC} values measured 8 min after addition of the compounds are given. Results are expressed as means ± SD (n = 3-15). The statistical significance of the differences is expressed as *, $P < 0.05$ and **, $P < 0.01$ versus the basal I_{SC}, I_{SC} in Na^+-free KRB, as well as the I_{SC} in the presence of 60 μM icilin.

[1]: substance was added first

[2]: substance was added 30 min after the first compound

Effects of sodium removal from the bathing solution of H441 cell monolayers on the response to 60 μM icilin are shown in **Figure 11**. While decreasing the I_{SC} to 78.6 ± 4.8% of the basal level (n = 8) under standard conditions, icilin failed to produce a significant effect in Na^+-free KRB (I_{SC} levels of 0.5 ± 0.5 and 0.4 ± 0.4 μA/cm^2 (n = 3) were measured in the absence and presence of 60 μM icilin, respectively). When amiloride was added after icilin, an additional inhibition of the short-circuit current was observed. The resulting I_{SC} was not significantly different from the I_{SC} inhibited by amiloride alone. This indicates that, in H441 cell monolayers, currents inhibited by icilin were also amiloride-sensitive Na^+ currents.

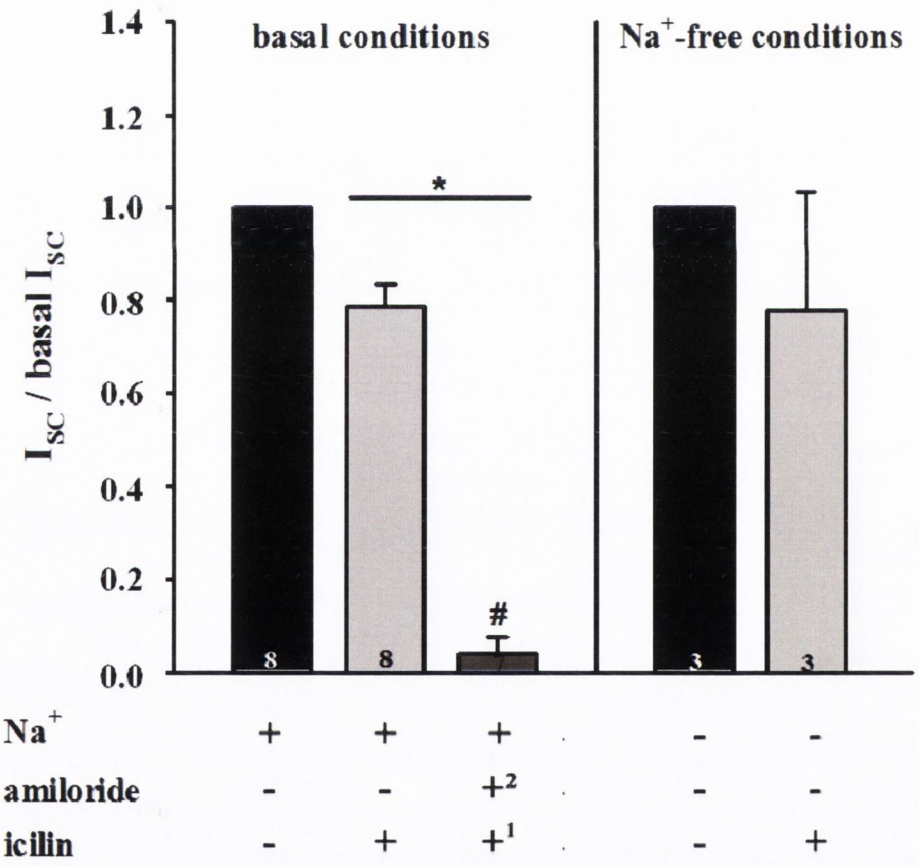

Figure 11. Sodium-dependence of the apical response to 60 μM icilin in H441 cells. Results are expressed as means ± SD (n = 3-8). The statistical significance of the differences is expressed as *, $P < 0.01$ versus the basal I_{SC} and as #, $P < 0.01$ versus the I_{SC} in the presence of 60 μM icilin.

4.5 Overview: Effects of the alleged δ-ENaC modulators in human respiratory epithelial cells

The pharmacological effects of the δ-ENaC activators, capsazepine and icilin, as well as of the inhibitor, Evans blue, were investigated in human respiratory epithelial cells as described above. **Table 2** gives an overview of the pharmacological effects observed and characterised in Ussing chamber studies as well as of those reported in literature.

Table 2. Summary of the effects of δ-ENaC modulators on δ-ENaC-mediated currents in *Xenopus laevis* oocytes and human nasal epithelial cells, as reported in literature, and on short-circuit currents in human respiratory epithelial cells, as determined in Ussing chamber measurements in this work. ↑ indicates current activation, ↓ indicates current inhibition. For Calu-3 and H441 cells, the nature of the activated or inhibited currents is described in regard to sodium and chloride dependence as well as amiloride-sensitivity and dependence on the function of the CFTR channel.

Compound	**δ- and δβγ-ENaC expressing *X. laevis*** (Yamamura *et al.* 2004b, 2005a, 2005b, Zhao *et al.* 2012)	**Human nasal epithelial cells** (Bangel-Ruland *et al.* 2010)	**Calu-3**	**H441**	**ATI-like cells**
Evans blue	↓ (Yamamura: IC_{50}: 143 μM)	↓ (19.8 ± 1.9% of total Na^+ absorption is sensitive to 300 μM EB)	↑ (EC_{50}: 70.7 ± 38.4 μM) • Na^+-dependent • amiloride-insensitive • Cl^--dependent • not CFTR-mediated	↓ • Na^+-dependent • amiloride-sensitive (73.4 ± 10.7% of basal I_{SC} is sensitive to 300 μM EB)	↓ (76.3±4.2% of basal I_{SC} is sensitive to 300 μM EB)
Capsazepine	↑ (Yamamura: EC_{50}: 8 μM) (Zhao: EC_{50}: 11.9 and 6.3 μM for $\delta_1\beta\gamma$- and $\delta_2\beta\gamma$, respectively)		↓ (IC_{50}: 20.2 ± 3.2 μM) • Na^+-dependent • amiloride-insensitive • Cl^--independent • not CFTR-mediated	↓ • Na^+-dependent • amiloride-sensitive	↓
Icilin	↑ (Yamamura: EC_{50}: 33 μM)		↑ (EC_{50}: 41.0 ± 9.2 μM) • Na^+-dependent • amiloride-insensitive • Cl^--dependent • CFTR-mediated	↓ • Na^+-dependent • amiloride-sensitive	↓

CHAPTER 5

Effects of down- and up-regulation of δ-ENaC expression in human respiratory epithelial cells

5.1 Effects of δ-ENaC knock-down in human respiratory epithelial cells

The presence of δ-ENaC protein in human respiratory epithelial H441 and Calu-3 cell lines as well as in human primary alveolar epithelial cells was demonstrated using biomolecular techniques, albeit no full-length protein could be detected in the cell membranes of the respective cells. In transepithelial measurements, application of the alleged δ-ENaC modulators, Evans blue, capsazepine and icilin led to pharmacological responses in the three cell models tested (i.e., Calu-3, H441 and ATI-like cell monolayers). Only the effects of Evans blue in H441 and ATI-like cells and icilin effects in Calu-3 cells were consistent with the observations reported by Yamamura *et al.* (2004, 2005, 2005a). In addition, analysis of the respective actions with respect to their Na^+ and Cl^- dependencies, and also involvement of CFTR, revealed their distinct nature, at least in Calu-3 cells. Taken together, these results seem incompatible with the assumption that the observed outcomes were exclusive to δ-ENaC activation and/or inhibition. Indeed, the compounds, which have been characterised as specific δ-ENaC modulators in a heterologous expression system, are also known to modulate other epithelial ion channels. Hence, it is conceivable that at least part of the effects observed in respiratory epithelial cell monolayers originated from interactions with proteins other than δ-ENaC. In particular, TRPM8, activated by icilin (Andersson *et al.* 2004), and P_2X-purinergic receptors, inhibitable by Evans blue (Bultmann and Starke, 1993), are candidates to be considered, since their functional expression has previously been described in human respiratory epithelial cells (Sabnis *et al.* 2008, Taylor *et al.* 1999).

Thus, in order to confirm the functional expression of δ-ENaC in human respiratory epithelial cell monolayers, it was studied which of the stimulatory/inhibitory effects of

the alleged δ-ENaC modulators, was the result of a specific and exclusive interaction with δ-ENaC. To this end, RNAi technique was utilised, aiming at down-regulation of δ-ENaC expression.

5.1.1 Transient knock-down strategies to down-regulate δ-ENaC expression

Initially, transient knock-down strategies were employed, in order to down-regulate δ-ENaC expression and, thus, its activity in human respiratory epithelial cells *in vitro*. In Calu-3 cells, transfection with specific siRNA directed against δ-ENaC was performed. H441 cells were transfected with dominant negative cDNA constructs (E35X), leading to knock-down of the functional full-length protein by over-expression of a truncated version.

In both cases, transfections were carried out using a number of different conditions, in the attempt to optimise the procedures. Protein samples were isolated 24, 48 and 72 h after transfection and analysed by Western blot to test for changes in protein abundance. Expression levels of δ-ENaC were evaluated by densitometric analysis and normalised by comparison to the β-actin loading control. However, no efficient knock-down could be obtained under any of the conditions tested. Some of the results from Calu-3 and H441 cell studies are shown in **Figure 1** and **2**, respectively.

Immunoblots of Calu-3 cells, which were transfected with 50 nM of δ-ENaC siRNA on day 3 after seeding, were probed with SC anti-δ-ENaC antibody. Lysates of cells transfected with scrambled, non-silencing siRNA were used as negative controls. Densitometric analysis was carried out for protein bands at 85 and 100 kDa. No reduction in δ-ENaC expression was detected 24 h after transfection **(Figure 1 (A))**. After 48 hours (**Figure 1 (B)**), signal intensity at 100 kDa showed a significant

reduction in δ-ENaC siRNA transfected cells, when compared to both non-transfected

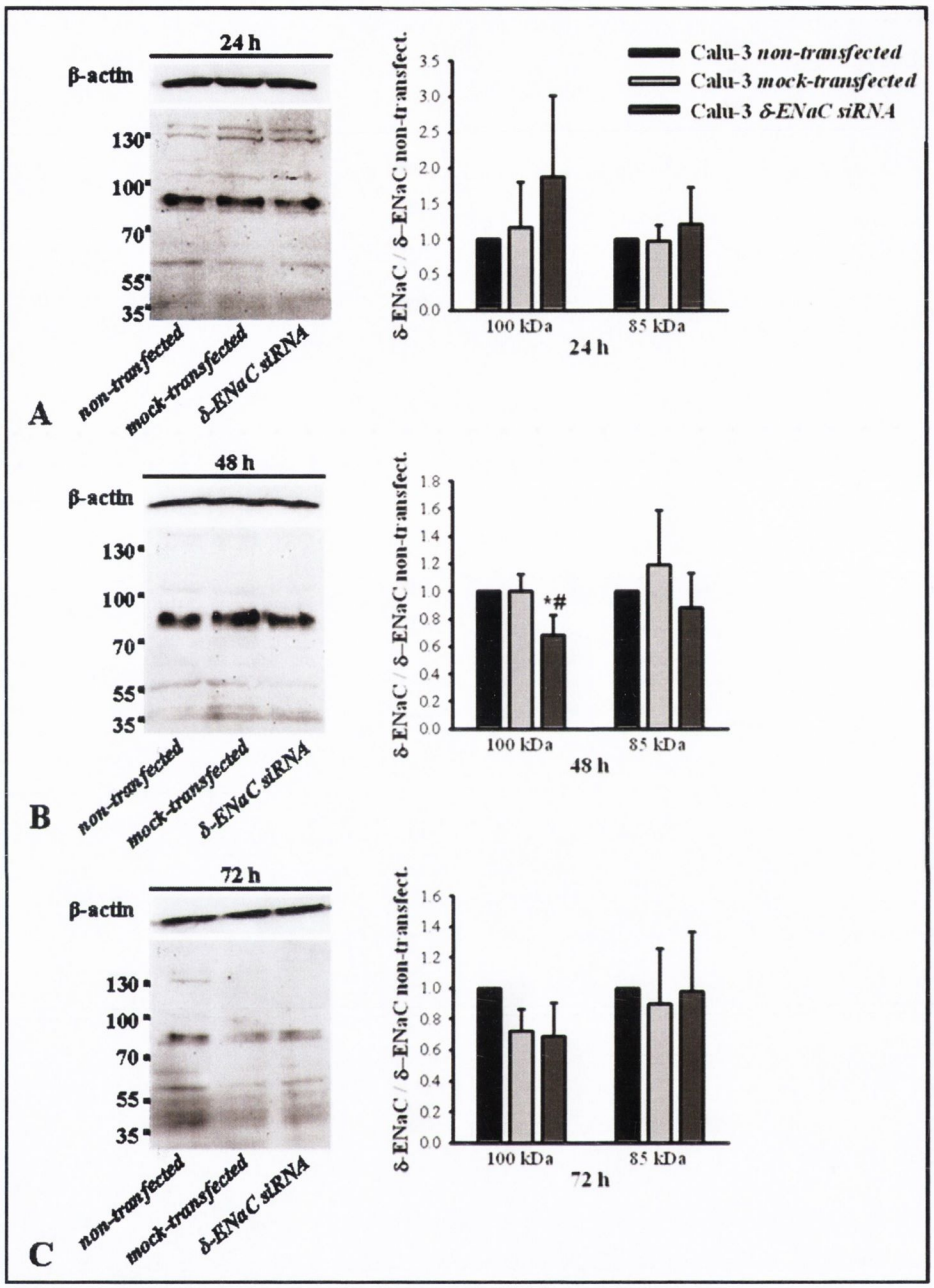

Figure 1. Transient δ-ENaC knockdown in Calu-3 cells using siRNA. Calu-3 cells were transfected with scrambled, non-silencing siRNA (*mock-transfected*) or 50 nM of δ-ENaC siRNA (*δ-ENaC siRNA*) 3 days after seeding. Protein samples were isolated 24, 48 and 72 h after transfection and analysed by Western blot using SC anti-δ-ENaC antibody. Beta-actin was used as loading control. Respective immunoblots as well as densitometric analysis of 85 and 100 kDa protein bands are shown above (**A, B, C**). Results are expressed as means ± SD ($n = 3$). The statistical significance of the difference is expressed as *, $P < 0.05$ versus non-transfected Calu-3 and as #, $P < 0.05$ versus mock-transfected Calu-3 cells.

and mock-transfected controls (32 ± 15%, $n = 3$, $P<0.05$). However, the 100 kDa band, although referenced to as specific for δ-ENaC by others (Bangel-Ruland *et al.* 2009), has been shown to be unspecific in our hands. Additionally, no significant reduction in band intensity at 85 kDa (i.e., the molecular weight of the full-length protein) was detected 48 h after transfection. At 72 h after transfection, no significant reduction in δ-ENaC expression was detected in δ-ENaC siRNA transfected cells (**Figure 1 (C)**).

H441 cells were transfected with 1.6 μg E35X cDNA one day after seeding. Cell lysates were probed with both DAR and SC anti-δ-ENaC antibodies (**Figure 2 (A)** and **(B)**, respectively). Densitometric analysis was carried out for 75 and 100 kDa protein bands as well as for 85 and 100 kDa bands, detected with DAR and SC antibodies, respectively. No significant differences in band intensities were detected for either of the bands, when quantified 24, 48 and 72 h after transfection.

In summary, both transient knock-down strategies that were used failed to down-regulate δ-ENaC expression at protein level in Calu-3 and H441 cells. Moreover, a major drawback of the transient approach consists in the fact that, on one hand, transient transfection needs to be performed preferably within 24 h after seeding in order to obtain high knock-down efficiencies, with the knock-down effect wearing off within 72 h following the transfection procedure. On the other hand, cell monolayers require longer than 72 h in culture to develop electrical resistances sufficient for transepithelial measurements, which are necessary to determine the consequences of δ-ENaC knock-down at the functional level. Since it proved to be very challenging to optimise the transient knock-down procedure in a way that both requirements were fulfilled, an attempt to generate a cell line with stably down-regulated expression of δ-ENaC was undertaken.

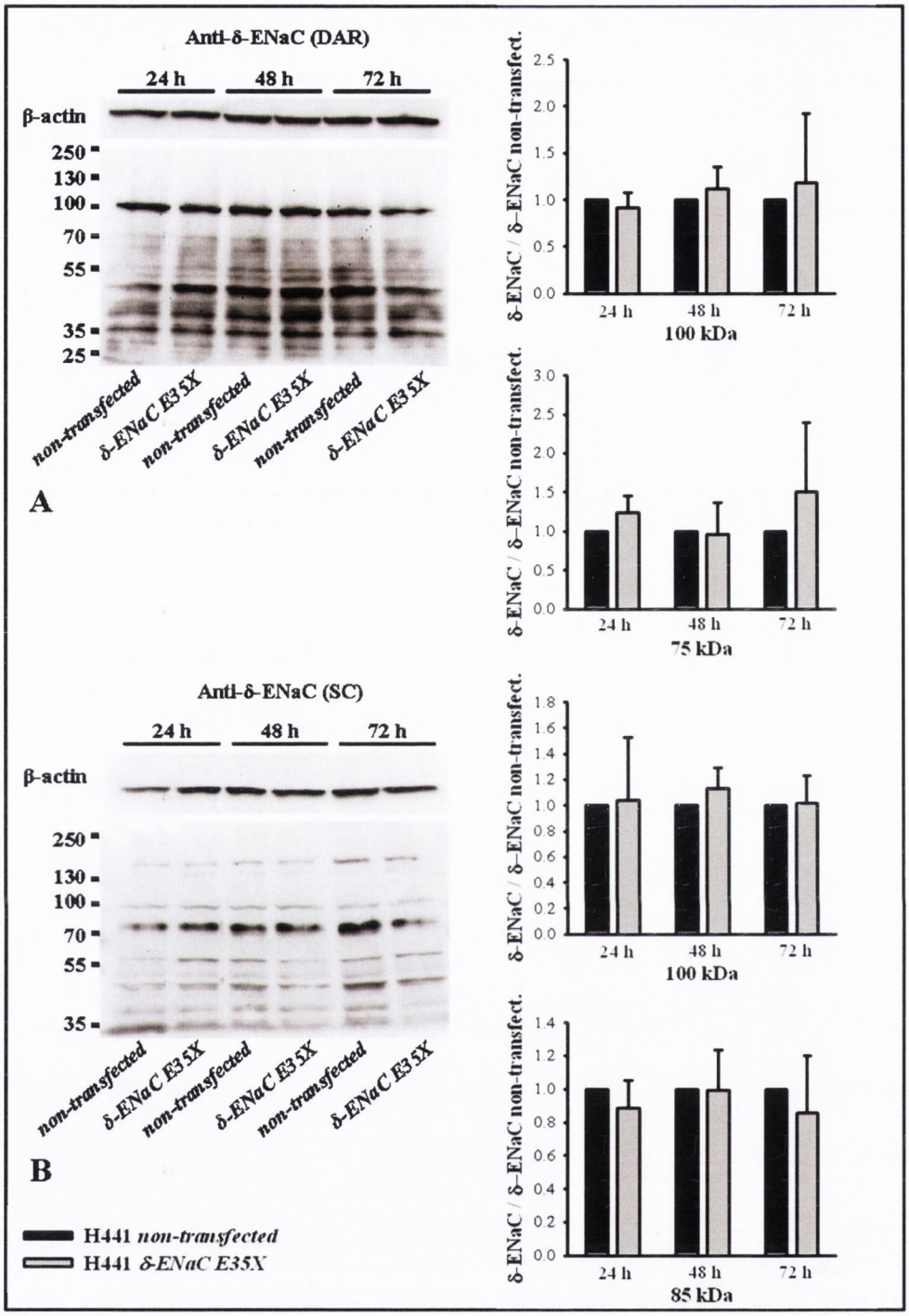

Figure 2. Transient δ-ENaC knockdown in H441 cells using dominant-negative cDNA constructs. H441 cells were transfected with 1.6 µg of dominant negative cDNA (*δ-ENaC E35X*) one day after seeding. Protein samples were isolated 24, 48 and 72 h after transfection and analysed by Western blot using DAR (**A**) and SC (**B**) anti-δ-ENaC antibodies. Beta-actin was used as loading control. Respective immunoblots as well as densitometric analysis of protein bands at 100 kDa and of those corresponding to the full-length protein (75 and 85 kDa, respectively) are shown above. Results are expressed as means ± SD ($n = 3$).

5.1.2 Stable knock-down strategy to down-regulate δ-ENaC expression

Western blot analysis as well as the Ussing chamber measurements with stably transfected cells were performed by Svenja Sladek (Trinity College Dublin, Ireland).

To stably down-regulate δ-ENaC expression, H441 and Calu-3 cells were transduced with lentiviral particles containing constructs of a puromycin resistance gene and either scrambled shRNA or shRNA designed to knock-down δ-ENaC. Successfully transduced, shRNA expressing cell colonies were selected by exposure to puromycin. Subsequently, protein samples deriving from three different passages of non-transfected H441 and Calu-3 cells, mock-transfected and δ-ENaC shRNA transfected cells were analysed by means of Western blot to estimate the knock-down efficiency. All samples were probed with both DAR and SC anti-δ-ENaC antibodies. Delta-ENaC expression levels, normalised to the β-actin loading control, were compared.

Figure 3 (A) shows a representative immunoblot of H441 cell lysates probed with DAR antibody and the densitometric analysis of bands detected at 75 and 100 kDa (n = 3). The obtained band patterns were comparable between non-transfected, mock-transfected and δ-ENaC shRNA transfected H441 samples. No significant differences in band intensities could be detected at 100 kDa, not unexpectedly, since the 100 kDa band is most likely unspecific, as demonstrated previously. Also, at the molecular weight of 75 kDa, corresponding to the full-length δ-ENaC protein, no relevant differences were measured, although band intensities in mock-transfected cells were significantly higher than those in non-transfected and δ-ENaC shRNA transfected cells ($P < 0.05$). Additionally, quantification of band intensities at lower molecular weights did not reveal any significant down-regulation of δ-ENaC expression in δ-ENaC shRNA transfected cells (data not shown).

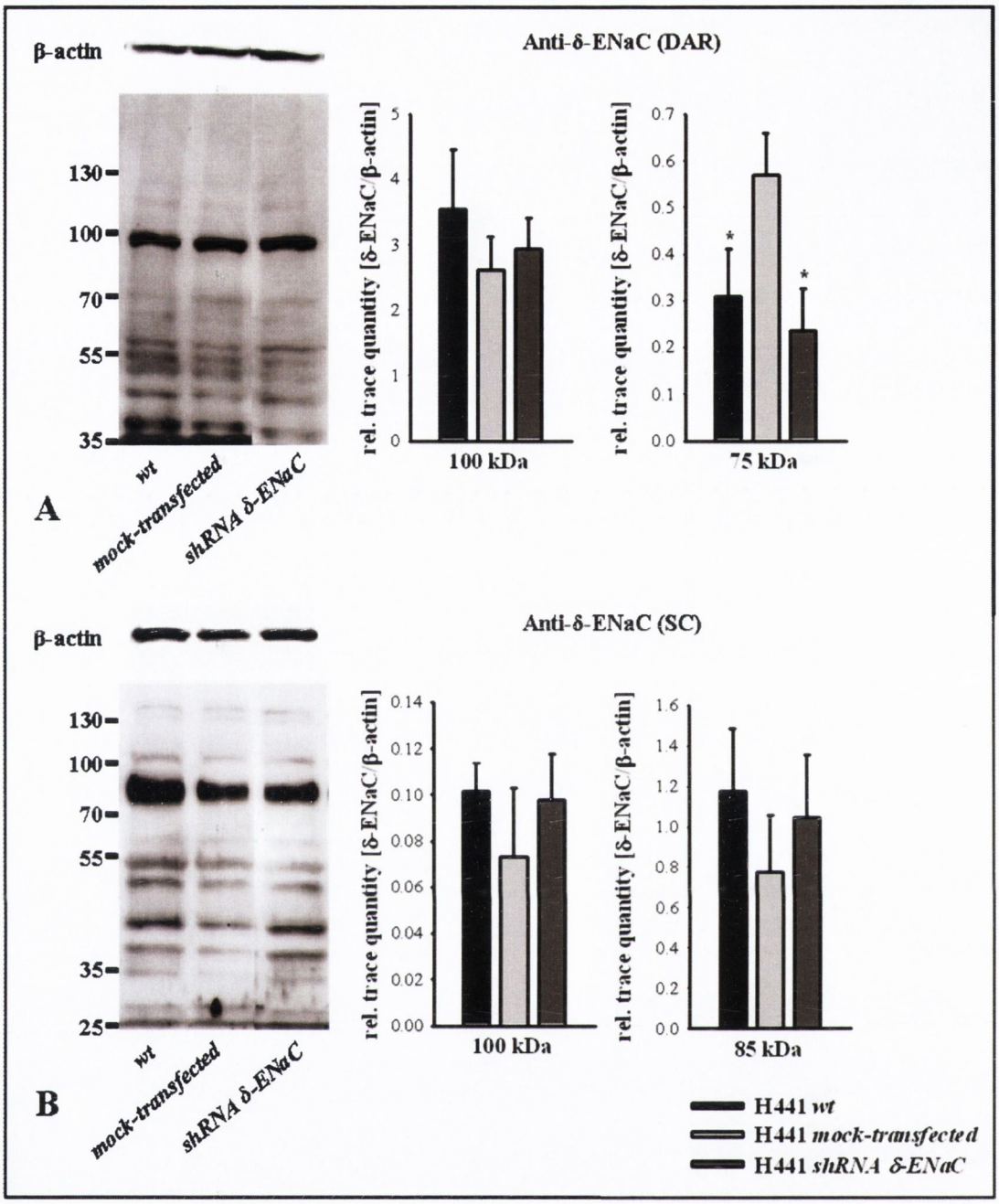

Figure 3. Representative Western blots showing expression of δ-ENaC in non-transfected H441cells (H441 *wt*) as well as in cells, stably transfected with scrambled shRNA and shRNA, designed to knock-down δ-ENaC (H441 *mock-transfected* and H441 *shRNA δ-ENaC*, respectively). Cell lysates derived from three different passages were probed with anti-δ-ENaC DAR **(A)** and SC **(B)** antibodies. Beta-actin was used as loading control. Intensities of protein bands at 100 kDa and of those corresponding to the full-length protein (75 and 85 kDa, respectively) were analysed by means of densitometry. Results are expressed as means ± SD (n = 3). The statistical significance of the difference is expressed as *, $P < 0.05$ versus mock-transfected H441.

Corresponding immunoblots probed with SC anti-δ-ENaC antibody are presented in **Figure 3 (B)**. Similar to the results obtained with the DAR antibody, densitometric analysis of protein bands did not show any reduction of δ-ENaC expression in δ-ENaC shRNA transfected cells, regardless of which bands were analysed. Quantification of signal intensities at 85 and 100 kDa is shown in **Figure 3 (B)**. Comparable results were obtained when protein bands at lower molecular weights were quantified (data not shown).

Similar results were obtained by Western blot analysis of Calu-3 cell lysates. Immunoblots obtained using DAR and SC anti-δ-ENaC antibodies are presented in **Figure 4 (A)** and **(B)**, respectively. Densitometric analysis of 100 kDa bands (detected with both antibodies) as well as of the full-length δ-ENaC protein bands (75 kDa for DAR and 85 kDa for SC antibody) did not reveal any significant reduction of δ-ENaC protein levels in δ-ENaC shRNA transfected cells, when compared to those in non-transfected or mock-transfected Calu-3 cells. Also, quantification of signal intensities at lower molecular weights did not show any significant decrease in δ-protein abundance in δ-ENaC shRNA transfected cells (data not shown).

In summary, no decrease in the abundance of δ-ENaC protein was detected in either δ-ENaC shRNA transfected H441 or Calu-3 cells, when δ-ENaC expression levels were compared to those in the respective non-transfected and mock-transfected cells by means of Western blot analysis. These findings were obtained consistently with both anti-δ-ENaC antibodies used. However, due to the specificity of the SC antibody being unreliable and full-length δ-ENaC protein band detected with the DAR antibody at 75 kDa being very weak, even a significant down-regulation of δ-ENaC expression in shRNA transfected cells may be difficult to detect using Western blot technique. For

this reason, Ussing chamber experiments with cell monolayers of shRNA transfected H441 and Calu-3 cells were carried out, despite the negative results at the protein expression level.

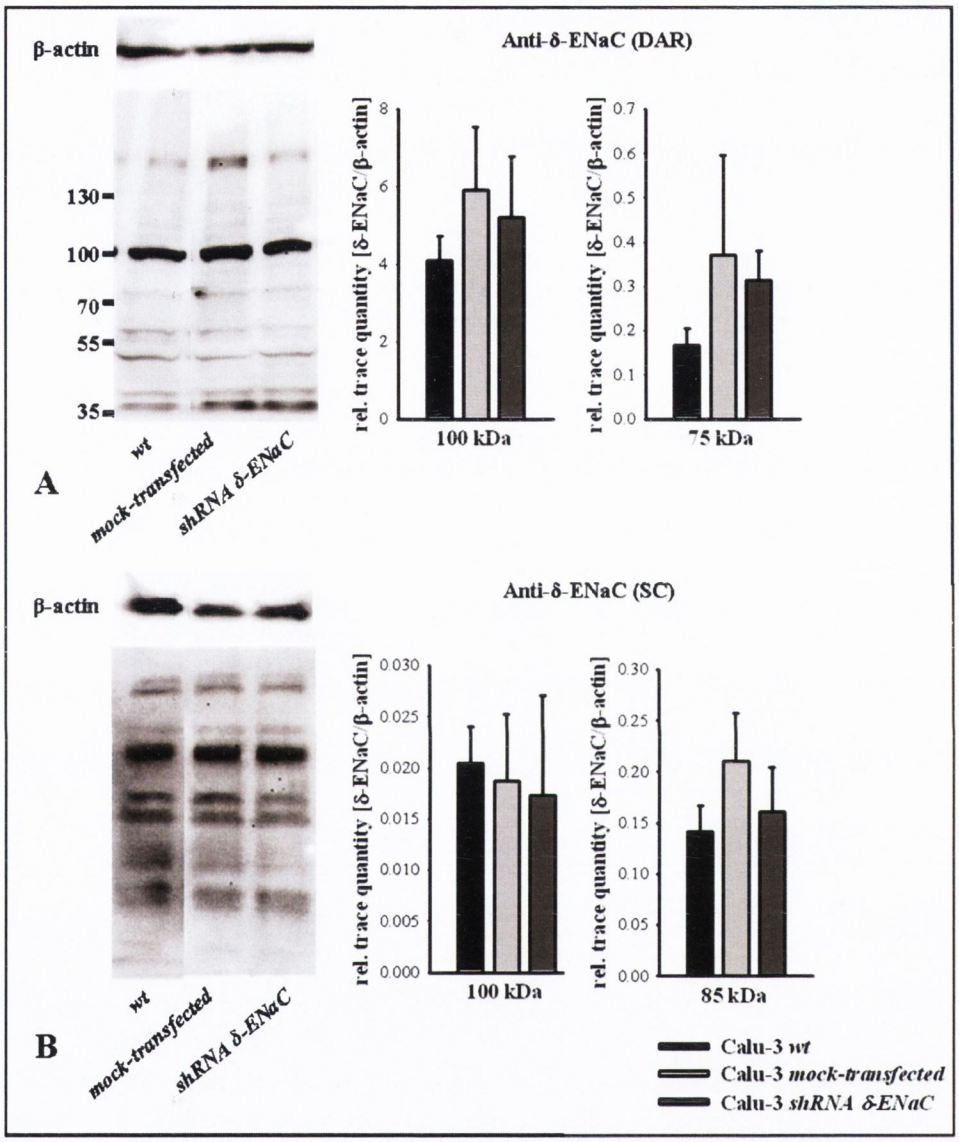

Figure 4. Representative Western blots showing expression of δ-ENaC in non-transfected Calu-3 cells (Calu-3 *wt*) as well as in cells, stably transfected with scrambled shRNA and shRNA, designed to knock-down δ-ENaC (Calu-3 *mock-transfected* and Calu-3 *shRNA δ-ENaC*, respectively). Cell lysates derived from three different passages and were probed with anti-δ-ENaC DAR **(A)** and SC **(B)** antibodies. Beta-actin was used as loading control. Intensities of protein bands at 100 kDa and of those corresponding to the full-length protein (75 and 85 kDa, respectively) were analysed by means of densitometry. Results are expressed as means ± SD (*n* = 3).

As shown in **Figure 5 (A)**, when Evans blue, capsazepine or icilin were applied to the apical compartments of H441 cell monolayers, short-circuit currents were reduced, with no significant differences in response to the pharmacological agents measured between non-transfected, mock-transfected and δ-ENaC shRNA transfected H441 cells. Likewise, no significant reduction in the compound effects was detected in δ-ENaC shRNA transfected Calu-3 cells, when compared to the effects in non-transfected and mock-transfected cells. Here, short-circuit currents were stimulated by application of Evans blue and icilin and inhibited by capsazepine, as shown in **Figure 5 (B)**.

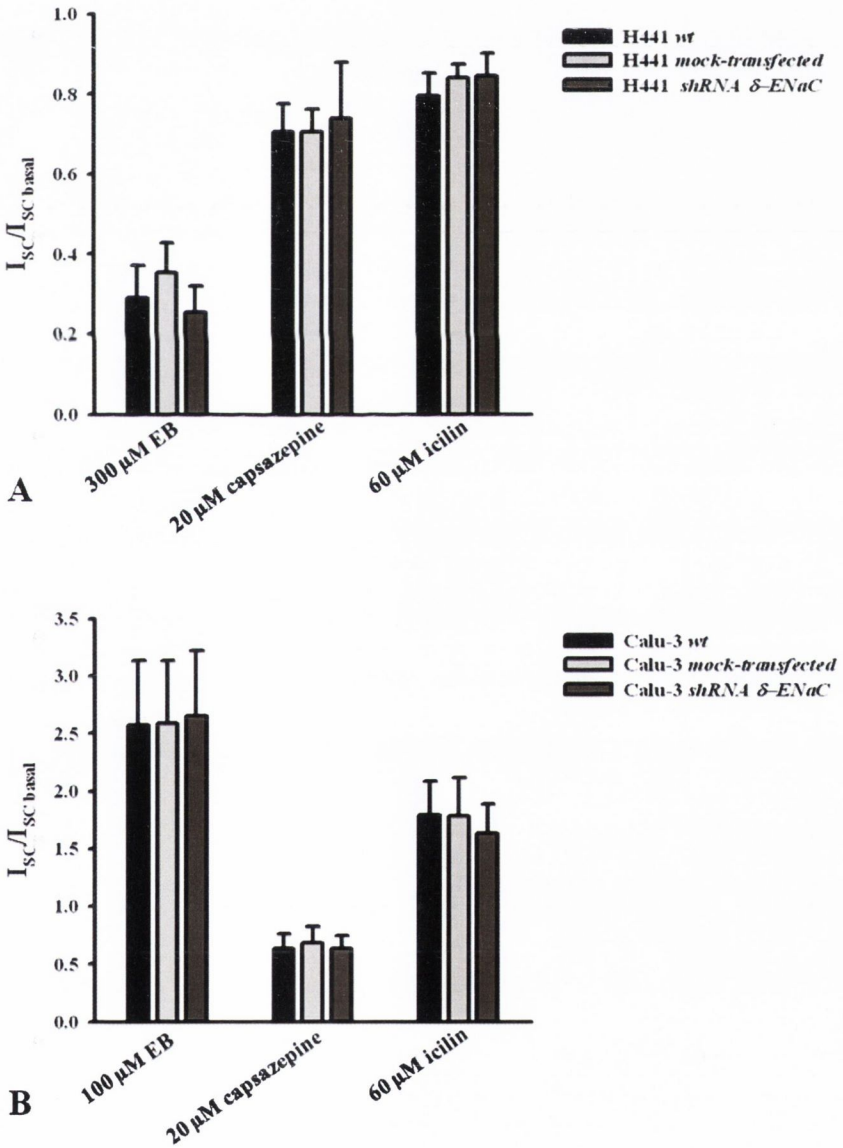

Figure 5. Effects of the δ-ENaC inhibitor, Evans blue (EB), and of the activators, capsazepine and icilin, on H441 **(A)** and Calu-3 **(B)** cell monolayers of non-transfected cells (*wt*) as well as of cells, stably transfected with scrambled shRNA and shRNA, designed to silence δ-ENaC (*mock-transfected* and *shRNA δ-ENaC*, respectively). Short-circuit currents (I_{SC}) resulting after administration of the relevant compounds were measured and normalised to the I_{SC} measured prior to the addition of the substances (basal I_{SC}). Results are expressed as means ± SD (n = 3-15).

Thus, it can be concluded that the attempt to generate cell lines with stably down-regulated δ-ENaC expression levels failed. No reduction in δ-ENaC protein abundance or in activity of the reported δ-ENaC modulators could be detected in δ-ENaC shRNA transfected cells. Therefore, it remains unclear whether the effects, observed in respiratory epithelial cells in response to the pharmacological agents used, were δ-ENaC-specific and, consequently, whether δ-ENaC is functionally expressed in these cells.

5.2 Effects of δ-ENaC over-expression in human respiratory epithelial cells

Since the knock-down approach failed to provide conclusive information regarding the functional expression of δ-ENaC in the airway epithelium, the reverse strategy was tried, i.e., δ-ENaC protein was over-expressed in H441 cells. To generate a cell line stably over-expressing δ-ENaC, H441 cells were transfected with δ_1-ENaC plasmid cDNA and subsequently exposed to geneticin for selection. Unlike *X. laevis* oocytes or other commonly used heterologous expression systems, H441 cells endogenously express δ-ENaC. This led to the assumption that the over-expressed protein will be processed in the same way as endogenous δ-ENaC. Thus, effects of δ-ENaC modulators are expected to be similar, however, more pronounced in δ-ENaC over-expressing cells.

5.2.1 Expression and localisation of δ_1-ENaC protein over-expressed in H441 cells

Western blot analysis was performed by Svenja Sladek (Trinity College Dublin, Ireland).

Expression of δ-ENaC in transfected H441 cells was assessed by Western blot of cell lysates deriving from different geneticin-resistant clones. A representative immunoblot, probed with DAR anti-δ-ENaC antibody, is shown in **Figure 6**. Lysates of non-transfected and transiently transfected H441 cells were used as negative and positive controls, respectively. In one of the tested clones (**Figure** 6, Lane 4), a prominent protein band at 75 kDa was detected confirming over-expression of δ-ENaC. This clone was expanded and cells deriving thereof are referred to as δ_1-ENaC over-expressing or transfected cells in the further course of this chapter. In protein samples from different passages of transfected cells, the 75 kDa band was of a significantly higher intensity

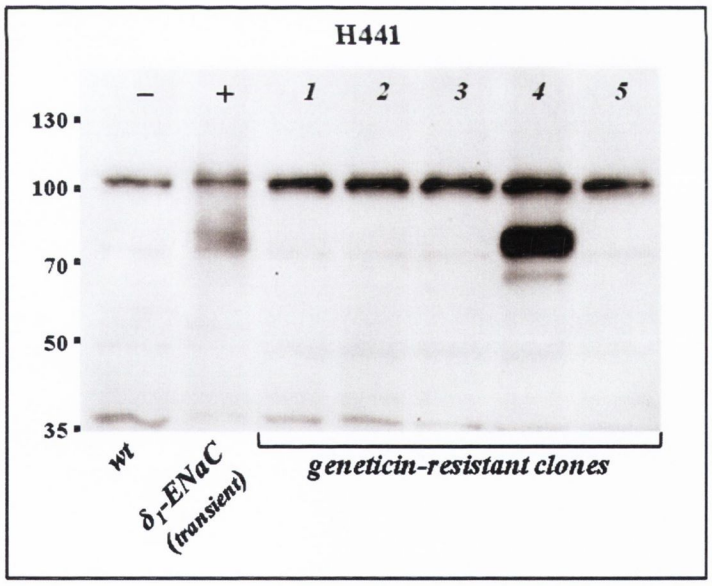

Figure 6. To generate a stably over-expressing cell line, H441 cells were transfected with δ_1-ENaC plasmid and exposed to geneticin for selection. Protein samples deriving from different geneticin-resistant clones (Lanes *1-5*) were tested for δ-ENaC over-expression using the DAR anti-δ-ENaC antibody. Lysates of non-transfected (*-/wt*) and transiently transfected H441 cells (*+/δ_1-ENaC transient*) were used as negative and positive controls, respectively.

than in non-transfected specimens (n = 4, $P < 0.05$). Additionally, a band at 70 kDa, only occasionally observed in wild-type H441 cells, was observed consistently in all samples from transfected cells. This suggests both protein bands to be specific for δ-ENaC. Densitometric analysis revealed that the ratio between signal intensities of 70 and 75 kDa bands was comparable in both non-transfected and δ_1-ENaC over-expressing H441 cells. In the wild-type cells, the 75 kDa protein was 6.3 ± 3.0-fold (n = 3) more abundant than the 70 kDa product (**Figure 7 (A)**). In the transfected cells, the ratio was 7.4 ± 2.0 (n = 4) (**Figure 7 (B)**). Following PNGase F treatment, the 75 kDa band shifted to the molecular weight of 70 kDa, while the 70 kDa band showed no migration (**Figure 7 (C)**), indicating that these bands represented *N*-glycosylated and non-glycosylated forms of δ_1-ENaC protein. This observation was consistent with previous reports of δ-ENaC protein being *N*-glycosylated (Haerteis *et al.* 2009; Chang *et al.* 2011). According to the results of densitometric quantification, the glycosylation rate was similar in wild-type and transfected cells, supporting the idea of identical processing of endogenous and over-expressed δ-ENaC protein in H441 cells.

As described in the Chapter 3, section 3.2.4, no full-length or truncated δ-ENaC protein was detected in the biotinylated membrane fractions of the wild-type H441 cells using the DAR anti-δ-ENaC antibody. In contrast, when biotinylated membrane protein fractions from δ_1-ENaC over-expressing H441 cells were analysed by Western blot, the 75 kDa band was detected in both apical and basolateral membrane samples. The 70 kDa band, however, was only observed in the basolateral membrane (**Figure 7 (D)**). No further bands were observed at lower molecular weights.

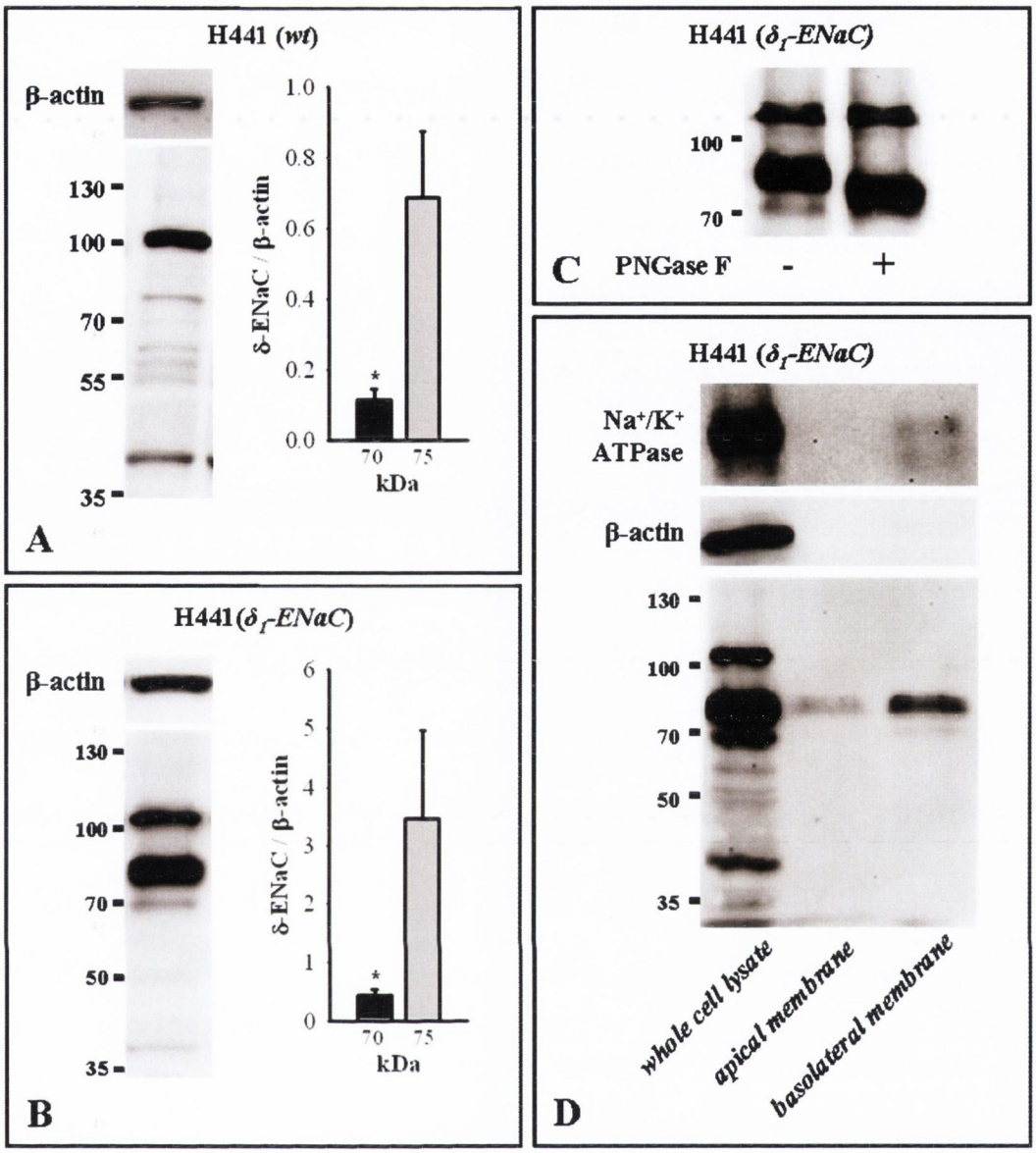

Figure 7. Over-expression of δ_1-ENaC in H441 cells. Representative immunoblots of wild-type (*wt*, **A**) and δ_1-ENaC over-expressing H441 cells (*δ_1-ENaC*, **B**), probed with DAR anti-δ-ENaC antibody. Specific δ-ENaC protein bands at 70 and 75 kDa were analysed by means of densitometry and normalised to the β-actin loading control. Results are expressed as means ± SD (n = 3 - 4). The statistical significance of the difference is expressed as *, $P < 0.01$ versus the signal intensity at 75 kDa. **(C)** Glycosylation of over-expressed δ_1-ENaC protein in H441 cells. Untreated control samples were run in parallel to PNGase F treated cell lysates. **(D)** Representative Western blot of whole cell lysate as well as of apically and basolaterally biotinylated surface protein fractions from H441 (*δ_1-ENaC*) cells. Beta-actin and Na^+/K^+-ATPase were used as controls to exclude potential contamination of the biotinylated samples with intracellular non-biotinylated protein and contamination of apical protein fraction with basolateral protein, respectively.

Thus, over-expression of δ_1-ENaC in H441 cells resulted in an increase in cellular abundance of the full-length δ-ENaC protein and its enhanced insertion into the cell membranes. Whilst the *N*-glycosylated form of 75 kDa was detected on both cellular aspects, the non-glycosylated protein of 70 kDa was observed only in the basolateral membrane. This discrepancy may, however, be an artefact originating from less efficient recovery of the apically biotinylated protein. The resulting lower protein concentration in the apical samples could have interfered with the detection of the non-glycosylated protein. Since bands for Na^+/K^+-ATPase were only observed in the basolateral membrane samples, apical samples were free from basolateral contaminants. Regrettably, the possibility of contamination of basolaterally biotinylated samples with apical protein could not be ruled out, so that the presence of the full-length δ-ENaC protein on the basolateral aspect of transfected H441 cells still remains controvertible. Since, however, β-actin was detected only in the untreated whole cell lysates, contamination of the membrane fractions with intracellular protein can be excluded. Hence, evidence has been provided that full-length δ-ENaC protein is localised to the cell surface of δ_1-ENaC over-expressing H441 cells, even though, the specification of the relevant cell aspects was not satisfactory.

To further support these data, δ_1-ENaC over-expressing H441 cells grown on Transwell filter inserts were immunostained using SC, DAR and TF anti-δ-ENaC antibodies. To allow a direct comparison, the immunofluorescence images (**Figure 8**) were obtained using the same pinhole settings and the detector gains for both, the transfected and the wild-type specimens. As expected, no differences in the intensity and the localisation of the fluorescent signal were observed between the monolayers of non-transfected and transfected H441 cells, when these were stained with SC antibody. Also, the localisation of the signal obtained with TF antibody remained unchanged. However, the signal

intensity in the δ_1-ENaC over-expressing cells was slightly increased. In contrast, higher intensity as well as clearly changed distribution pattern of the fluorescent signal was observed, when δ_1-ENaC over-expressing cells were immunostained with the DAR antibody and the resulting images were compared to those of the wild-type H441 cells. Whilst staining of non-transfected cells showed cytoplasmic, perinuclear pattern, strong accumulation of the fluorescent signal in the apical membranes of the transfected cells was observed, providing additional evidence for abundance of δ-ENaC protein at the apical surfaces of these cells. Cytoplasmic staining, on the other hand, was of lower intensity. Signal localisation in the basolateral cell membrane was not observed as distinctly as the results of the cell surface biotinylation would suggest. However, the obtained immunofluorescence images do not rule out the basolateral localisation of δ-ENaC protein, either.

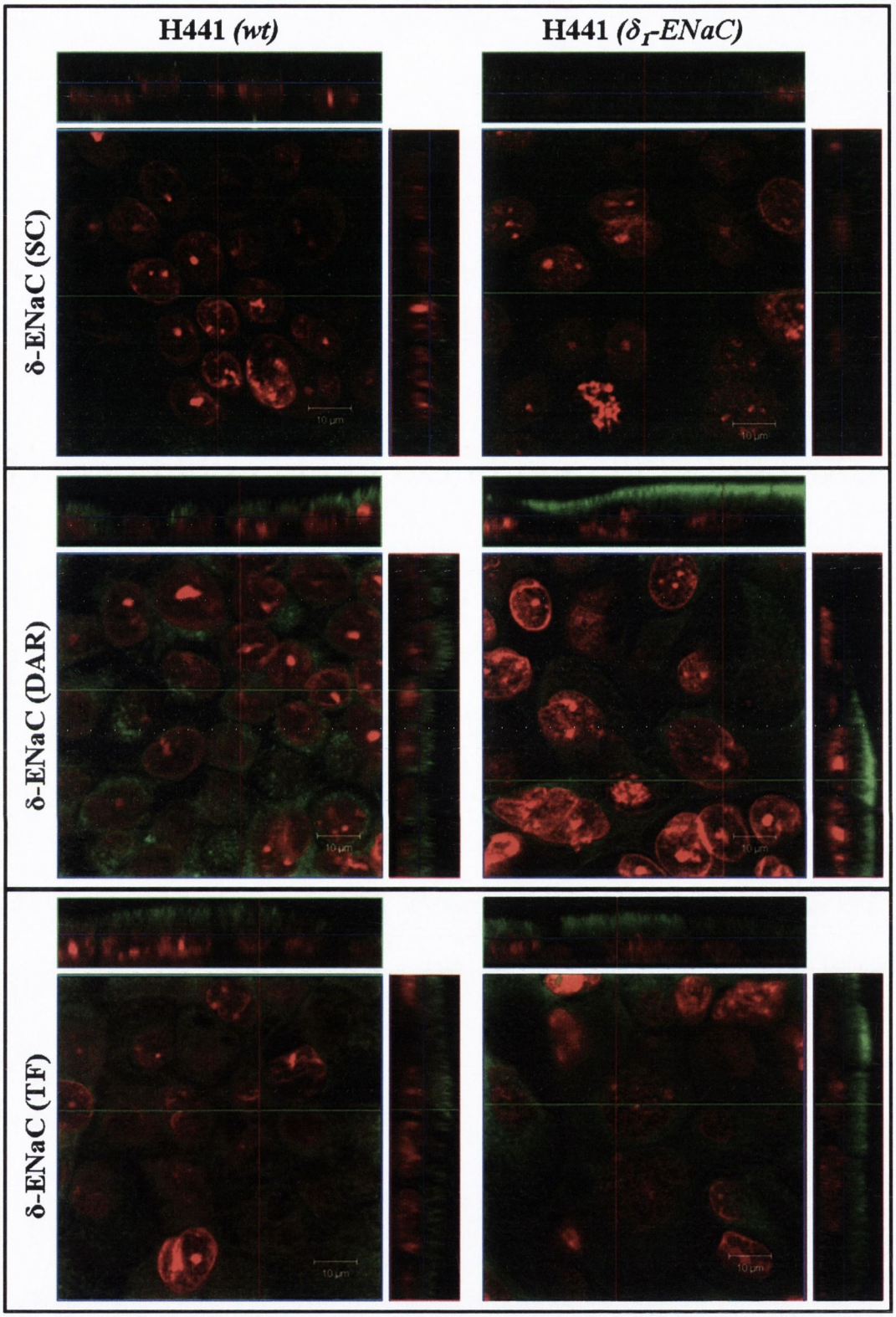

Figure 8. Immunofluorescence microscopy for δ-ENaC in wild-type (*wt*) and δ_1-ENaC over-expressing H441 cells (*δ_1-ENaC*). Delta-ENaC signals were detected using anti-δ-ENaC SC, DAR and TF antibodies (green). Cell nuclei were counterstained with propidium iodide (red).

5.2.2 Assessment of δ_1-ENaC function in δ_1-ENaC over-expressing H441 cells

Part of the Ussing chamber measurements were performed by Svenja Sladek (Trinity College Dublin, Ireland).

After successful over-expression of δ-ENaC in H441 cells had been confirmed, functional transepithelial measurements in modified Ussing chambers were performed in order to test the effects of the alleged δ-ENaC modulators in the δ_1-ENaC over-expressing cells.

5.2.2.1 Amiloride-sensitivity of Na^+ currents in δ_1-ENaC over-expressing H441 cells

The epithelial sodium channel blocker, amiloride significantly reduced short-circuit currents in δ_1-ENaC over-expressing H441 cells. Representative I_{SC} traces obtained by consecutive administration of 10 μM and 100 μM amiloride are shown in **Figure 9 (A)**. Interestingly, quantification of the inhibitory effects revealed significant differences in amiloride-sensitivity between wild-type and transfected H441 cells (**Figure 9 (B)**). Administration of 10 μM amiloride to the cell monolayers of δ_1-ENaC over-expressing H441 cells significantly reduced the basal I_{SC} by 26.3 ± 10.1% (n = 9). However, the effect was significantly smaller than in the wild-type cells, where 88.3 ± 5.9% (n = 9) of the basal I_{SC} were inhibited by 10 μM amiloride. Increase of the amiloride concentration to 100 μM led to a further significant decrease in current to 20.3 ± 1.1% (n = 3) of the initial value in the transfected and to 3.0 ± 3.5% (n = 9) in the non-transfected cells, respectively. Inhibition of Na^+-K^+-ATPase by ouabain (1 mM) led to comparable reduction of I_{SC} in both cell types (by 78.5 ± 19.4% and 69.7 ± 5.2% (n = 4-5) in the wild-type and transfected cells, respectively; **Figure 9(C)**).

Whilst the major part of I_{SC} was sensitive to 10 μM amiloride in the non-transfected

cells, a 10-fold higher concentration was required to inhibit the main portion of I_{SC} in the transfected cells. Thus, basal currents in δ_1-ENaC over-expressing H441 cells were less amiloride-sensitive than those in the wild-type cells, although total sodium-currents were similar in both cell types.

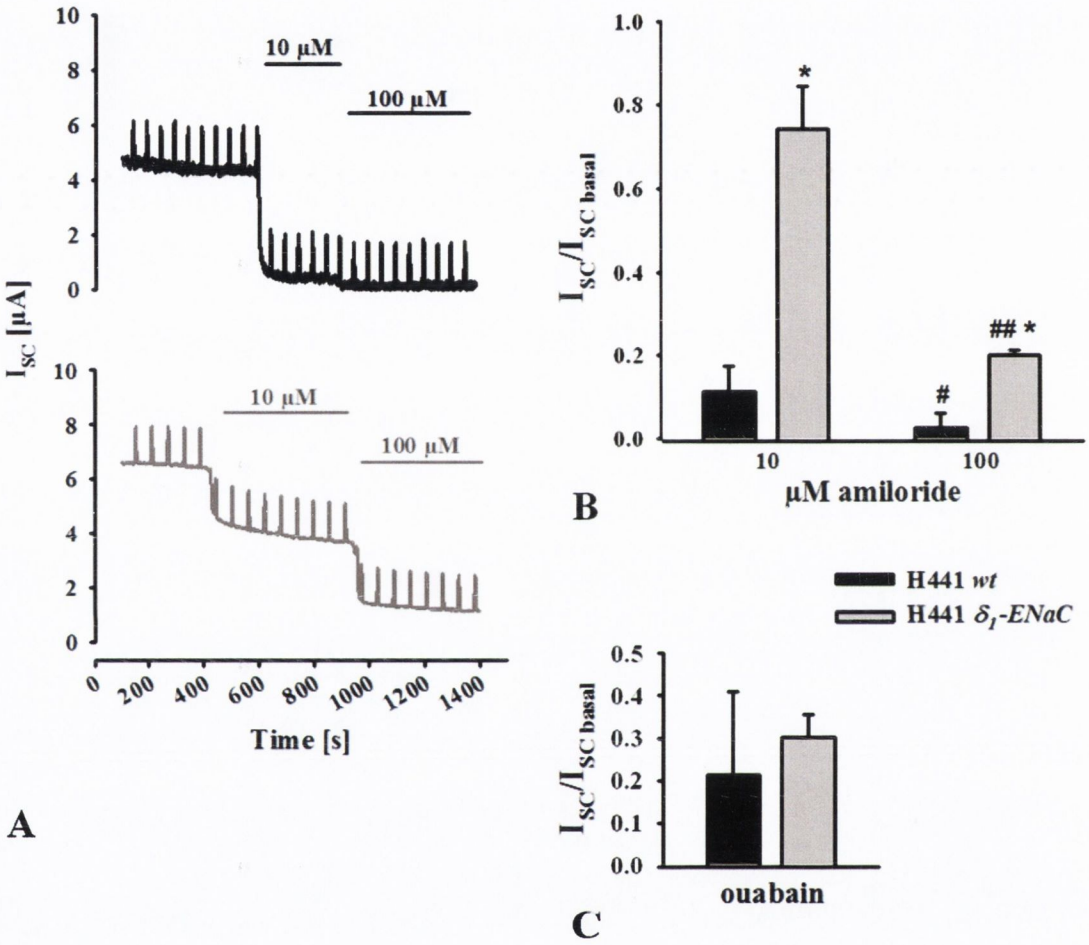

Figure 9. Amiloride and ouabain-dependence of the short-circuit currents in the wild-type (*black*) and δ_1-ENaC over-expressing H441 cells (*grey*). Representative I_{SC} traces as well as the quantification of the responses to 10 µM and 100 µM amiloride (**(A)** and **(B)**, respectively) and to 1 mM ouabain **(C)** are shown. Short-circuit current values were measured after adding the respective concentration of amiloride or ouabain and normalised against I_{SC}, measured in the absence of the compounds (I_{SC} basal). Results are expressed as means ± SD (n = 3 - 9). The statistical significance of the effect is expressed as #, $P < 0.05$ and ##, $P < 0.01$ versus the I_{SC} in the presence of 10 µM amiloride and as *, $P < 0.01$ versus the respective I_{SC} in the wild-type H441 cells.

5.2.2.2 Effects of the alleged δ-ENaC modulators in δ_1-ENaC over-expressing H441 cells

When applied apically to the cell monolayers, the alleged δ-ENaC modulators showed pronounced effects on the short-circuit currents in δ_1-ENaC over-expressing H441 cells. **Figure 10 (A)**, **(B)** and **(C)** shows the representative short-circuit current traces in response to 300 μM Evans blue, 20 μM capsazepine and 60 μM icilin, respectively. Observed effects were quantified by normalisation against basal I_{SC} and compared to the compound effects in the wild-type cells (**Figure 11**). Delta-ENaC inhibitor Evans blue, added to the transfected H441 cells, led to a significant reduction of the short-circuit current, which was comparable to that in the non-transfected cells (decrease by 70.1 ± 19.1% (n = 11) and 72.5 ± 11.2% (n = 9), respectively). Both activators of δ-ENaC function, capsazepine and icilin, elevated I_{SC} levels in δ_1-ENaC over-expressing H441 cells (significant activation by 33.0 ± 7.7% (n = 9) and 30.4 ± 10.1% (n = 9), respectively), contrary to the inhibitory effects, exhibited by these compounds in the wild-type cells.

Albeit responses to the δ-ENaC modulators in the transfected cells were expected to be of greater amplitude, but of similar quality compared to the wild-type cells, quite the opposite was observed; at least in cases of capsazepine and icilin. Of note, the compounds' effects in δ-ENaC over-expressing cells were consistent with the observations reported by others (i.e., Yamamura *et al.* 2004b, 2005a, 2005b).

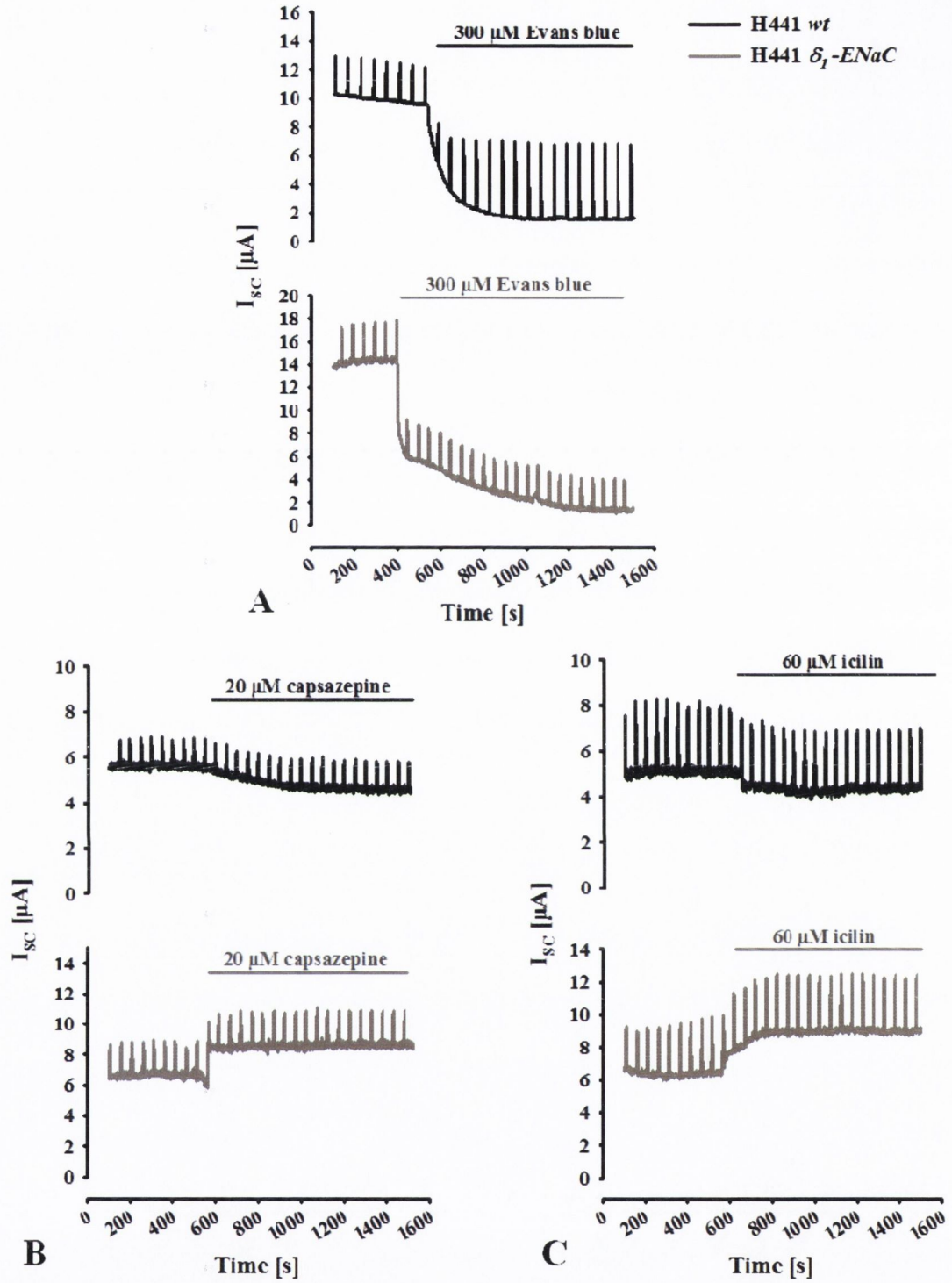

Figure 10. All alleged δ-ENaC modulators exhibited inhibitory effects in wild-type H441 cells, however, only the δ-ENaC inhibitor, Evans blue, decreased short-circuit currents in δ_1-ENaC over-expressing cells. The reported activators, capsazepine and icilin, had stimulatory effects on I_{SC}. Representative I_{SC} traces of responses to **(A)** 300 μM Evans blue, **(B)** 20 μM capsazepine and **(C)** 60 μM icilin are shown, after the compounds were applied apically to monolayers of the wild-type (*black*) or δ_1-ENaC over-expressing H441 cells (*grey*).

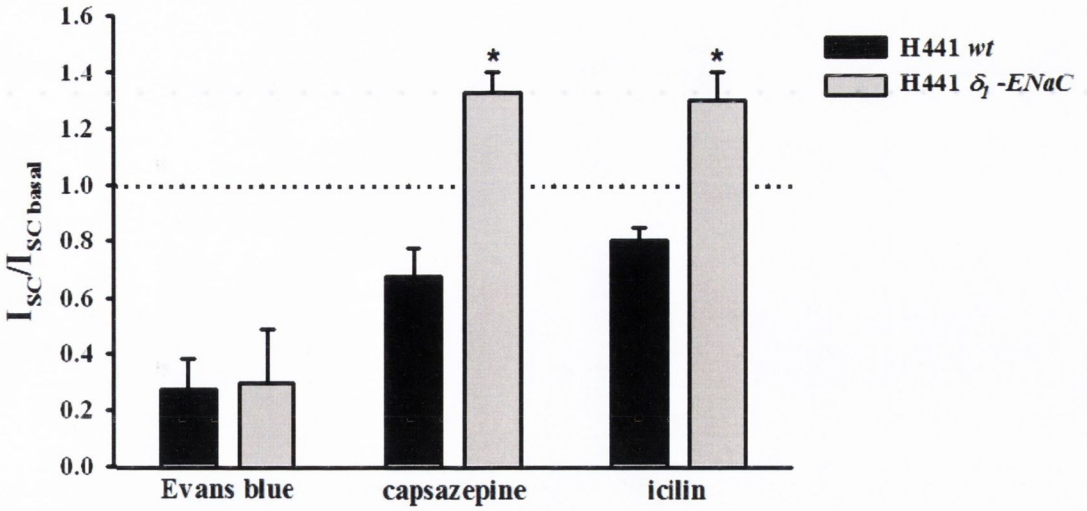

Figure 11. Quantification of the responses to 300 μM Evans blue, 20 μM capsazepine and 60 μM icilin in the wild-type (*black bars*) and δ_1-ENaC over-expressing H441 cell monolayers (*grey bars*). Short-circuit current values were measured after addition of the respective compound and normalised against I_{SC}, measured in the absence of the substance (I_{SC} basal). Results are expressed as means ± SD (n = 9 - 11). The statistical significance of the effect is expressed as *, $P < 0.01$ versus the respective I_{SC} in the wild-type H441 cells.

5.2.2.3 Amiloride-sensitivity of the effects induced by the alleged δ-ENaC modulators in δ_1-ENaC over-expressing H441 cells

Figure 12 shows the effects of 10 μM and 100 μM amiloride on transfected H441 cell monolayers, which had previously been treated with 300 μM Evans blue, 20 μM capsazepine or 60 μM icilin, respectively.

Short-circuit currents inhibited by Evans blue (28.9 ± 16.3% of the basal I_{SC}; n = 6) were slightly decreased by the subsequent addition of 10 and 100 μM amiloride (24.3 ± 18.6% and 20.8 ± 18.2% of the basal I_{SC}, respectively; n = 6). The effects, however, did not reach significance.

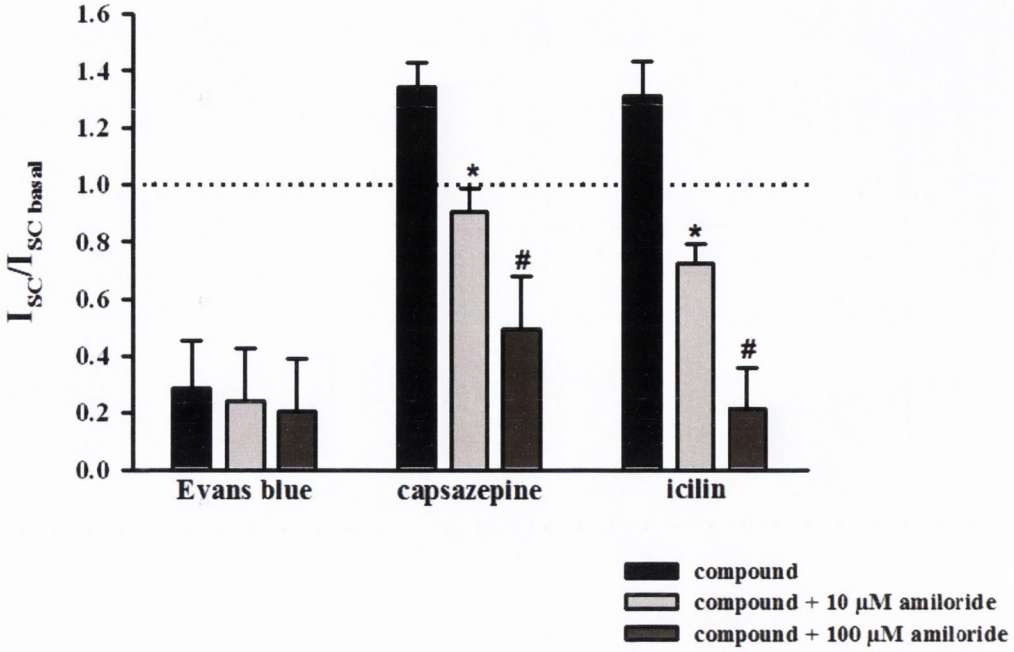

Figure 12. Amiloride-sensitivity of the effects induced by the administration of Evans blue, capsazepine and icilin to the monolayers of δ_1-ENaC over-expressing H441 cells. Short-circuit current values, measured after adding the relevant compound and after the subsequent application of 10 µM and 100 µM amiloride, respectively, were normalised against the I_{SC}, measured in the absence of the substance (I_{SC} basal). Results are expressed as means ± SD (n = 6). The statistical significance of the effects is expressed as *, $P < 0.01$ versus the I_{SC} in the presence of the respective compound as well as as #, $P < 0.01$ versus the I_{SC} in the presence of the relevant substance and 10 µM amiloride.

Capsazepine and icilin-induced increases in I_{SC} (by 34.4 ± 8.4% and 31.3 ± 11.8% of the basal I_{SC}, respectively; n = 6) were completely abolished by administration of 10 µM amiloride (90.6 ± 8.2% and 72.6 ± 6.7% of the basal I_{SC}, respectively; n = 6). Subsequent application of 100 µM amiloride led to a further significant decrease in short-circuit currents (49.4 ± 18.6% and 21.5 ± 14.5% of the basal I_{SC}, respectively; n = 6). However, addition of capsazepine or icilin still significantly stimulated currents across cell monolayers pre-treated with 10 µM amiloride (by 11.3 ± 5.2% and 12.5 ± 2.6% of the amiloride-insensitive I_{SC}, respectively; n = 3), although the amplitudes of

the increases were significantly smaller than in the absence of amiloride (**Figure 13**). Thus, currents stimulated by δ-ENaC activators in the transfected H441 cells were, at least partially, insensitive to lower concentrations of amiloride.

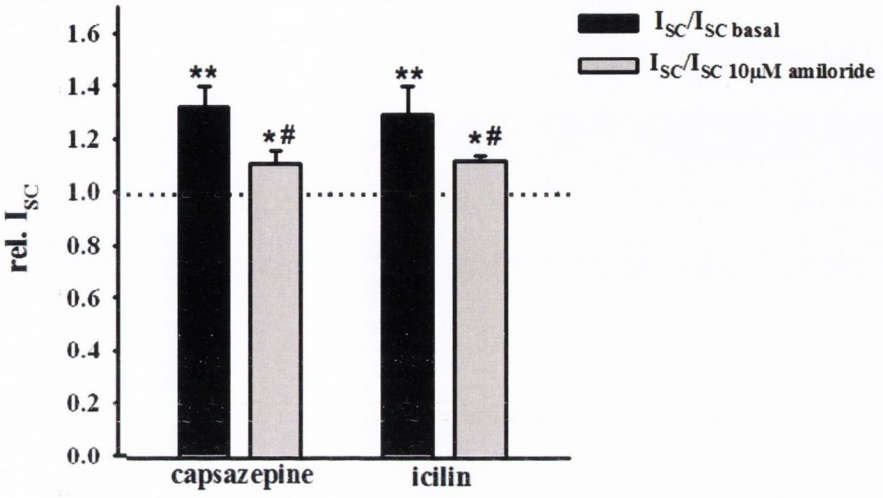

Figure 13. Amiloride-sensitivity of the effects induced by δ-ENaC activators. Capsazepine (20 μM) or icilin (60 μM) were added to the monolayers of δ_1-ENaC over-expressing H441 cells in the presence or absence of 10 μM amiloride. Short-circuit current values were measured after adding the relevant compound and normalised against the I_{SC}, measured prior to adding the substance (by basal I_{SC} in the absence of amiloride/*black bars* or by I_{SC} in the presence of 10 μM amiloride/*grey bars*). Results are expressed as means ± SD (n = 3 - 9). The statistical significance of the effect is expressed as *, $P < 0.05$ and **, $P < 0.01$ versus the basal I_{SC} or I_{SC} in the presence of 10 μM amiloride, respectively, and as #, $P < 0.01$ versus the compound effect in the absence of amiloride.

5.2.2.4 Evans blue-sensitivity of the effects induced by δ-ENaC activators in δ_1-ENaC over-expressing H441 cells

Capsazepine-induced current increase (30.2 ± 6.4% of the basal I_{SC}; n = 3) was completely abolished by application of 300 μM Evans blue with the resulting I_{SC} (10.6 ± 12.1% of the basal I_{SC}; n = 3) being not significantly different from I_{SC} in the presence of Evans blue alone (29.9 ± 19.1% of the basal I_{SC}; n = 11). Furthermore, capsazepine

failed to activate currents in Evans blue pre-treated cell monolayers, decreasing the I_{SC} slightly, however, not significantly (from 42.3 ± 25.8% to 34.1 ± 26.0% of the basal I_{SC}; n = 3). Representative I_{SC} traces and quantification of the effects are shown in **Figure 14**.

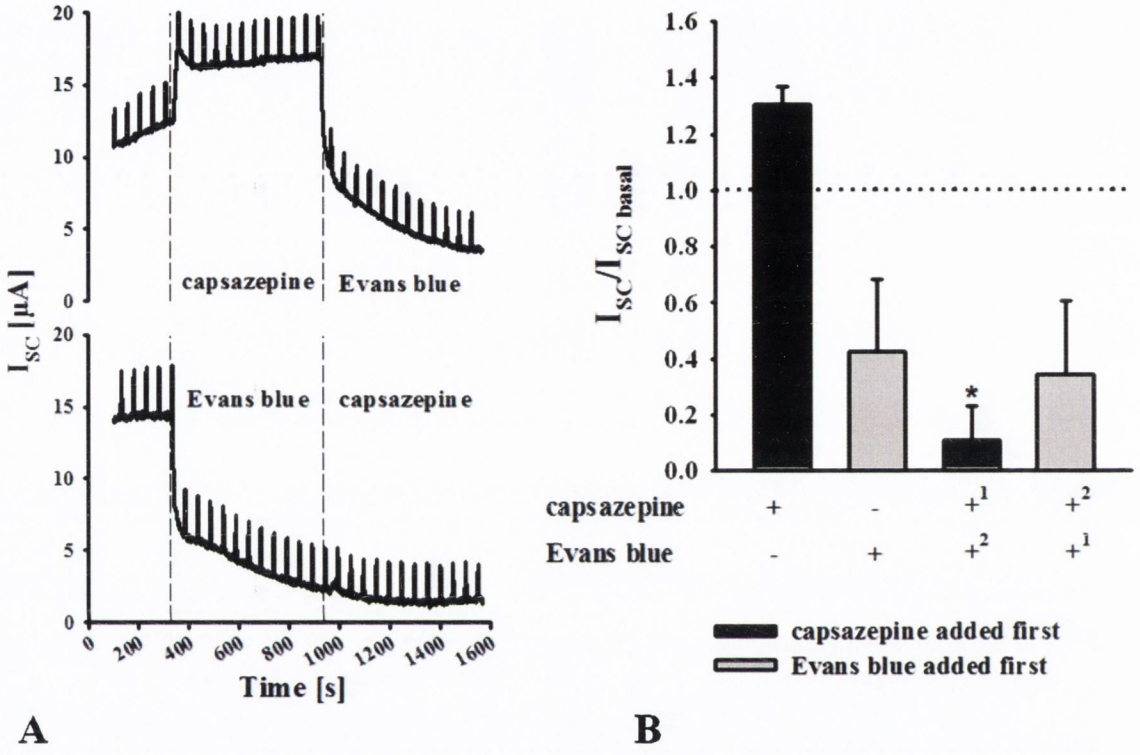

Figure 14. Capsazepine-induced I_{SC} increase was sensitive to Evans blue in δ_1-ENaC overexpressing H441 cell monolayers. **(A)** Representative I_{SC} traces in response to consecutive administration of 20 µM capsazepine and 300 µM Evans blue and *vice versa*. **(B)** Short-circuit current values were measured after administration of the respective compound and normalised against I_{SC}, measured in the absence of the substances (I_{SC} basal). Results are expressed as means ± SD (n = 3). The statistical significance of the effect is expressed as *, $P < 0.01$ versus I_{SC} in the presence of 20 µM capsazepine.

[1]: substance was added first

[2]: substance was added 10 min after the first compound

Similar results were obtained with icilin (**Figure 15**). In the presence of Evans blue, no significant current stimulation by icilin was observed. On the contrary, icilin further reduced short-circuit currents already diminished by Evans blue (from 24.2 ± 17.2% to 20.2 ± 18.0% of the basal I_{SC}; $n = 3$), albeit the effect did not reach significance. On the other hand, currents, initially activated by application of icilin by 28.5 ± 7.1% of the initial level ($n = 3$), were significantly reduced by Evans blue. The resulting I_{SC} level (11.3 ± 4.6% of the basal I_{SC}; $n = 3$) was not significantly different from I_{SC} in the presence of Evans blue alone (29.9 ± 19.1% of the basal I_{SC}; $n = 11$).

Thus, currents induced by the δ-ENaC activators capsazepine and icilin in δ_1-ENaC over-expressing H441 cells were sensitive to the δ-ENaC inhibitor Evans blue. Moreover, in cell monolayers pre-treated with Evans blue, both substances exhibited slight inhibitory effects.

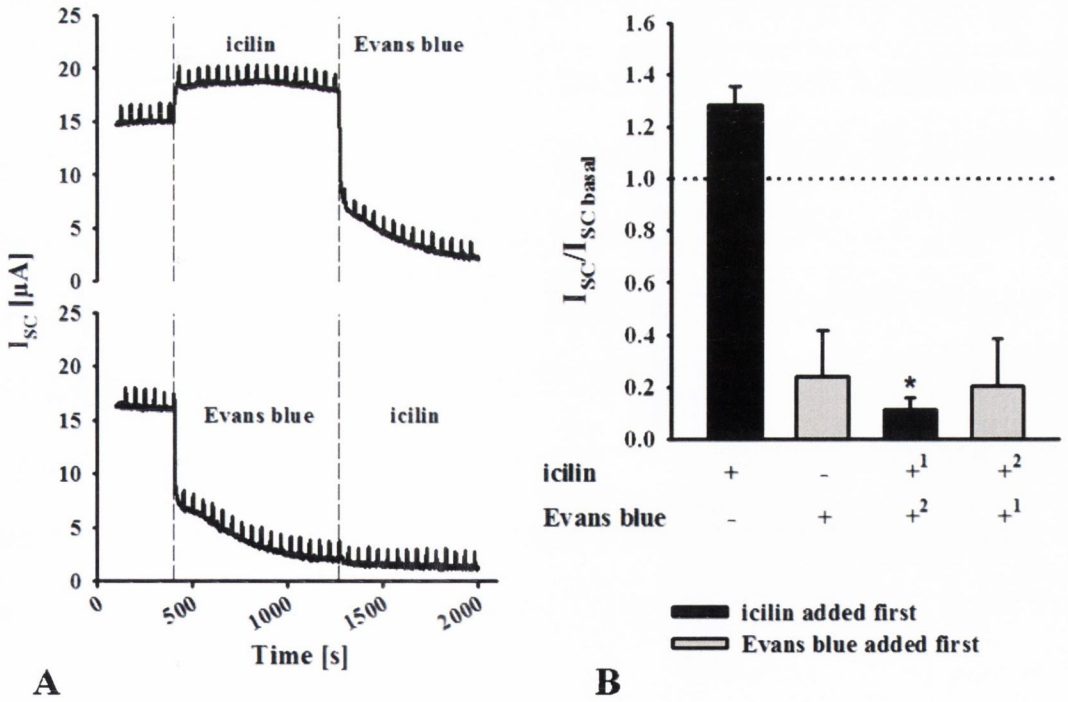

Figure 15. Icilin-induced I_{SC} increase was sensitive to Evans blue in δ_1-ENaC over-expressing H441 cell monolayers. **(A)** Representative I_{SC} traces in response to consecutive administration of 60 μM icilin and 300 μM Evans blue and *vice versa*. **(B)** Short-circuit current values were measured after administration of the respective compound and normalised against I_{SC}, measured in the absence of the substances (I_{SC} basal). Results are expressed as means ± SD (n = 3). The statistical significance of the effect is expressed as *, $P < 0.01$ versus I_{SC} measured after addition of the first compound.

[1]: substance was added first

[2]: substance was added 10 min after the first compound

5.2.3 Functional expression of δ-ENaC in δ-ENaC over-expressing and wild-type H441 cells

All three alleged modulators of δ-ENaC exhibited inhibitory effects in the wild-type H441 cells and freshly isolated human alveolar epithelial cells in primary culture. We now used over-expression of the δ-subunit as a means to investigate if the observed pharmacological responses indeed originated from the compounds' interaction with δ-ENaC.

In native epithelia, highly Na^+ selective cation channels (HSC), likely to be represented by αβγ-ENaC channels, and the nonselective cation channels (NSC), the molecular basis of which remains controversial, differ in their sensitivity to the potassium-sparing diuretic, amiloride (reviewed by Matalon *et al.* 2002). In heterologous expression systems, similar is true for α- and δ-ENaC-mediated currents, with α-ENaC containing channels exhibiting an approximately 30-fold higher sensitivity to this commonly used ENaC blocker (Waldmann *et al.* 1995). As a rule of thumb, α-ENaC-mediated currents are considered to be inhibited by 10 μM, δ-mediated currents by 100 μM concentration of amiloride (Canessa *et al.* 1993; Waldmann *et al.* 1995). Applied at higher

concentrations, amiloride also inhibits currents mediated by other ion channels, e.g., by ASIC1-3 (Alvarez de la Rosa *et al.* 2000), or channels and transporters unrelated to ENaC (Kleyman, Cragoe, 1988). In the wild-type cells, amiloride concentration of 10 μM was sufficient to inhibit the main portion of the I_{SC} (~ 90%), whilst merely ~ 5% of the basal currents showed additional sensitivity to 100 μM amiloride. This was consistent with the observations by Albert *et al.* (2008), who described two distinct populations of sodium channels in the membranes of H441 cells (HSC and NSC), with 56 ± 5% of total I_{SC} being sensitive to 1 μM amiloride, further 30 ± 3% to 10 μM and approx 5% to 100 μM. In δ_1-ENaC over-expressing H441 cells, on the other hand, only ~ 25% of the basal short-circuit current were inhibited by addition of 10 μM amiloride. An additional 55% were sensitive to 100 μM amiloride. Importantly, contribution of sodium-currents to the total I_{SC} was similar in both cell types, as demonstrated by inhibition of Na^+/K^+-ATPase by ouabain. Non sodium-dependent currents were likely to be responsible for the remaining I_{SC}, insensitive to 100 μM amiloride. These results suggest that, in comparison to the wild-type cells, the less amiloride-sensitive δ-ENaC-mediated currents contribute to a larger extent to the total sodium current in the δ_1-ENaC over-expressing H441 cells. Certainly, this observation could also be an unspecific effect of the transfection procedure, an artefact, with re-assembly of the surface channels population causing a shift in favour of NSC channels in the over-expressing cells. However, the latter would not explain the effects of the selective δ-ENaC modulators in the transfected cells, as described below.

Yamamura and colleagues characterised Evans blue as a selective inhibitor (2005b) and both capsazepine and icilin as selective activators of δ-ENaC function (2004b, 2005a) in patch-clamp experiments conducted in *X. laevis* oocytes expression system. In our hands, Evans blue reduced short-circuit currents in transepithelial measurements

conducted in the wild-type H441 cells, which were used as organotypic model of human respiratory epithelium. The stimulatory effects of the alleged δ-ENaC activators, however, could not be reproduced in these cells. In the δ_1-ENaC over-expressing H441 cells, on the other hand, both capsazepine and icilin activated net ion transport, while Evans blue still acted as an inhibitor of the I_{SC}. Hence, the modes of action of three modulators in the transfected H441 cells were consistent with the observations reported by Yamamura *et al.* (2004a, 2005a, 2005b). Moreover, activation of short-circuit currents by capsazepine and icilin was, at least partially, insensitive to 10 μM amiloride, since both compounds were able to produce significant increases in I_{SC} in the presence of 10 μM amiloride. Furthermore, the stimulatory effects were completely abolished by application of 100 μM amiloride or 300 μM Evans blue, suggesting that the observed increases in I_{SC} indeed resulted from specific activation of δ-ENaC containing channels.

These data taken together with the confirmed localisation of δ-ENaC in the cell membranes of the transfected cells suggests that the over-expressed δ-ENaC protein is functional in the δ_1-ENaC over-expressing H441 cells and confirms the specificity of the alleged δ-ENaC modulators, at least, in this model.

Since capsazepine and icilin elevated short-circuit currents in δ_1-ENaC over-expressing H441 cells, and these effects could be characterised as δ-ENaC-specific due to their sensitivity to amiloride and Evans blue, it is conceivable that the inhibitory effects, observed with both substances in the wild-type H441 cells, did not originate from specific interactions of the compounds with δ-ENaC, but with other proteins. Interestingly, small, albeit not significant, reductions of I_{SC} by capsazepine and icilin were observed in monolayers of δ_1-ENaC over-expressing cells, pre-treated with Evans blue. Hence, the compounds showed effects similar to those in the wild-type cells, when

the activity of the over-expressed δ-ENaC protein was pharmacologically suppressed, providing further evidence for the icilin-effects in the non-transfected H441 cells being not δ-ENaC-specific. Against this background, the effect of Evans blue in the wild-type cells was, most likely, also due to modulation of a target distinct from δ-ENaC, even though the substance showed the same mode of action in both, wild-type and transfected cells.

CHAPTER 6

Discussion and conclusions

6.1 Discussion

The overall aim of this work was to gain insight into the physiological role of the epithelial sodium channel δ-subunit in human respiratory epithelium. In particular, the objective was to prove the hypothesis that δ-ENaC contributes to the net transepithelial ion transport in the lung.

6.1.1 The relevance of the work and experimental models

Despite newly arisen interest and increased number of studies focusing on this homologous ENaC subunit, a lot still remains unknown. In particular, whilst our knowledge about the spatial expression of δ-ENaC in different tissues and its biophysical properties is becoming more detailed and comprehensive, what we know about its (patho)physiological role is merely putative. This is also the case for the probably most investigated expression site of δ-ENaC outside neuronal tissues – the lung. There is a growing body of evidence confirming the presence of δ-ENaC in human respiratory epithelium. Delta-ENaC mRNA transcripts as well as protein have been detected in various continuously growing respiratory epithelial cell lines (i.e., A549, H441 and 16HBE14o-), freshly isolated respiratory epithelial cells in primary culture (ATII, HNE) and in human lung tissue *in situ* (Ji *et al.* 2006; Bangel-Ruland *et al.* 2010; Nie *et al.* 2009b; Zhao *et al.* 2012). As a functional role of δ-ENaC in these epithelia, contribution to transepithelial sodium transport in human alveolar epithelium in health and disease has been suggested. However, as with most other postulates regarding δ-ENaC function, this hypothesis was based on data acquired in δ-ENaC expressing *X. laevis* oocytes (Ji *et al.* 2006). Supportive evidence in organotypic epithelial cells *in vitro* or *in situ*, on the other hand, is missing to date. Additionally,

absence of δ-ENaC gene expression in mice and rats hinders the development of experimental animal models to study the physiological relevance of δ-ENaC *in vivo*.

In this work, organotypic cell models of respiratory epithelium, commonly employed to investigate pulmonary solute and ion transport in the airways, were used to study the functional expression of δ-ENaC *in vitro*, i.e., A549, H441, Calu-3 and 16HBE14o- cell lines as well as freshly isolated human alveolar epithelial type I and type II cells in primary culture. Whilst δ-ENaC had been reported in A549, H441 and ATII cells prior or parallel to the start of this work (Ji *et al.* 2006; Nie *et al.* 2009b), evidence for the presence of δ-ENaC in 16HBE14o- has emerged only very recently (Zhao *et al.* 2012). Expression of δ-ENaC in Calu-3 bronchial epithelial cells has not yet been reported.

6.1.2 Delta-ENaC expression at mRNA level

Messenger RNA transcripts encoding δ-ENaC were detected in A549 and Calu-3 cell lines by means of RT-PCR. Since primers used were not designed to distinguish between δ_1- and δ_2-isoforms, only one PCR product was observed in both cases. Messenger RNA expression levels of homologous α-, β-, γ- and δ-ENaC subunits were quantified by q-PCR in these and 16HBE14o- cells. Signal intensities obtained for δ-ENaC were comparable to those of γ-ENaC, but 10-100fold lower than for α- and β-ENaC. Importantly, there is no direct link between mRNA expression levels and the efficiency of mRNA translation, so that low mRNA abundance, in our case of δ-ENaC, does not necessary lead to low protein expression levels. The results of PCR experiments were in agreement with reports of homologous α-, β-, γ- and δ-ENaC subunits being co-expressed in A549 cells (Ji *et al.* 2006) and of δ-ENaC mRNA abundance in 16HBE14o- cells (Zhao *et al.* 2012). In Calu-3 cells, transcriptional expression of δ-ENaC was demonstrated for the first time.

6.1.3 Delta-ENaC expression at protein level

6.1.3.1 Specificity of anti-δ-ENaC antisera

To study δ-ENaC protein expression and localisation, a selection of currently available antibodies directed against δ-ENaC was tested. The only custom-made anti-δ-ENaC antibody (Wesch *et al.* 2012), was kindly provided to us by Dr. Diego Alvarez de la Rosa (Universidad de La Laguna, La Laguna, Spain; DAR antibody). The commercially available antibodies, polyclonal anti-δ-ENaC antibody from Santa Cruz Biotechnology (the most frequently used in literature (Nie *et al.* 2009a, 2009b; Kapoor *et al.* 2009; Bangel-Ruland *et al.* 2010; SC antibody)) and the polyclonal anti-δ-ENaC antibody from Pierce were used (TF antibody).

First, the specificities of the selected anti-δ-ENaC antibodies were tested. As positive control, a commercially available δ-ENaC control peptide was used as well as the full-length δ_1-ENaC protein, heterologously expressed in HEK-293 cells. It is noteworthy that the antibodies tested were raised against amino acid regions present in both δ-ENaC isoforms, so that the δ_1-protein was regarded as a suitable positive control. Cell lysates of non-transfected and mock-transfected HEK-293 cells were used as negative controls. Since the protein band at 100 kDa was detected throughout positive and negative control samples with both anti-δ-ENaC SC and DAR antibodies, this signal was labelled as unspecific, albeit the 100 kDa band was δ-ENaC-specific according to manufacturer's specification in case of SC antibody. The δ-ENaC control peptide was recognised by both antibodies tested. Full-length δ_1-ENaC protein, on the other hand, only appeared as an additional band in the immunoblots probed with the DAR antibody. Thus, the specificity of anti-δ-ENaC-antibody DAR was confirmed, whereas the SC antibody proved to be unreliable. The anti-δ-ENaC TF antibody could not be optimised for the Western blot application.

6.1.3.2 Delta-ENaC expression and localisation

In literature, distinct molecular weights have been reported for the δ-ENaC protein detected by Western blot. The observed differences appear to depend on the type of the experimental model tested. In particular, the protein processing, cleavage and glycosylation may differ between endogenously and heterologously expressed proteins. Moreover, differences between various expression systems, i.e. *X. laevis* oocytes *versus* HEK-293 cells, and organ systems, i.e. the skin *versus* the lung, may not be excluded. For endogenous δ-ENaC, a single protein band was observed in samples from human skin and keratinocytes (~70 kDa, Yamamura *et al.* 2008b) as well as mouse sperm (~80 kDa, Harnández-González *et al.* 2006), whilst a double band at 80-90 kDa was detected in the lysates of human bronchiolar epithelial H441 and pleural mesothelial M9K cells (Nie *et al.* 2009b) as well as in human glioma D54-MG cell line (Kapoor *et al.* 2009). Also, for heterologously expressed δ-ENaC, products of various molecular weights have been reported. In CHO cells, only a 70 kDa δ-ENaC protein has been observed (Yamamura *et al.* 2008b). In COS-7 cells, two δ-ENaC-specific bands at 85 and 95 kDa appeared, with the upper band shifting downwards to 90 kDa following the PNGase F treatment (Chang *et al.* 2011). In *X. laevis* oocytes expressing δ-ENaC, on the other hand, Haerteis and colleagues (2009) detected two prominent bands at 75 and 86 kDa, representing an *N*-glycosylated and a non-glycosylated form of the same protein.

In our hands, a prominent band at the molecular weight of ~80-85 kDa was detected in Calu-3, H441 and ATI-like as well as in A549 and 16HBE14o- cell lysates with the anti-δ-ENaC SC antibody, similar to the protein bands reported in the lysates of H441 cells and human lung tissue (Nie *et al.* 2009a) as well as in D54-MG cells (Kapoor *et al.* 2009) using the same antibody. This band may potentially correspond to a glycosylated form of the full-length δ-ENaC protein, whilst the protein bands detected at lower

molecular weights may represent cleaved protein fragments. However, this assumption remains unverified due to the uncertain specificity of the SC antibody in our hands.

With the DAR anti-δ-ENaC antibody, a specific protein band of approximately 75 kDa was detected in the lysates of HEK-293 cells, heterologously expressing δ-ENaC. Faint bands at the corresponding molecular weight were also observed in the whole cell lysates of Calu-3, H441 and ATI-like cells. Although it can be argued that the endogenous δ-ENaC protein in the respiratory cell lysates may display a molecular weight different from the δ-ENaC heterologously expressed in HEK-293 cells, questioning the specificity of the 75 kDa band in the organotypic cells, the later over-expression of δ-ENaC in H441 cells led to potentiation of the aforesaid band and thus confirmed its specificity. Further, multiple bands at lower molecular weights, potentially representing cleaved δ-ENaC fragments, were obtained using DAR antibody.

Cell surface biotinylation and immunofluorescence microscopy were carried out to study the subcellular localisation of δ-ENaC protein in the respiratory epithelial cells. Hereby, DAR antibody detected no signals in the biotinylated membrane protein fractions of H441 and ATI-like cells, in contrast to Calu-3 cells, where a 36 kDa fragment was detected in the isolations of both apical and basolateral membrane proteins. The latter band may either represent a C-terminal 36 kDa cleavage product of δ-ENaC or be a result of an unspecific antibody binding to a 36 kDa protein, exclusively present to the membranes of bronchial, however, not of bronchiolar and alveolar cells. However, considering the fact that the extracellular proteases are highly active in H441 cells, as demonstrated by the high abundance of cleaved α- and γ-ENaC fragments in these cells (Tan *et al.* 2011), the existence of a cleavage product, exclusive to Calu-3 cells, appears unlikely. The results of the cell surface biotinylation were further

confirmed by IFM, since no fluorescent signal was detected in the cell membranes. Similar, intracellularly localised immunofluorescent staining was obtained using both, anti-δ-ENaC DAR and TF antibodies.

In the literature, the presence of δ-ENaC was demonstrated in H441 cells by means of Western blot as well as by IFM using an anti-δ-ENaC antibody from Open Biosystems (Ji *et al.* 2006). Nie and colleagues (2009b) reported δ-ENaC protein expression in H441 cells as well as in human lung tissue, however, using SC antibody. Here, expression of δ-ENaC in human bronchiolar epithelial H441 cell line as well as in human alveolar epithelial cells in primary culture was confirmed at protein level, using an antibody of confirmed specificity (DAR). In human bronchial epithelial Calu-3 cells, δ-ENaC protein was detected for the first time. Additionally, new insights into the intracellular localisation of δ-ENaC were provided, which, surprisingly, showed absence of the full-length δ-ENaC protein from the cell surfaces of respiratory epithelial cells.

6.1.4 Effects of pharmacological modulators of δ-ENaC on the short-circuit currents in human respiratory epithelial cells in vitro

For a long time, the tools for the functional characterisation of δ-ENaC had been limited to the distinct sensitivity of α- and δ-ENaC-containing channels to the well known ENaC blocker, amiloride, with α-ENaC showing ~30-fold higher amiloride affinity (Waldman *et al.* 1995). Evans blue, capsazepine and icilin have been described to specifically modulate δ- but not α-ENaC-containing channels expressed in *X. laevis* oocytes expression system (Yamamura *et al.* 2004b, 2005a, 2005b). Albeit high hopes were initially set in these substances to enable dissecting the contribution of δ-subunit to the total ENaC currents across epithelia and helping to elucidate its physiological role,

only Evans blue has been used as an inhibitor of δ-ENaC function *in vitro* by others (Bangel-Ruland *et al.* 2010). In addition, all three compounds are known to be pharmacological modulators of other targets (Bultmann and Starke, 1993; Bevan *et al.* 1992; Behrendt *et al.* 2004; Andersson *et al.* 2004). However, since more suitable pharmacological tools are currently unavailable, Evans blue, capsazepine and icilin were utilised for functional assessment of δ-ENaC in this work.

In Ussing chamber studies, all alleged modulators of δ-ENaC function showed effects on the short-circuit currents across Calu-3, H441 and ATI-like cell monolayers. Intriguingly though, our observations partially differed from those documented in the literature. According to its characterisation as a specific inhibitor of δ-ENaC activity by Yamamura *et al.* (2005b) and effects observed in human primary nasal epithelial cells (Bangel-Ruland *et al.* 2010), Evans blue reduced currents across both H441 and ATI-like cell monolayers, whilst showing concentration-dependent stimulatory effects on the I_{SC} in Calu-3 cells. Capsazepine, on the other hand, decreased I_{SC} in all cells tested, albeit being suggested as a δ-ENaC activator (Yamamura *et al.* 2004b). Moreover, icilin, another alleged activator (Yamamura *et al.* 2005a), expectedly caused a concentration-dependent I_{SC} increase in Calu-3 cell monolayers, but exhibited inhibitory effects in H441 and ATI-like cells.

Differences observed between the cell types were consistent with the allocation of the cells to the different segments of the respiratory epithelium. While Calu-3 cells reflect the transport properties of native submucosal gland serous cells, H441 and ATI-like cells represent the Na^+ absorbing epithelium of the distal lung. In both latter cell types, all alleged modulators of δ-ENaC function exhibited inhibitory effects. The short-circuit currents in Calu-3 cells, on the other hand, were decreased only by capsazepine, while Evans blue and icilin showed stimulatory effects. Moreover, when dependence of the

observed effects on the presence of Na^+ was tested, currents inhibited by δ-ENaC modulators in H441 and ATI-like cells were shown to be sodium-dependent and amiloride-sensitive. In contrast, currents stimulated or inhibited in Calu-3 cells were amiloride-insensitive, albeit sodium-dependent. Since Calu-3 cells are of serous phenotype, effects of Cl^- removal and CFTR inhibition were also studied in these cells. While reduction of I_{SC} by capsazepine did not depend on the presence of Cl^- or activity of CFTR, both icilin and Evans blue-induced increases in I_{SC} were carried by Cl^- ions. However, current stimulation was CFTR-mediated in the case of icilin, but independent from CFTR in case of Evans blue, indicating involvement of Cl^- channels different from CFTR.

6.1.5 Delta-ENaC knock-down studies

When trying to explain the obvious contradictions between the compound effects in our hands and observations by others (Yamamura *et al.* 2004b, 2005a, 2005b; Bangel-Ruland *et al.* 2010), one must consider that the respective substances had only been characterised as modulators of δ-ENaC function in the *X. laevis* oocytes expression system. While oocytes allow an accurate analysis of the biophysical properties of single membrane molecules, their obvious limitation is that the presence of other ion channels, receptors, transporters and their respective underlying pathways is missing. Thus, it is possible that in cells *in vitro*, inhibition/activation of δ-ENaC subunit does not necessary give rise to effects as they were observed by Yamamura and co-workers in *X. laevis* oocytes, but through complex signalling pathways, to responses observed in our experiments. The range of ion channels co-expressed may be essentially different in different cell models, i.e., in bronchial and alveolar epithelial (in our hands) or in human nasal epithelial cells (Bangel-Ruland *et al.* 2010), which could explain distinct results

between the cell lines. Whilst some of the discrepancies could be explained, at least theoretically, others could not be accounted for, i.e., different ion dependencies of the compound effects in Calu-3 cells, clearly indicating that the observed pharmacological responses were not derived from substance interactions with the same target, in our case δ-ENaC. Thus, studies aiming to down-regulate δ-ENaC expression were carried out to determine whether any of the observed responses were due to specific modulation of δ-ENaC.

To this end, several knock-down strategies were employed. Firstly, transient down-regulation of δ-ENaC expression was tried, using siRNA as well as dominant negative cDNA constructs (E35X) encoding a truncated δ-ENaC variant in Calu-3 as well as in H441 cells, respectively. Secondly, an attempt to stably down-regulate δ-ENaC expression was undertaken in both cell lines using lentiviral shRNA particles. However, none of the chosen approaches was successful. On the expression level, no reduction of the protein abundance was detected, regardless of the anti-δ-ENaC antibody used or the molecular weight of the band analysed. Also, no significant differences were revealed on the functional level, since amplitudes of the pharmacological responses to the alleged δ-ENaC modulators were comparable between non-transfected, mock-transfected and δ-ENaC shRNA transfected Calu-3 and H441 cell monolayers, respectively. In the case of transient transfection, functional analysis was rather difficult, as the time frame of 72 h after transfection was not always sufficient to obtain confluent cell monolayers suitable for transepithelial measurements.

While stable down-regulation of δ-ENaC expression has not been yet reported, two successful attempts of transient knock-down have been described so far. Kapoor and colleagues (2009) achieved ~50% knock-down of δ-ENaC in the human glioblastoma D54-MG cell line using dominant negative cDNA constructs (E35X). The knock-down

efficiency was determined by densitometric analysis of protein bands detected with anti-δ-ENaC SC antibody, once again raising controversy about the specificity of the latter. In addition to glioma cells being potentially more receptive for transfection than epithelial cells, a method of higher transfection efficiency than lipofection, i.e., electroporation, was used. Moreover, two-electrode voltage-clamp technique was employed, allowing functional assessment of the knock-down within 72 h after transfection. Taken together, these methodological differences may have been decisive, causing the disappointing outcome of our transient knock-down attempt with negative dominant cDNA. In the second report, siRNA technique was used to down-regulate δ-ENaC in freshly isolated human nasal epithelial cells in primary culture (Bangel-Ruland *et al.* 2010). Commercially available anti-δ-ENaC siRNA, also used in our siRNAi approach, was utilised. The protein bands detected with the anti-δ-ENaC SC antibody at 100 kDa, regarded as δ-ENaC-specific due to manufacturer's specifications, showed a decrease in intensity in the transfected HNE cells. Regrettably, neither β-actin loading control nor data of densitometric analysis were provided by the authors, so that the overall knock-down efficiency at protein level remained unclear. Interestingly, Evans blue-sensitive currents across HNE cells monolayers were almost completely abolished in transfected HNE cells, indicating ~100% reduction of δ-ENaC function. This notable knock-down efficiency on the functional level, however, raises questions, not addressed by the authors, about the contribution of δ-ENaC protein, unaffected by siRNA, to the total δ-ENaC activity in the HNE cells. Although methodological differences may not be completely ruled out as a potential reason for the failure of the RNAi technique in our hands, the striking difference in the knock-down outcomes in the respiratory epithelial cells is difficult to explain from our perspective.

6.1.6 Delta-ENaC over-expression studies

As an alternative strategy to test the functional expression of δ-ENaC in the airway epithelium, δ-ENaC was stably over-expressed in H441 cells. The approach was based on the assumption that, since H441 cells endogenously express δ-ENaC, over-expressed protein would be processed in the same way as endogenous δ-ENaC, with elevated protein expression levels leading to a potentiation of the pharmacological effects deriving from the specific modulation of δ-ENaC protein.

First, over-expression of δ-ENaC was confirmed at protein level. The specific δ-ENaC protein band at 75 kDa was of a significantly higher intensity in the transfected cells, and was demonstrated to be an *N*-glycosylated form of a 70 kDa protein. The glycosylation rate was similar in the wild-type and the transfected cells, supporting the idea of identical processing of endogenous and over-expressed δ-ENaC protein in H441 cells. Moreover, elevated protein levels led to an increased insertion of the over-expressed δ-ENaC into the cell membranes, to a level detectable by Western blot analysis of biotinylated membrane protein and IFM.

In the Ussing chamber studies, Na^+ currents across δ-ENaC over-expressing cell monolayers displayed significantly lower sensitivities to amiloride than in the wild-type cells, while the overall sodium-dependence remained unchanged, suggesting a greater contribution of δ-ENaC to the total Na^+ currents in the transfected cells. Expectedly, Evans blue still exhibited inhibitory effects on the short-circuit currents in δ-ENaC over-expressing cells. Capsazepine and icilin, on the other hand, increased I_{SC} levels, as opposed to the current reduction observed with both substances in the wild-type cells. Currents stimulated by the alleged δ-ENaC activators were, at least partially, insensitive to 10 μM amiloride and inhibitable by Evans blue. Hence, effects induced by the tested pharmacological agents in δ-ENaC over-expressing H441 cells were consistent with the

observations by Yamamura and colleagues (2004b, 2005a, 2005b). Moreover, interdependencies of the inhibitors, amiloride and Evans blue, with the activators, capsazepine and icilin, were compatible with the idea of these compounds interacting with the same target, i.e., δ-ENaC. Thus, evidence was provided that the δ-ENaC protein, over-expressed and localised to the cell surface in H441 cells, was functional and generated Na^+ currents. More importantly, it was demonstrated that, also in the complex cell model of human respiratory epithelium, the δ-ENaC-specific compounds' effects were the same as in *X. laevis* oocytes, i.e. δ-ENaC-mediated currents were indeed inhibited by Evans blue and activated by both, capsazepine and icilin.

As a consequence of these observations, it was concluded that the inhibitory effects of capsazepine and icilin in the wild-type cells were not mediated by the endogenous δ-ENaC. This was additionally confirmed by the fact that, when the function of the over-expressed δ-ENaC was inhibited by Evans blue in the transfected cells, both capsazepine and icilin slightly decreased the I_{SC}, exhibiting the same mode of action as in the wild-type cells. This, in turn, leads to the conclusion that δ-ENaC protein cannot be activated and is per se non-functional in the wild-type cells. Consequently, it appears unlikely that the Evans blue effect in the non-transfected H441 cells was due to the modulation of the endogenous δ-ENaC, even though the compound displayed the same mode of action in the wild-type as in δ-ENaC over-expressing cells and reduced short circuit-currents. Hence, despite the presence of endogenous δ-ENaC protein in H441 cells, as demonstrated in this work and also by others (Ji *et al.* 2006; Nie *et al.* 2009b), effects observed with the alleged δ-ENaC modulators in the wild-type H441 cells were likely not δ-ENaC-mediated. Thus, endogenous δ-ENaC does not contribute to the net Na^+ transport in these cells.

No over-expression experiments were carried out in Calu-3 cells, in which the specificities of the pharmacological responses to Evans blue, capsazepine and icilin were also uncertain. However, considering the data obtained in H441 cells as well as the fact that, also in Calu-3 cells, no δ-ENaC was detected in the cell membranes, Evans blue-induced increase and capsazepine-mediated decrease in the I_{SC} were indirectly confirmed not to originate from inhibition or stimulation of δ-ENaC in Calu-3 cells. Also, the response to icilin, albeit being of stimulatory nature, was likely not to be δ-ENaC-mediated. Thus, as in the case of H441 cells, the function of δ-ENaC protein was not affected by the administration of pharmacological δ-ENaC modulators in Calu-3 cells.

6.1.7 Molecular identity of alternative targets of alleged δ-ENaC modulators in the wild-type human respiratory epithelial cells

Certainly, since the contribution of endogenous δ-ENaC to the effects observed with δ-ENaC modulators in human respiratory epithelial cells was ruled out, the question about their molecular basis remains. As previously mentioned, all three compounds are known for interactions with targets different from δ-ENaC. For instance, whilst capsazepine acts as a competitive antagonist on both TRPV1 and TRPM8 receptors (Bevan *et al.* 1992; Behrendt *et al.* 2004), icilin as a "super-cooling agent" activates TRPM8, which is also stimulated by menthol and cold-stimuli (Andersson *et al.* 2004). As expression of both TRPV1 and TRPM8 receptors has been reported in human respiratory epithelial cells, their regulation by capsazepine and icilin may account for the outcomes observed with these compounds. In particular, a truncated variant of TRPM8 receptor has been described in normal bronchial epithelial cells (NHBE) and in human bronchial epithelial BEAS-2B cell line (Sabnis *et al.* 2008), however, not in alveolar epithelium so far.

Transient receptor potential vanilloid subfamily 1, on the other hand, has been detected in both human bronchial and alveolar epithelial cells, i.e., bronchial NHBE and BEAS-2B cells as well as in human alveolar epithelial A549 cells (Thomas *et al.* 2012: Reilly *et al.* 2003). Hence, despite the absence of direct evidence, it is conceivable that these ion channels may be differentially expressed in bronchial Calu-3, bronchiolar H441 and ATI-like cells, with inhibition of TRPM8 and TRPV1 by capsazepine and activation of TRPM8 by icilin leading to the respective inhibitory or stimulatory effects. Moreover, capsazepine also blocks voltage-dependent potassium channels (Kuenzi *et al.* 1996). Expression of the latter has been reported in rat alveolar epithelial cells in primary culture and in Calu-3 cells with localisation at the apical cell surfaces (Lee *et al.* 2003b; Moser *et al.* 2008), offering an alternative explanation for the observed capsazepine-induced I_{SC} decreases in Calu-3, H441 and ATI-like cell monolayers.

Among the substances tested, Evans blue is probably the least specific compound, since it has been reported to interact with a range of different proteins: *inter alia* P_2X-purinergic receptors, glutamate transporters, large-conductance, Ca^{2+}-activated K^+ channels and δ-ENaC (Bultmann and Starke, 1993; Roseth *et al.* 1995; Hollywood *et al.* 1998; Yamamura *et al.* 2005b). In the lung, expression of P_2X-receptors is cell type specific. While there is no evidence for their presence in ATII cells, apical P_2X_4 and P_2X_7 receptors are present in ATI cells and have been suggested as specific cellular markers of pneumocyte differentiation (Qiao *et al.* 2003; Chen *et al.* 2004). Also in the bronchial epithelium, expression of P_2X-receptors has been described, i.e., P_2X_4, P_2X_5 and P_2X_6 in 16HBE14o-, Calu-3 and BEAS-2B cell lines (Taylor *et al.* 1999; Liang *et al.* 2005). Purinergic signals are most likely involved in cell differentiation, proliferation and migration in these epithelia. Moreover, apical purinergic receptors mediate the autocrine regulation of Cl^- secretion and Na^+ absorption by CFTR in airway

epithelia. Activation of CFTR promotes extracellular ATP release, which leads to elevation of intracellular Ca^{2+} levels via activation of purinergic receptors in human bronchial epithelial cells (Walsh *et al.* 2000). Increase in $[Ca^{2+}]_i$, in turn, stimulates Ca^{2+} dependent Cl^- secretion via CaCC channels (Stutts *et al.* 1992; Paradiso *et al.* 2001). When the effect is triggered by the direct activation of purinergic receptors rather than CFTR, the current stimulation occurs in a Cl^--dependent, however, non-CFTR-mediated manner, which is similar to the Evans blue-stimulated I_{SC} increase in Calu-3 cells. Furthermore, Na^+ uptake is diminished via purinergic stimuli and subsequently elevated $[Ca^{2+}]_i$ (Graham *et al.* 1992). Notably, Na^+ currents were inhibited by Evans blue in H441 and ATI-like cells, in which Cl^- currents do not contribute greatly to the total ion flow. Thus, activation of P_2X-purinergic receptors appears as a sound base for Evans blue effects as observed in our hands. However, interaction of Evans blue with P_2X receptors is of inhibitory, rather than stimulatory kind (Bultmann and Starke, 1993), undermining the latter explanation. Activation of large-conductance, Ca^{2+} activated K^+ channels (BK) is another mode of action exhibited by Evans blue (Hollywood *et al.* 1998; Wu *et al.* 1999). Indeed, presence of functional BK channels at the apical surface of NHBE cells has been most recently described by Manzanares and colleagues (2011). Most importantly, not only did activation of these channels stimulate apical K^+ secretion, it also triggered an increase in apical Cl^- efflux, suggesting that current stimulation by Evans blue in Calu-3 cells may indeed occur via BK channels.

Ultimately, it would go beyond the scope of this work to identify the exact molecular pathways leading to the observed, albeit not δ-ENaC-specific, pharmacological effects of δ-ENaC modulators in human respiratory epithelial cells. Nevertheless, it is noteworthy to highlight the potential relevance to further investigate the nature of Evans-blue induced increase in short-circuit currents in Calu-3 cells. Evans blue

stimulated I_{SC} in a chloride-dependent, but CFTR-independent manner, potentially via activation of apical BK channels. In cystic fibrosis (CF), the defect of CFTR gives rise to an impaired Cl^- transport across bronchial epithelial barriers, resulting in thickened mucus and subsequent infections of the airways. A promising strategy in CF therapy is to decrease the mucus' viscosity. This can be achieved through, e.g., inhaled rhDNase (Pulmozyme®) or indeed through an increase in transepithelial ion flux. The Evans blue-mediated mechanism could, hence, serve as a novel therapeutic approach in the treatment of CF. Furthermore, identification of the pharmacophore responsible for the interaction with the respective target would enable developing of novel promising drugs for CF therapy.

6.1.8 Contribution of δ-ENaC to ENaC-mediated currents

This work demonstrated that administration of compounds, previously characterised as specific δ-ENaC modulators, did not lead to δ-ENaC-specific responses in the short-circuit currents in human respiratory epithelial cells *in vitro*. This suggests that δ-ENaC, expressed at both mRNA and protein levels in these cells, is likely non-functional and does not contribute to the net transepithelial ion transport, at least under basal conditions. Nevertheless, existence of stimuli able to up-regulate δ-ENaC activity, e.g., via mobilisation of intracellularly stored protein and its increased insertion into the cell membrane, cannot be ruled out and requires further investigation. Another issue to be addressed is the composition of the δ-ENaC-containing channels in the wild-type and δ-ENaC over-expressing H441 cells and/or the characterisation of the effects of Evans blue, capsazepine and icilin on the δαβγ-ENaC channels. As demonstrated in this work and by others (Ji *et al.* 2006), α-, β-, γ-, and δ-ENaC are expressed in human bronchiolar epithelial H441 cells. According to Ji and colleagues, ENaC proteins physically interact

in H441 cells, as shown by means of co-immunoprecipitation. Therefore, in a cell expressing all four homologous subunits, co-existence of differently composed ENaC channels is likely (i.e., α-, δ-, αβγ-, δβγ- as well as δαβγ-ENaC). Over-expression of a single subunit, in our case δ, shifts the natural composition of the ion channel population of the cell towards one or two particular channel types. Hence, it is conceivable that the observed effects (or absence thereof) may be due to the primary involvement of δ-ENaC protein in the assembly of different channel types in the wild-type and δ-ENaC over-expressing cells (i.e., δαβγ- and δβγ-channels, respectively). This consideration is important to the extent that the composition of the heteromeric channel defines its biophysical properties. For instance, the IC_{50} values for amiloride of αβγ-, δβγ- and δαβγ-channels, determined in *X. laevis* oocytes, were 0.3 μM, 13.1 μM and 3.8 μM, respectively (Ji *et al.* 2006). The relevant values for the alleged δ-ENaC modulators have not been described in literature so far. Hence, the effects of Evans blue, capsazepine and icilin, reported to affect δ- and δβγ-ENaC, but not α- and αβγ-ENaC-mediated currents (Yamamura *et al.* 2004, 2005a, 2005b), on δαβγ-channels remain unknown. It is highly likely though that their modes of action for δβγ- and δαβγ-channels are of the same quality, although different amplitude. In this case, our conclusions regarding the function of δ-ENaC in human respiratory epithelium remain valid. However, to ultimately confirm our findings, characterisation of Evans blue, capsazepine and icilin in their action on δαβγ-ENaC channels would be desirable.

6.2 Conclusions

Recently, there has been emerging evidence for the expression of the epithelial sodium channel δ-subunit in human bronchial and alveolar epithelial cells. Studies of biophysical properties of δ-ENaC, heterologously expressed in *Xenopus laevis* oocytes, gave rise to the hypothesis that δ-ENaC may contribute to the transepithelial Na^+ transport across native epithelia, in particular in the lung. This work disproves this assumption by providing an insight into δ-ENaC expression and function in human respiratory epithelial cells *in vitro*. The conclusions are stated below.

Comparison of different anti-δ-ENaC antibodies, employing positive and negative controls, revealed uncertain specificity of commercially available biomolecular tools. Hence, some of the previously reported expression sites of δ-ENaC, especially in human respiratory epithelium, would need to be reviewed and reconfirmed.

Evans blue as well as capsazepine and icilin have been previously characterised in *X. laevis* oocytes heterologous expression system as selective inhibitor and activators of δ-ENaC, respectively. However, the suitability of these compounds as modulators of δ-ENaC in complex *in vitro* models is highly limited due to their interaction with multiple other targets, in particular, their interference with purinergic pathways as well as with K^+ transport.

Expression of δ-ENaC was confirmed in human respiratory epithelial A549, 16HBE14o- and H441 cell lines, consistently with previous reports. For the first time, the presence of δ-ENaC was demonstrated in the human bronchial epithelial Calu-3 cell line as well as in freshly isolated human alveolar epithelial type I-like cells in primary culture. However, the abundance levels of δ-ENaC protein were very low, and no δ-ENaC was detected at the cell surfaces.

In our hands, inhibitory and stimulatory effects, exhibited by alleged modulators of δ-ENaC function on the short-circuit currents across cell monolayers of Calu-3, H441 and ATI-like cells, differed from the compound effects, as observed in heterologous expression systems. Over-expressing δ-ENaC in H441 cells identified effects in the wild-type human respiratory epithelial cells as not δ-ENaC-mediated.

Collectively, this work demonstrates that, despite its expression at mRNA and protein levels, δ-ENaC function was not detectable in human respiratory epithelial cells *in vitro*. Thus, relevant contribution of endogenous δ-ENaC to the net transepithelial ion transport across respiratory epithelium, as suggested by data previously acquired in heterologous expression systems, could not be confirmed. Since our studies focused on the transepithelial ion movement under basal, unstimulated conditions, future work will be required to clarify whether and via which stimuli activity of δ-ENaC can be up-regulated in human airway epithelium. Moreover, based on our findings, the specificities of currently available biomolecular and pharmacological tools for characterisation of δ-ENaC expression and function are highly unsatisfactory. Therefore, there is demand for more and specific anti-δ-ENaC antibodies as well as pharmacological modulators of δ-ENaC function that would help specifically dissect the contribution of the δ-subunit to ENaC-mediated sodium transport and elucidate the physiological role of δ-ENaC in and outside the human lung.

Appendices

I Acknowledgements

First and foremost, I thank my supervisor Dr. Carsten Ehrhardt for the constant enthusiasm, encouragement, support and guidance provided over the course of my PhD. Thank you for the instant advice when experiments went wrong, for steady reassurance that things will work out eventually (also known as the "alles-wird-gut"-attitude) and for ensuring that working in the lab was both challenging and fun. I am especially grateful that I was given the great opportunity to attend numerous international conferences and the chance to present my work, to meet many interesting people and to enjoy science in its truest sense. Truly, this work would not have been possible without him and without that peculiar confocal picture he took years ago.

I am grateful to Dr. Horst Fischer and Dr. Beate Illek for providing me with the opportunity to spend three months in their lab at CHORI, to learn so much, and for making Berkeley feel like home to me. I also thank all my colleagues at CHORI; Ashok, Eric, Eric, Henrik, Johnny – for scientific support and advice as well as Lauren, Maria and Mark – for the fun aspect of it. Further, I wish to express my gratitude to Prof. Claus-Michael Lehr and his group for the supply with primary cells. I am especially grateful to Dr. Diego Alvarez de la Rosa for providing the δ-ENaC plasmid, the antibody and, by this means, the long-awaited turning point in this project.

I also acknowledge support and funding by the Irish Research Council for Science, Engineering and Technology (IRCSET), i.e., the EMBARK Postgraduate Scholarship Scheme.

Further, I wish to thank all people at Trinity College who supported and contributed to my work. Especially, I'd like to thank everyone who introduced me to the lab, taught me all the important techniques and gave advice, making my (first) steps in research

much easier. In particular, I am grateful to Dr. Stephen Buckley and Johanna Salomon for training me in confocal microscopy. I further thank the two of them for introducing me to cell culture, especially Johanna for her constant assistance in cell culture work and in so many other things over the whole period of my PhD. I thank Dr. Jose Corbalan, Dr. Serena Germano and Dr. Sibylle Endter for their assistance and advice in PCR as well as Dr. Michael Johnston for his help with my first ever Western blots. I am grateful to Stephany Micallef for her assistance in plasmid propagation. Further, I want to thank Dr. Sweta Rani for answering my never-ending questions about pretty much everything. I am grateful to Svenja Sladek for performing a part of the Western blot and Ussing chamber experiments and for sharing the unique DVC-1000 experience with me.

Thank you to all my great colleagues for being such fun in and outside the lab: Adrian, Anita, Brian, Christine, Claire, Edyta, Evelyn, Fred, Gary, Haris, Ines, Janani, Joanne, Johanna, Jose, Julia, Leonie, Keith, Krzysztof, Maria, Michael, Oli, Sanghee, Serena, Shane, Sibylle, Simona, Stefano, Stephany, Stephen, Susan, Svenja, Sweta, Vincent, Vincent and Youness. Especially, I want to thank Johanna, Stephen and Leonie for their support and for the fun time together outside the lab, in Dublin rain and Californian sun. To all my friends outside Trinity – thank you for your understanding, for all the fun and for reminding that life outside the lab does exist. Thanks to Marion for hours and hours on Skype, to Daniela for the latest up-dates, to Elli for warm-hearted welcomes, and to Valter for both, making me laugh and driving me crazy at times.

Finally, I wish to thank my family, especially my parents and my sister for their love, understanding, continued support and believe in me. None of what I've ever achieved would have been possible without them. Дорогие мои, все, чего я когда-либо достигла - это благодаря Вам! Спасибо Вам за любовь, заботу, понимание и веру в меня.

II List of publications

Abstracts and poster presentations:

- Schwagerus E, Buckley ST, Ehrhardt C (2010). Functional expression of the epithelial sodium channel delta subunit in human respiratory epithelial cells. FASEB J, *Experimental Biology Meeting 2010, Anaheim, CA, 24-28/04/2010*, 24, 2010, pp611.14

- Schwagerus E, Buckley ST, Ehrhardt C (2010). ENaC delta-subunit is functionally expressed in human respiratory epithelial cells. Am J Respir Crit Care Med, *Annual Meeting of the American Thoracic Society 2010, New Orleans, LA, 14-19/05/2010*, 181(1), 2010, ppA6454

- Schwagerus E, Buckley ST, Ehrhardt C (2011). Studies on the activity of the delta-ENaC in human respiratory epithelial cell lines. FASEB J, *Experimental Biology Meeting 2011, Washington, DC, 09-13/04/2011*, 25, 2011, pp659.1

- Schwagerus E, Buckley ST, Ehrhardt C (2011). Expression and function of the epithelial sodium channel delta subunit in human respiratory epithelial cells. Am J Respir Crit Care Med, *Annual Meeting of the American Thoracic Society 2011, Denver, CO, 13-18/05/2011*, 183, 2011, ppA4229

- Schwagerus E, Buckley ST, Fischer H, Illek B, Ehrhardt C (2011). Epithelial sodium channel delta subunit and its functional expression in human respiratory epithelial cells. The Physiologist, *2011 APS Conference: 7th International Symposium on Aldosterone and the ENaC/Degenerin Family of Ion Channels, Pacific Grove, CA, 18-22/09/2011,* 54(6), 2011, pp4.27

- Schwagerus E, Illek B, Fischer H, Ehrhardt C (2012). Studies on the functional expression of the epithelial sodium channel delta subunit (δ-ENaC) in human respiratory epithelial cells *in vitro*. FASEB J, *Experimental Biology Meeting 2012*, San Diego, *CA*, *21-25/04/2012*, 26, 2012, pp696.1

- Schwagerus E, Illek B, Fischer H, Ehrhardt C (2012). Functional expression of the epithelial sodium channel delta subunit in human respiratory epithelial cells *in vitro*. Am J Respir Crit Care Med, *Annual Meeting of the American Thoracic Society 2012, San Francisco, CA*, *18-23/05/2012*, 185, 2012, ppA3528

Oral presentations:

- Investigations on the functional expression of the epithelial sodium channel delta subunit in human respiratory epithelial cells, *29th West Coast Salt & Water Club Meeting, Morro Bay, CA, 13/03/2010, 2010*

- Expression and function of the epithelial sodium channel delta subunit in human respiratory epithelium, *Irish Epithelial Physiology Group Meeting 2010, Kilkenny, Ireland, 22/10/2010, 2010*

- Studies on the activity of the epithelial sodium channel delta subunit in human respiratory epithelial cell lines, *Pre-Experimental Biology Epithelial Transport Meeting 2011, Washington, DC, 09/04/2011, 2011*

- Epithelial sodium channel delta subunit (δ-ENaC) and its functional expression in human respiratory epithelial cells, *Irish Epithelial Physiology Group Meeting 2011, Kilkenny, Ireland, 21/10/2011, 2011*

- Delta-ENaC expression and function in the airways, *Pre-Experimental Biology Epithelial Transport Meeting 2012, San Diego, CA, 21/04/2012, 2012*

III List of abbreviations

16HBE14o-	human bronchial epithelial cell line
A549	human alveolar epithelial cell line
aa	amino acid
AFC	alveolar fluid clearance
AIP	aldosterone-induced protein
Akt1	protein kinase B
ALF	alveolar lining fluid
ALI	acute lung injury
ANOVA	analysis of variance
AQP	aquaporin
ARDS	acute respiratory distress syndrome
ASIC	acid-sensing ion channel
ATCC	American Type Culture Collection
ATI	alveolar epithelial type-I cell
ATII	alveolar epithelial type-II cell
ATP	adenosine triphosphate
BEAS-2B	human bronchial epithelial cell line
BK	large conductance, Ca^{2+} activated K^{+} channel
bp	base pair
BSA	bovine serum albumin
CaCC	Ca^{2+}-activated Cl^{-} channel
Caco-2	human colorectal epithelial cell line

Calu-3	human bronchial epithelial cell line
cAMP	cyclic-adenosine monophosphate
cDNA	complementary DNA
CF	cystic fibrosis
CFPAC	human cystic fibrosis pancreatic adenocarcinoma cell line
CFTR	cystic fibrosis conductance regulator
CHO	Chinese hamster ovary cells
CLC	Cl^- channel
CLSM	confocal laser scanning microscopy
CNG	cyclic nucleotide-gated channel
CNS	central nervous system
COMMD1	copper metabolism Murr1 domain 1
COS-7	green monkey kidney fibroblast-like cell line
D54-MG	human malignant glioma cell line
DEG	degenerin
DEPC	diethylpyrocarbonate
DMEM	Dulbecco's modified Eagle's medium
DMSO	dimethylsulfoxid
DNA	deoxyribonucleic acid
dNTP	deoxy-nucleotide-triphosphate
E35X	δ-ENaC dominant negative cDNA construct with a premature stop codon at serine 35
EB	Evans blue

EC_{50}	half maximal effective concentration
ECACC	European Collection of Animal Cell Cultures
ECL	extracellular loop
EMEM	Eagle's modified essential medium
ENaC	epithelial sodium channel
$F(ab')_2$	antigen-binding fragment
FaNaC	Phe-Met-Arg-Phe-amide-gated sodium channel
FBS	foetal bovine serum
G-361	human melanoma cell line
G418	geneticin
H441	human bronchiolar epithelial cell line
hAEpC	primary human alveolar epithelial cells
HEK-293	human embryonic kidney cell line
HEPES	N-2-hydroxyethylpiperazine-N'-2-ethanesulfonic acid
HNE	human nasal epithelial cells
HRP	horseradish peroxidise
HSC	highly selective cation channel
IC_{50}	half maximal inhibitory concentration
ICH	immunohistochemistry
IFM	immunofluorescence microscopy
IFU	infectious unit of virus
IgG	immunoglobulin G
I_{SC}	short-circuit current

ISH	*in situ* hybridisation
K_{ATP}	ATP-sensitive K^+ channel
KRB	Krebs-Ringer-Buffer
LCC	liquid-covered culture
M9K	human mesothelioma cell line
mRNA	messenger ribonucleic acid
NB	Northern blot
Nedd4-2	an E3 ubiquitin ligase (neural precursor cell expressed, developmentally down-regulated 4-2)
NHBE	normal human bronchial epithelial cells
NKCC	Na^+-K^+-$2Cl^-$ cotransporter
NSC	non-selective cation channels
P_2X	family of cation-permeable purinergic ion channels
PBS	phosphate buffered saline
pcDNA3.1(+)	mammalian expression vector
PCL	periciliary liquid
PCR	polymerase chain reaction
PD	transepithelial potential difference
$Pd(N)_6$	random hexamers 5'-phosphate
pEYFP-C1	mammalian expression vector
PHK16-0b	human keratinocyte cell line
PNGase F	*N*-glycosidase F
P_o	open probability

PPPxY (PY)	proline-rich motif (P = proline, x = any amino acid, Y = tyrosine)
qPCR	quantitative polymerase chain reaction
RNA	ribonucleic acid
RT	reverse transcriptase
RT-PCR	reverse transcriptase polymerase chain reaction
SAGM	small airway epithelial basal medium
SD	standard deviation
SDS-PAGE	sodium dodecyl sulphate polyacrylamide gel electrophoresis
SGK1	serum and glucocorticoid kinase 1
shRNA	small hairpin RNA or short hairpin RNA
siRNA	small interfering RNA
SOC	Super Optimal Broth medium
SP-A, SP-D	surfactant protein A, surfactant protein D
sulfo-NHS	N-Hydroxysulfosuccinimide
SV40	Simian vacuolating virus 40
TEER	transepithelial electrical resistance
TM	transmembrane domain
TRPM8	transient receptor potential melastatin subfamily 8
TRPV1	transient receptor potential vanilloid subfamily 1
VILI	ventilator-induced lung injury
WB	Western blot
wt	wild-type
ZO-1	zonula occludens protein 1

IV References

Abi-Antoun T, Shi S, et al. (2011). Second transmembrane domain modulates epithelial sodium channel gating in response to shear stress. Am J Physiol Renal Physiol 300(5):F1089-95

Adams CM, Anderson MG, et al. (1998). Ripped pocket and pickpocket, novel Drosophila DEG/ENaC subunits expressed in early development and in mechanosensory neurons. J Cell Biol 140:143-52

Al-Bazzaz FJ, Hafez N, et al. (2001). Detection of Cl^-/HCO_3^- and Na^+/H^+ exchangers in human airways epithelium. JOP 2:285-90

Albert AP, Woollhead AM, et al. (2008). AICAR decreases the activity of two distinct amiloride-sensitive Na^+-permeable channels in H441 human lung epithelial cell monolayers. Am J Physiol Lung Cell Mol Physiol 295(5):837-48

Althaus M, Pichl A, et al. (2011). Nitric oxide inhibits highly selective sodium channels and the Na^+/K^+-ATPase in H441 cells. Am J Respir Cell Mol Biol 44(1):53-65

Alvarez de la Rosa D, Canessa CM, et al. (2000). Structure and regulation of amiloride-sensitive sodium channels. Annu Rev Physiol 62:573-94

Alvarez de la Rosa D, Krueger SR, et al. (2003). Distribution, subcellular localization and ontogeny of ASIC1 in the mammalian central nervous system. J Physiol 546:77-87

Amin MS, Wang HW, et al. (2005). Distribution of epithelial sodium channels and mineralocorticoid receptors in cardiovascular regulatory centers in rat brain. Am J Physiol Regul Integr Comp Physiol 289: R1787-97

Andersson DA, Chase HW, Bevan S. (2004). TRPM8 activation by menthol, icilin and cold is differentially modulated by intracellular pH. J Neurosci 24:5364-9

Awayda MS, Bengrine A, et al. (2004). Nonselective cation transport in native esophageal epithelia. Am J Physiol Cell Physiol 287(2):C395-402

Babini E, Geisler HS, et al. (2003). A new subunit of the epithelial Na^+ channel identifies regions involved in Na^+ self-inhibition. J Biol Chem 278(31):28418-26

Bangel N, Dahlhoff C, et al. (2008). Upregulated expression of ENaC in human CF nasal epithelium. J Cyst Fibros 7(3):197-205

Bangel-Ruland N, Sobczak K, et al. (2010). Characterization of the epithelial sodium channel delta-subunit in human nasal epithelium. Am J Respir Cell Mol Biol 42(4):498-505

Bardou O, Trinh NT, Brochiero E (2009). Molecular diversity and function of K^+ channels in airway and alveolar epithelial cells. Am J Physiol Lung Cell Mol Physiol 296(2):L145-55

Barker PM, Nguyen MS, et al. (1998). Role of gamma ENaC subunit in lung liquid clearance and electrolyte balance in newborn mice. Insights into perinatal adaptation and pseudohypoaldosteronism. J Clin Invest 102:1634-40

Bastacky J, Lee CY, et al. (1995). Alveolar lining layer is thin and continuous: low-temperature scanning electron microscopy of rat lung. J Appl Physiol 79:1615-28

Bean BP (2007). The action potential in mammalian central neurons. Nat Rev Neurosci 8(6):451-65

Behrendt HJ, Germann T, et al. (2004). Characterization of the mouse cold-menthol receptor TRPM8 and vanilloid receptor type-1 VR1 using a fluorometric imaging plate reader (FLIPR) assay. Br J Pharmacol 141(4):737-45

Berdiev BK, Xia J, et al. (2003). Acid-sensing ion channels in malignant gliomas. J Biol Chem 278(17):15023-34

Bevan S, Hothi S, et al. (1992). Capsazepine: a competitive antagonist of the sensory neurone excitant capsaicin. Br J Pharmacol 107(2):544-52

Biasio W, Chang T, et al. (2004). Identification of Murr1 as a regulator of the human delta epithelial sodium channel. J Biol Chem 279(7):5429-34

Borok Z, Liebler JM, et al. (2002). Na^+ transport proteins are expressed by rat alveolar epithelial type I cells. Am J Physiol Lung Cell Mol Physiol 282: L599-608

Braiman A, Priel Z (2008). Efficient mucociliary transport relies on efficient regulation of ciliary beating. Respir Physiol Neurobiol 163(1-3):202-7

Brochiero E, Dagenais A, et al. (2004). Evidence of a functional CFTR Cl(−) channel in adult alveolar epithelial cells. Am J Physiol Lung Cell Mol Physiol 287: L382-92

Brockway LM, Zhou ZH, et al. (2002). Rabbit retinal neurons and glia express a variety of ENaC/DEG subunits. Am J Physiol Cell Physiol 283(1):C126-34

Brouard M, Casado M, et al. (1999). Epithelial sodium channel in human epidermal keratinocytes: expression of its subunits and relation to sodium transport and differentiation. J Cell Sci 112(19):3343-52

Brower M, Carney DN, et al. (1986). Growth of cell lines and clinical specimens of human non-small cell lung cancer in a serum-free defined medium. Cancer Res 46(29):798-806

Bultmann R, Starke K. (1993). Evans blue blocks P_2X-purinoceptors in rat vas deferens. Naunyn-Schmiedeberg's Arch Pharmacol 348:684-7

Burch LH, Talbot CR, et al. (1995). Relative expression of the human epithelial Na^+ channel subunits in normal and cystic fibrosis airways. Am J Physiol 269:C511-8

Butterworth MB, Edinger RS, et al. (2005). Acute ENaC stimulation by cAMP in a kidney cell line is mediated by exocytic insertion from a recycling channel pool. J Gen Physiol 125(1):81-101

Butterworth MB, Edinger RS, et al. (2007). The deubiquitinating enzyme UCH-L3 regulates the apical membrane recycling of the epithelial sodium channel. J Biol Chem 282(52):37885-93

Butterworth MB. (2010). Regulation of the epithelial sodium channel (ENaC) by membrane trafficking. Biochim Biophys Acta 1802(12):1166-77

Canessa CM, Horisberger JD, Rossier BC (1993). Epithelial sodium channel related to proteins involved in neurodegeneration. Nature 361(6411):467-70

Canessa CM, Schild L, et al. (1994). Amiloride-sensitive epithelial Na^+ channel is made of three homologous subunits. Nature 367(6462):463-7

Carattino MD, Hughey RP, Kleyman TR (2008). Proteolytic processing of the epithelial sodium channel gamma subunit has a dominant role in channel activation. J Biol Chem 283(37):25290-5

Chalfant ML, Denton JS, et al. (1999). Intracellular H^+ regulates the alpha-subunit of ENaC, the epithelial Na^+ channel. Am J Physiol 276(2 Pt 1):C477-86

Chang T, Ke Y, et al. (2011). COMMD1 regulates the delta epithelial sodium channel (δENaC) through trafficking and ubiquitination. Biochem Biophys Res Commun 411(3):506-11

Chen CC, England S, et al. (1998). A sensory neuron-specific, proton-gated ion channel. Proc Natl Acad Sci USA 95:10240-5

Chen JH, Stoltz DA, et al. (2010). Loss of anion transport without increased sodium absorption characterizes newborn porcine cystic fibrosis airway epithelia. Cell 143(6):911-23

Chen Z, Jin N, et al. (2004). Identification of two novel markers for alveolar epithelial type I and II cells. Biochem Biophys Res Commun 319(3):774-80

Clerici C, Matthay MA (2000). Hypoxia regulates gene expression of alveolar epithelial transport proteins. J Appl Physiol 88(5):1890-6

Collier DM, Snyder PM (2009). Extracellular protons regulate human ENaC by modulating Na^+ self-inhibition. J Biol Chem 284(2):792-8

Coppens JT, Van Winkle LS, et al. (2007). Distribution of Clara cell secretory protein expression in the tracheobronchial airways of rhesus monkeys. Am J Physiol Lung Cell Mol Physiol 292(5):L1155-62

Cozens AL, Yezzi MJ, et al. (1994). CFTR expression and chloride secretion in polarized immortal human bronchial epithelial cells. Am J Respir Cell Mol Biol 10(1):38-47

Dahlin K, Mager EM, et al. (2004). Identification of genes differentially expressed in rat alveolar type I cells. Am J Respir Cell Mol Biol 31:309-16

Debonneville C, Flores SY, et al. (2001). Phosphorylation of Nedd4-2 by Sgk1 regulates epithelial Na (+) channel cell surface expression. EMBO J 20(24):7052-9

DeCoursey TE, Jacobs ER, Silver MR (1988). Potassium currents in rat type II alveolar epithelial cells. J Physiol 395:487-505

Demling N, Ehrhardt C, et al. (2005). Promotion of cell adherence and spreading: a novel function of RAGE, the highly selective differentiation marker of human alveolar epithelial type I cells. Cell Tissue Res 323(3):475-88

Dobbs LG, Johnson MD (2007). Alveolar epithelial transport in the adult lung. Respir Physio Neurobiol 159(3):283-300

Docherty RJ, Yeats JC, Piper AS. (1997). Capsazepine block of voltage-activated calcium channels in adult rat dorsal root ganglion neurones in culture. Br J Pharmacol 121(7):1461-7

Driscoll M, Chalfie M. (1991). The mec-4 gene is a member of a family of Caenorhabditis elegans genes that can mutate to induce neuronal degeneration. Nature 349(6310):588-93

Duc C, Farman N, et al. (1994). Cell-specific expression of epithelial sodium channel alpha, beta, and gamma subunits in aldosterone-responsive epithelia from the rat: localization by *in situ* hybridization and immunocytochemistry. J Cell Biol 127: 1907-21

Dyka FM, May CA, Enz R. (2005). Subunits of the epithelial sodium channel family are differentially expressed in the retina of mice with ocular hypertension. J Neurochem 94, 120-8

Ehrhardt C, Kneuer C, et al. (2002). Influence of apical fluid volume on the development of functional intercellular junctions in the human epithelial cell line 16HBE14o-: implications for the use of this cell line as an *in vitro* model for bronchial drug absorption studies. Cell Tissue Res 308:391-400

Ehrhardt C, Kim KJ, Lehr CM (2005). Isolation and culture of human alveolar epithelial cells. Methods Mol Med 107:207-16.

Fang X, Fukuda N, et al. (2002). Novel role for CFTR in fluid absorption from the distal airspaces of the lung. J Gen Physiol 119:199-207

Fehrenbach H (2001). Alveolar epithelial type II cell: defender of the alveolus revisited. Respir Res 2(1):33-46

Filippidis AS, Zarogiannis SG, et al. (2012). Permeability of the arachnoid and pia mater. The role of ion channels in the leptomeningeal physiology. Childs Nerv Syst 28(4):533-40

Firsov D, Gautschi I, et al. (1998). The heterotetrameric architecture of the epithelial sodium channel (ENaC). EMBO J 17:344-52

Fogh J, Trempe G. (1975). Human tumor cells *in vitro*. Plenum Press, New York, Fogh J (ed.), 115-59.

Forbes B (2000). Human airway epithelial cell lines for *in vitro* drug transport and metabolism studies. Pharm Sci Technolo Today 3(1):18-27

Foster KA, Oster CG, et al. (1998). Characterization of the A549 cell line as a type II pulmonary epithelial cell model for drug metabolism. Exp Cell Res 243:359-66

Fuchs S, Hollins AJ, et al. (2003). Differentiation of human alveolar epithelial cells in primary culture: morphological characterization and synthesis of caveolin-1 and surfactant protein-C. Cell Tissue Res 311(1):31-45

Giard DJ, Aaronson SA, et al. (1973). *In vitro* cultivation of human tumors: establishment of cell lines derived from a series of solid tumors. J Natl Cancer Inst 51(5):1417-23

Giraldez T, Afonso-Oramas D, et al. (2007). Cloning and functional expression of a new epithelial sodium channel delta subunit isoform differentially expressed in neurons of the human and monkey telencephalon. J Neurochem 102(4):1304-15

Giraldez T, Rojas P, et al. (2012). Invited Review-The epithelial sodium channel δ subunit: new notes for an old song. Am J Physiol Renal Physiol 303(3):F328-38

Graham A, Steel DM, et al. (1992). Second-messenger regulation of sodium transport in mammalian airway epithelia. J Physiol 453:475-91

Grainger CI, Greenwell LL, et al. (2006). Culture of Calu-3 cells at the air interface provides a representative model of the airway epithelial barrier. Pharm Res 23(7):1482-90

Haerteis S, Krueger B, et al. (2009). The delta-subunit of the epithelial sodium channel (ENaC) enhances channel activity and alters proteolytic ENaC activation. J Biol Chem 284(42):29024-40

Hernández-González EO, Sosnik J, et al. (2006). Sodium and epithelial sodium channels participate in the regulation of the capacitation-associated hyperpolarization in mouse sperm. J Biol Chem 281(9):5623-33

Hollywood MA, Cotton KD, et al. (1998). Enhancement of Ca^{2+}-dependent outward current in sheep bladder myocytes by evans blue dye. Pflueg Arch Eur J Physiol 435:631-6

Hughey RP, Mueller GM, et al. (2003). Maturation of the epithelial Na^{+} channel involves proteolytic processing of the alpha- and gamma-subunits. J Biol Chem 278(39):37073-82

Hughey RP, Bruns JB, et al. (2004a). Distinct pools of epithelial sodium channels are expressed at the plasma membrane. J Biol Chem 279(49):48491-4

Hughey RP, Bruns JB, et al. (2004b). Epithelial sodium channels are activated by furin-dependent proteolysis. J Biol Chem 279(18):18111-4

Hummler E, Barker P, et al. (1996). Early death due to defective neonatal lung liquid clearance in alpha-ENaC-deficient mice. Nat Genet 12:325-8

Huque T, Cowart BJ, et al. (2009). Sour ageusia in two individuals implicates ion channels of the ASIC and PKD families in human sour taste perception at the anterior tongue. PLoS One 4(10):e7347

Itani OA, Auerbach SD, et al. (2002). Glucocorticoid-stimulated lung epithelial Na(+) transport is associated with regulated ENaC and sgk1 expression. Am J Physiol Lung Cell Mol Physiol 282(4):L631-41

Itani OA, Chen JH, et al. (2011). Human cystic fibrosis airway epithelia have reduced Cl^- conductance but not increased Na^+ conductance. Proc Natl Acad Sci USA 108(25):10260-5

Jasti J, Furukawa H, et al. (2007). Structure of acid-sensing ion channel 1 at 1.9 Å resolution and low pH. Nature 449(7160):316-23

Ji HL, Benos DJ. (2004). Degenerin sites mediate proton activation of deltabetagamma-epithelial sodium channel. J Biol Chem 279(26):26939-47

Ji HL, Su XF, et al. (2006). Delta-subunit confers novel biophysical features to alpha beta gamma-human epithelial sodium channel (ENaC) via a physical interaction. J Biol Chem 281(12):8233-41

Johnson MD, Widdicombe JH, et al. (2002). Alveolar epithelial type I cells contain transport proteins and transport sodium, supporting an active role for type I cells in regulation of lung liquid homeostasis. Proc Natl Acad Sci USA 99:1966-71

Johnson MD, Bao HF, et al. (2006). Functional ion channels in pulmonary alveolar type I cells support a role for type I cells in lung ion transport. Proc Natl Acad Sci USA 103:4964-9

Johnson M, Allen L, Dobbs L (2009). Characteristics of Cl^- uptake in rat alveolar type I cells. Am J Physiol Lung Cell Mol Physiol 297(5):L816-27

Junor RW, Benjamin AR, et al. (1999). A novel role for cyclic nucleotide-gated cation channels in lung liquid homeostasis in sheep. J Physiol 520(1):255-60

Kabra R, Knight KK, et al. (2008). Nedd4-2 induces endocytosis and degradation of proteolytically cleaved epithelial Na^+ channels. J Biol Chem 283(10):6033-9

Kapoor N, Bartoszewski R, et al. (2009). Knockdown of ASIC1 and epithelial sodium channel subunits inhibits glioblastoma whole cell current and cell migration. J Biol Chem 284(36):24526-41

Ke Y, Butt AG, et al. (2010). COMMD1 downregulates the epithelial sodium channel through Nedd4-2. Am J Physiol Renal Physiol 298(6):F1445-56

Kellenberger S, Schild L. (2002). Epithelial sodium channel/degenerin family of ion channels: a variety of functions for a shared structure. Physiol Rev 82(3):735-67

Kemp PJ, Kim KJ, et al. (2001). Re-evaluating the Na(+) conductance of adult rat alveolar type II pneumocytes: evidence for the involvement of cGMP-activated cation channels. J Physiol 536:693-701

Kim JK, Kim SS, et al. (2007). Expression and localization of surfactant proteins in human nasal epithelium. Am J Physiol Lung Cell Mol Physiol 292(4):L879-84

Kleyman TR, Cragoe EJ Jr. (1988). Amiloride and its analogs as tools in the study of ion transport. J Membr Biol 105(1):1-21

Kleyman TR, Carattino MD, Hughey RP. (2009). ENaC at the cutting edge: regulation of epithelial sodium channels by proteases. J Biol Chem 284(31):20447-51

Krueger B, Schlötzer-Schrehardt U, et al. (2012). Four subunits (αβγδ) of the epithelial sodium channel (ENaC) are expressed in the human eye in various locations. Invest Ophthalmol Vis Sci 53(2):596-604

Kuenzi FM, Dale N. (1996). Effect of capsaicin and analogues on potassium and calcium currents and vanilloid receptors in *Xenopus* embryo spinal neurones. Br J Pharmacol 119(1):81-90

Kunzelmann K, Kathöfer S, Greger R (1995). Na^+ and Cl^- conductances in airway epithelial cells: increased Na^+ conductance in cystic fibrosis. Pflugers Arch 431(1):1-9

Lazrak A, Samanta A, Matalon S. (2000). Biophysical properties and molecular characterization of amiloride-sensitive sodium channels in A549 cells. Am J Physiol Lung Cell Mol Physiol 278(4):L848-57

Lee SY, Maniak PJ, et al. (2003a). Basolateral Cl^- transport is stimulated by terbutaline in adult rat alveolar epithelial cells. J Membr Biol 191(2):133-9

Lee SY, Maniak PJ, et al. (2003b). Adult alveolar epithelial cells express multiple subtypes of voltage-gated K^+ channels that are located in apical membrane. Am J Physiol Cell Physiol 284(6):C1614-24

Leroy C, Dagenais A, et al. (2004). Molecular identity and function in transepithelial transport of K(ATP) channels in alveolar epithelial cells. Am J Physiol Lung Cell Mol Physiol 286:L1027-37

Leroy C, Prive A, et al. (2006). Regulation of ENaC and CFTR expression with K^+ channel modulators and effect on fluid absorption across alveolar epithelial cells. Am J Physiol Lung Cell Mol Physiol 291:L1207-19

Li T, Folkesson HG (2006). RNA interference for alpha-ENaC inhibits rat lung fluid absorption *in vivo*. Am J Physiol Lung Cell Mol Physiol 290:L649-60

Liang L, Zsembery A, et al. (2005). RNA interference targeted to multiple P_2X receptor subtypes attenuates zinc-induced calcium entry. Am J Physiol Cell Physiol 289(2):C388-96

Lieber M, Smith B, et al. (1976). A continuous tumor-cell line from a human lung carcinoma with properties of type II alveolar epithelial cells. Int J Cancer 17(1):62-70

Lingueglia E, Renard S, et al. (1994). Different homologous subunits of the amiloride-sensitive Na^+ channel are differently regulated by aldosterone. J Biol Chem 269(19):13736-9

Lingueglia E, Champigny G, et al. (1995). Cloning of the amiloride-sensitive FMRFamide peptide-gated sodium channel. Nature 378:730-3

Liu L, Simon SA. (1997). Capsazepine, a vanilloid receptor antagonist, inhibits nicotinic acetylcholine receptors in rat trigeminal ganglia. Neurosci Lett 228(1):29-32

Ma T, Fukuda N, et al. (2000). Lung fluid transport in aquaporin-5 knockout mice. J Clin Invest 105:93-100

Mall M, Bleich M, et al. (1998). The amiloride-inhibitable Na^+ conductance is reduced by the cystic fibrosis transmembrane conductance regulator in normal but not in cystic fibrosis airways. J Clin Invest 102(1):15-21

Malnic G, Berliner RW, Giebisch G (1989). Flow dependence of K^+ secretion in cortical distal tubules of the rat. Am J Physiol Renal Fluid Electrolyte Physiol 256:F932-41

Manzanares D, Gonzalez C, et al. (2011). Functional apical large conductance, Ca^{2+}-activated, and voltage-dependent K^+ channels are required for maintenance of airway surface liquid volume. J Biol Chem 286(22):19830-9

Matalon S, Lazrak A, et al. (2002). Invited review: biophysical properties of sodium channels in lung alveolar epithelial cells. J Appl Physiol 93:1852-9

Matsushita K, McCray PB Jr, et al. (1996). Localization of epithelial sodium channel subunit mRNAs in adult rat lung by *in situ* hybridization. Am J Physiol Lung Cell Mol Physiol 271:L332-9

Matthay MA, Folkesson HG, Clerici C (2002). Lung epithelial fluid transport and the resolution of pulmonary edema. Physiol Rev 82:569-600

McDonald FJ, Yang B, et al. (1999). Disruption of the gamma-subunit of the epithelial Na^+ channel in mice: hyperkalemia and neonatal death associated with a pseudohypoaldosteronism phenotype. Proc Natl Acad Sci USA 96:1727-31

Moser SL, Harron SA, et al. (2008). Multiple KCNQ potassium channel subtypes mediate basal anion secretion from the human airway epithelial cell line Calu-3. J Membr Biol 221(3):153-63

Mutlu GM, Sznajder JI (2005). Mechanisms of pulmonary edema clearance. Am J Physiol Lung Cell Mol Physiol 289(5):L685-95

Nici L, Dowin R, et al. (1991). Upregulation of rat lung Na^+-K^+-ATPase during hyperoxic injury. Am J Physiol Lung Cell Mol Physiol 261(1):L307-14

Nie HG, Tucker T, et al. (2009a). Expression and regulation of epithelial Na^+ channels by nucleotides in pleural mesothelial cells. Am J Respir Cell Mol Biol 40(5):543-54

Nie HG, Chen L, et al. (2009b). Regulation of epithelial sodium channels by cGMP/PKGII. J Physiol 587:2663-76

Nielsen S, King LS, et al. (1997). Aquaporins in complex tissues. II. Subcellular distribution in respiratory and glandular tissues of rat. Am J Physiol 273:C1549-61

Olver RE, Strang LB (1974). Ion fluxes across the pulmonary epithelium and the secretion of lung liquid in the foetal lamb. J Physiol 241:327-57

O'Reilly MA, Gazdar AF, et al. (1988). Differential effects of glucocorticoid on expression of surfactant proteins in a human lung adenocarcinoma cell line. Biochim Biophys Acta 970:194-204

O'Sullivan BP, Freedman SD (2009). Cystic fibrosis. The Lancet 373(9678):1891-1904

Paradiso AM, Ribeiro CM, et al. (2001). Polarized signaling via purinoceptors in normal and cystic fibrosis airway epithelia. J Gen Physiol 117(1):53-67

Patterson CE, Rhoades RA, Garcia JG. (1992). Evans blue dye as a marker of albumin clearance in cultured endothelial monolayer and isolated lung. J Appl Physiol 72(3):865-73

Ramsden CA, Markiewicz M, (1992). Liquid flow across the epithelium of the artificially perfused lung of fetal and postnatal sheep. J Physio 448:579-97

Reilly CA, Taylor JL et al. (2003). Capsaicinoids cause inflammation and epithelial cell death through activation of vanilloid receptors. Toxicol Sci 73:170-81

Ricard JD, Dreyfuss D, Saumon G (2003). Ventilator-induced lung injury. Eur Respir J Suppl 42:2-9

Rich DP, Anderson MP, et al. (1990). Expression of cystic fibrosis transmembrane conductance regulator corrects defective chloride channel regulation in cystic fibrosis airway epithelial cells. Nature 347(6291):358-63

Rock JR, O'Neal WK, et al. (2009). Transmembrane protein 16A (TMEM16A) is a Ca^{2+}-regulated Cl^- secretory channel in mouse airways. J Biol Chem 284(22):14875-80

Roseth S, Fykse EM, Fonnum F. (1995). Uptake of *L*-glutamate into rat brain synaptic vesicles: effect of inhibitors that bind specifically to the glutamate transporter. J Neurochem 65:96-103

Qiao R, Zhou B et al. (2003). Identification of three genes of known function expressed by alveolar epithelial type I cells. Am J Respir Cell Mol Biol 29:98-105

Sabnis AS, Shadid M et al. (2008). Human lung epithelial cells express a functional cold-sensing TRPM8 variant. Am J Respir Cell Mol Biol 39(4):466-74

Sakuma T, Okaniwa G, et al. (1994). Alveolar fluid clearance in the resected human lung. Am J Respir Crit Care Med 150(2):305-10

Satlin LM, Sheng S, et al. (2001). Epithelial Na^+ channels are regulated by flow. Am J Physiol Renal Physiol 280:F1010-8

Schwiebert EM, Potter ED, et al. (1997). cGMP stimulates sodium and chloride currents in rat tracheal airway epithelia. Am J Physiol 272:C911-22

Shen BQ, Finkbeiner WE, et al. (1994). Calu-3: a human airway epithelial cell line that shows cAMP-dependent Cl^-secretion. Am J Physiol 266:L493-501

Shimkets RA, Lifton RP, Canessa CM. (1997). The activity of the epithelial sodium channel is regulated by clathrin-mediated endocytosis. J Biol Chem 272(41):25537-41

Simon A, Shenton F, et al. (2010). Amiloride-sensitive channels are a major contributor to mechanotransduction in mammalian muscle spindles. J Physiol 588(1):171-85

Smith DE, Otulakowski G, et al. (2000). Epithelial Na(+) channel (ENaC) expression in the developing normal and abnormal human perinatal lung. Am J Respir Crit Care Med 161(1):1322-31

Snyder PM, Cheng C, et al. (1998). Electrophysiological and biochemical evidence that DEG/ENaC cation channels are composed of nine subunits. J Biol Chem 273:681-4

Sporty JL, Horalkova L, Ehrhardt C (2008). *In vitro* cell culture models for the assessment of pulmonary drug disposition. Expert Opin Drug Metab Toxicol 4(4):333-45

Stockand JD, Staruschenko A, et al. (2008). Insight toward epithelial Na^+ channel mechanism revealed by the acid-sensing ion channel 1 structure. IUBMB Life 60(9):620-8

Stone KC, Mercer RR, et al. (1992). Allometric relationships of cell numbers and size in the mammalian lung. Am J Respir Cell Mol Biol 6:235-43

Story GM, Peier AM, et al. (2003). ANKTM1, a TRP-like channel expressed in nociceptive neurons, is activated by cold temperatures. Cell 112:819-29

Stutts MJ, Chinet TC, et al. (1992). Regulation of Cl^- channels in normal and cystic fibrosis airway epithelial cells by extracellular ATP. Proc Natl Acad Sci USA 89(5):1621-5

Take-Uchi M, Kawakami M, et al. (1998). An ion channel of the degenerin/epithelial sodium channel superfamily controls the defecation rhythm in *Caenorhabditis elegans*. Proc Natl Acad Sci USA 95(20):11775-80

Talbot CL, Bosworth DG, et al. (1999). Quantitation and localization of ENaC subunit expression in fetal, newborn, and adult mouse lung. Am J Respir Cell Mol Biol 20:398-406

Tan CD, Selvanathar IA, Baines DL (2011). Cleavage of endogenous γENaC and elevated abundance of αENaC are associated with increased Na^+ transport in response to apical fluid volume expansion in human H441 airway epithelial cells. Pflugers Arch 462(3):431-41

Taylor AL, Schwiebert LM, et al. (1999). Epithelial P2X purinergic receptor channel expression and function. J Clin Invest 104:875-84

Tessier GJ, Traynor TR, et al. (1990). Mechanisms of sodium and chloride transport across equine tracheal epithelium. Am J Physiol 259:L459-67

Thomas KC, Roberts JK, et al. (2012). Contributions of TRPV1, endovanilloids, and endoplasmic reticulum stress in lung cell death *in vitro* and lung injury. Am J Physiol Lung Cell Mol Physiol 302(1):L111-9

Waldmann R, Champigny G, et al. (1995). Molecular cloning and functional expression of a novel amiloride-sensitive Na^+ channel. J Biol Chem 270:27411-4

Waldmann R, Champigny G, et al. (1997). A proton-gated cation channel involved in acid-sensing. Nature 386:173-7

Waldmann R, Champigny G, et al. (1999). H(+)-gated cation channels. Ann N Y Acad Sci 868:67-76

Walsh DE, Harvey BJ, et al. (2000). CFTR regulation of intracellular calcium in normal and cystic fibrosis human airway epithelia. J Membr Biol 177(3):209-19

Ware LB, Matthay MA (2001). Alveolar fluid clearance is impaired in the majority of patients with acute lung injury and the acute respiratory distress syndrome. Am J Respir Crit Care Med 163:1376-83

Weibel ER (1963). Morphometry of the Human Lung. Heidelberg: Springer-Verlag

Wesch D, Miranda P, et al. (2010). The neuronal-specific SGK1.1 kinase regulates {delta}-epithelial Na^+ channel independently of PY motifs and couples it to phospholipase C signaling. Am J Physiol Cell Physiol 299(4):C779-90

Wesch D, Althaus M, et al. (2012). Differential N termini in epithelial Na^+ channel δ-subunit isoforms modulate channel trafficking to the membrane. Am J Physiol Cell Physiol 302(6):C868-79

Wiemuth D, Ke Y et al. (2007). Epithelial sodium channel (ENaC) is multi-ubiquitinated at the cell surface. Biochem J 405(1):147-55

Wu SN, Jan CR et al. (1999). Stimulation of large-conductance Ca^{2+}-activated K^+ channels by Evans blue in cultured endothelial cells of human umbilical veins. Biochem Biophys Res Commun 254(3):666-74

Yamamura H, Ugawa S, et al. (2004a). Protons activate the delta-subunit of the epithelial Na^+ channel in humans. J Biol Chem 279(13):12529-34

Yamamura H, Ugawa S, et al. (2004b). Capsazepine is a novel activator of the delta subunit of the human epithelial Na^+ channel. J Biol Chem 279(43):44483-9

Yamamura H, Ugawa S, et al. (2005a). Icilin activates the delta-subunit of the human epithelial Na^+ channel. Mol Pharmacol 68(4):1142-7

Yamamura H, Ugawa S, et al. (2005b). Evans blue is a specific antagonist of the human epithelial Na^+ channel delta-subunit. J Pharmacol Exp Ther 315(2):965-9

Yamamura H, Ugawa S, et al. (2006). A novel spliced variant of the epithelial Na^+ channel delta-subunit in the human brain. Biochem Biophys Res Commun 349(1):317-21

Yamamura H, Ugawa S, et al. (2008a). Expression analysis of the epithelial Na^+ channel delta subunit in human melanoma G-361 cells. Biochem Biophys Res Commun 366(2):489-92

Yamamura H, Ugawa S, et al. (2008b). Epithelial Na^+ channel delta subunit mediates acid-induced ATP release in the human skin. Biochem Biophys Res Commun 373(1):155-8

Yamamura H, Ugawa S, et al. (2008c). Epithelial Na^+ channel delta subunit is an acid sensor in the human oesophagus. Eur J Pharmacol 600(1-3):32-6

Zhang L, Whitsett JA, Stripp BR (1997). Regulation of Clara cell secretory protein gene transcription by thyroid transcription factor-1. Biochim Biophys Acta 350:359-67

Zhao RZ, Nie HG, et al. (2012). Characterization of a novel splice variant of δ ENaC subunit in human lungs. Am J Physiol Lung Cell Mol Physiol 302(12):L1262-72

Zhou R, Patel SV, Snyder PM. (2007). Nedd4-2 catalyzes ubiquitination and degradation of cell surface ENaC. J Biol Chem 282(28):20207-12